THEORETICAL BIOLOGY AND MEDICAL MODELLING

RESEARCH Open Access

Modeling CICR in rat ventricular myocytes: voltage clamp studies

Abhilash Krishna[1], Liang Sun[2], Miguel Valderrábano[3], Philip T Palade[4], John W Clark Jr[1*]

* Correspondence: jwc@rice.edu
[1]Department of Electrical and Computer Engineering, Rice University, 6100 Main Street, Houston, 77005, USA

Abstract

Background: The past thirty-five years have seen an intense search for the molecular mechanisms underlying calcium-induced calcium-release (CICR) in cardiac myocytes, with voltage clamp (VC) studies being the leading tool employed. Several VC protocols including lowering of extracellular calcium to affect Ca^{2+} loading of the sarcoplasmic reticulum (SR), and administration of blockers caffeine and thapsigargin have been utilized to probe the phenomena surrounding SR Ca^{2+} release. Here, we develop a deterministic mathematical model of a rat ventricular myocyte under VC conditions, to better understand mechanisms underlying the response of an isolated cell to calcium perturbation. Motivation for the study was to pinpoint key control variables influencing CICR and examine the role of CICR in the context of a physiological control system regulating cytosolic Ca^{2+} concentration ($[Ca^{2+}]_{myo}$).

Methods: The cell model consists of an electrical-equivalent model for the cell membrane and a fluid-compartment model describing the flux of ionic species between the extracellular and several intracellular compartments (cell cytosol, SR and the dyadic coupling unit (DCU), in which resides the mechanistic basis of CICR). The DCU is described as a controller-actuator mechanism, internally stabilized by negative feedback control of the unit's two diametrically-opposed Ca^{2+} channels (trigger-channel and release-channel). It releases Ca^{2+} flux into the cyto-plasm and is in turn enclosed within a negative feedback loop involving the SERCA pump, regulating $[Ca^{2+}]_{myo}$.

Results: Our model reproduces measured VC data published by several laboratories, and generates graded Ca^{2+} release at high Ca^{2+} gain in a homeostatically-controlled environment where $[Ca^{2+}]_{myo}$ is precisely regulated. We elucidate the importance of the DCU elements in this process, particularly the role of the ryanodine receptor in controlling SR Ca^{2+} release, its activation by trigger Ca^{2+}, and its refractory characteristics mediated by the luminal SR Ca^{2+} sensor. Proper functioning of the DCU, sodium-calcium exchangers and SERCA pump are important in achieving negative feedback control and hence Ca^{2+} homeostasis.

Conclusions: We examine the role of the above Ca^{2+} regulating mechanisms in handling various types of induced disturbances in Ca^{2+} levels by quantifying cellular Ca^{2+} balance. Our model provides biophysically-based explanations of phenomena associated with CICR generating useful and testable hypotheses.

Background

Contraction of cardiac muscle is triggered by a transient rise in intracellular Ca^{2+} concentration $[Ca^{2+}]_{myo}$. Sarcolemmal (SL) membrane depolarization triggers Ca^{2+} influx from the extracellular medium by opening dihydropyridine (DHP)-sensitive L-type Ca^{2+} channels. Following diffusion across a small sub-membrane dyadic space, this influx activates ryanodine receptors (RyRs) controlling ryanodine-sensitive Ca^{2+} release channels in the junctional portion of the sarcoplasmic reticulum (jSR). Fabiato and Fabiato [1] named the process calcium-induced calcium release (CICR). Ca^{2+} subsequently diffuses from the dyadic space into the cytosol. Ultimately, intracellular Ca^{2+} concentration $[Ca^{2+}]_{myo}$ is returned to resting levels by combination of: (a) Ca^{2+} buffering in the dyadic space and cytosol; (b) sequestration of Ca^{2+} by sarcoplasmic/endoplasmic reticulum Ca^{2+}-ATPase (SERCA)-type calcium pumps lining the longitudinal portion of the sarcoplasmic reticulum (LSR); and (c) Ca^{2+} extrusion from the cytosol by Na^{+}/Ca^{2+} exchangers and Ca^{2+}-ATPase pumps on the sarcolemmal membrane.

CICR in cardiac muscle exhibits both graded behavior and a high gain. Graded behavior refers to the obser-vation that SR Ca^{2+} release is proportional to the influx of trigger Ca^{2+} [2], whereas high gain indicates that the SL trigger current elicits a high SR Ca^{2+} release flux. Graded Ca^{2+} release with high gain is somewhat paradoxical according to Stern [3], in that the positive feedback inherent in such high-gain systems tend to produce regenerative, nearly all-or-none release rather than graded release. Several deterministic models have been developed to explain excitation-contraction (E-C) coupling [4,5], but none of them can explain the mechanism of graded release at high gain over a wide range of values for sarcolemmal Ca^{2+} current. Stern [3] proposed that such a gradation paradox might be explained if the stimulus for Ca^{2+} release by RyRs were actually the local nanodomains of $[Ca^{2+}]$ generated by nearby L-type channels, rather than the global cytosolic $[Ca^{2+}]_{myo}$. According to this hypothesis, graded control of macroscopic SR Ca^{2+} release can be achieved by graded statistical recruitment of individual, autonomous, all-or-none stochastic release events [6]. In these studies, a distributed differential model of high order that included dynamic interactions between large numbers of individual channels was used to demonstrate this concept. However, rather large amounts of computation time are required with distributed stochastic models of this type. Additional models have sought to characterize the Ca^{2+} release complex, including several [7-9] based on the stochastic release process adopted by Stern et al. These statistical models have solved the graded release problem, however, they too are complicated and computationally very expensive. Other models based on the simplified local control model of CICR developed by Hinch et al. [10] sought to adopt a lower order description of the E-C coupling process [11,12] by making an approximation of rapid equilibrium in the dyadic space. The latency from onset of Ca^{2+} entry via the $I_{Ca,L}$ channel to triggered SR Ca^{2+} release is known to increase with decrease in the magnitude of $I_{Ca,L,TT}$ [13], the modeling of which is made possible by considering Ca^{2+} diffusion in the dyadic medium. These models [11,12] also approximate the SR as a single volume compartment with no distinction between junctional versus the longitudinal (network) SR compartments. However, recent work [14] points towards the important role of the Ca^{2+} refilling rate from the network to junctional SR in controlling RyR release termination via the luminal sensor. Shiferaw et al. [15] developed a computationally tractable model of Ca^{2+} cycling to represent the release of calcium from the SR as a sum of spatially localized events

that correspond to Ca^{2+} sparks, assuming the recruitment rate of Ca^{2+} sparks is directly proportional to the whole-cell $I_{Ca,L}$ current. This assumption overlooks the complex calmodulin mediated interaction (calcium dependent facilitation (CDF) and calcium dependent inactivation (CDI)) of the $I_{Ca,L}$ channel with calcium in its vicinity. It also demands a large amount of computation.

Numerically, distributed as well as statistical models tend to be computationally expensive due to the in-herent repetition involved in the computation. In a spatially distributed model, simultaneous solution for dynamics in identical compartments distributed in space would amount to a large computational cost. In statistical models inference is drawn based on multiple runs of identical events which translate into a prolonged simulation time. Hence, these models are cumbersome to implement, particularly in larger multiple-cell simulations. Consequently, we consider a deterministic approach to the characterization of CICR. Specifically, we develop a lumped model of the Ca^{2+} release complex that includes: (a) a sub-sarcolemmal dyadic cleft space separating the SL and jSR membranes; (b) a single DHP-sensitive Ca^{2+} channel on the SL membrane; and (c) a single equivalent Ry-sensitive channel arranged symmetrically on the opposing jSR membrane that represents the output of a local cluster of Ry-sensitive channels facing the DHP-sensitive channel. Based on morphological data compiled by Bers [16], we further assume that each ventricular cell contains 10,000 of these dyadic Ca^{2+} release units, and that they are associated with the fraction of the SL membrane that is coupled with the jSR. That is, we partition the sarcolemma into free and dyadically coupled SL membrane, and associate each with a different fluid compartment: the cell cytosolic medium in the case of the free SL membrane, and the dyadic cleft space medium in the case of the dyadic-coupled fraction. In a sense, we build on Stern's [3] local domain concept by considering the aforementioned local nanodomains identical, but focusing on the nonlinear dynamics of the two different types of Ca^{2+} channel in the dyadic coupling unit. Our deterministic model although is very descriptive, is computationally tractable and has a run time of 21 sec (including recording of 73 variables of type double on a data file) for 1 cycle of 4 Hz voltage clamp stimulation.

Methods

Experimental Methods

Rat ventricular myocytes were prepared from 200-300 g male Sprague Dawley rats by dissociation with collagenase, as previously described [17]. All experiments were performed under conventional whole cell recording conditions with a List EPC-7 patch clamp, recording fluorescence from nearly the entire cell, as described by Fan and Palade [17]. Recordings from an individual cell were rarely extended beyond 10 min in order to reduce as much as possible both escape of dye from the cell and Ca^{2+} current rundown. External solution in the bath was normal Tyrode (1 mM Ca^{2+}) with Cs^{+} substituted for K^{+} for purposes of blocking inward rectifier K^{+} currents. The internal solution in the pipette contained Cs aspartate supplemented with 20 mM $CsCl$, 3 mM Na_2ATP , 3.5 mM $MgCl_2$ and 5 mM HEPES. Holding potential used was -40 mV.

Computational Aspects

All simulations and analysis were performed on a 2.8 GHz Intel® Core™2 Duo CPU-based computer using Microsoft Windows XP operating system. To find the

parameters involved in the 6 state Markovian model for $I_{Ca,L}$, a non-linear least-squares method [18] was used to obtain the solution of the system of non-linear ordinary differential equations. Specifically, we have employed an algorithm given by Lau [19]. The numerical integration scheme used to solve the full set of forty two 1st-order differential equations describing the dynamic model was the Merson-modified Runge-Kutta 4th-order method [20,21] with a conservative fixed time step, chosen small enough to allow the local truncation error to be of fourth order. The explicit finite difference scheme was used to numerically solve the Laplacian equations of Ca^{2+} diffusion in the cleft space. Detailed numerical methods are similar to those presented by Smith et al. [22]. The results were visualized using Matlab by Mathworks and Origin by Microcal Software.

Model Development

Our objective was to develop a model of the rat ventricular cell which could be used to explain Ca^{2+} signaling at the nanoscale level of the dyad and integrate the contributions of many dyads to produce a Ca^{2+} transient and continuous Ca^{2+} balance at the whole-cell level. Therefore, we start with a broad discussion of the elements of the DCU and its Ca^{2+} supply (the jSR), and continue with a progressively more detailed description of the whole cell model. It is important to note that all Ca^{2+} concentrations discussed in the model pertain to unbound Ca^{2+} unless specified.

Membrane Classification

We assume that a continuous membrane barrier exists between the cytoplasm and the external bathing medium (Figure 1A; Figure 2), which consists of two components: a surface sarcolemma (SL) (M_{FreeSL} in Figure 3) free of any sub-membrane contact with the junctional sarcoplasmic reticulum (jSR) and the remnant membrane ($M_{JunctionalSL}$ in Figure 3) that does make contact with the jSR via a dyadic space (nanodomain) (Figure 1A). These membrane components have the same basic plasma membrane, but differ in content with regard to total membrane surface area, type and distribution of transmembrane ion channels, ATPase pumps and exchangers, as well as their functional coupling with a dyadic space. Ultrastructural information from several cardiac preparations including the rat ventricular cell has been compiled by Bers [16], which can be used to estimate the percentage of the cell membrane in contact with a dyadic space, for either the free surface plasmalemma or for the transverse tubule (TT) which brings the extracellular medium to the plasma membrane of the dyadic coupling unit. Thus, the bounding membrane is divided into two lumped parts (free and coupled) based on the existence of sub-membrane coupling to a dyadic space (Table 1). A portion of membrane could be part of a transverse tubular membrane, but if there is no dyadic coupling involved, that membrane would be classified as belonging to the free surface plasmalemma. Another portion of membrane might be part of the bounding outer surface of the cylindrical cell and yet have submembrane coupling to a dyadic space. In this case, it would be classified as belonging to the coupled category. Table 2 gives values for volumes of the fluid compartments (shown in Figure 3) assumed for the rat ventricular cell, which are largely based on measured data from rat ventricular myocytes [16].

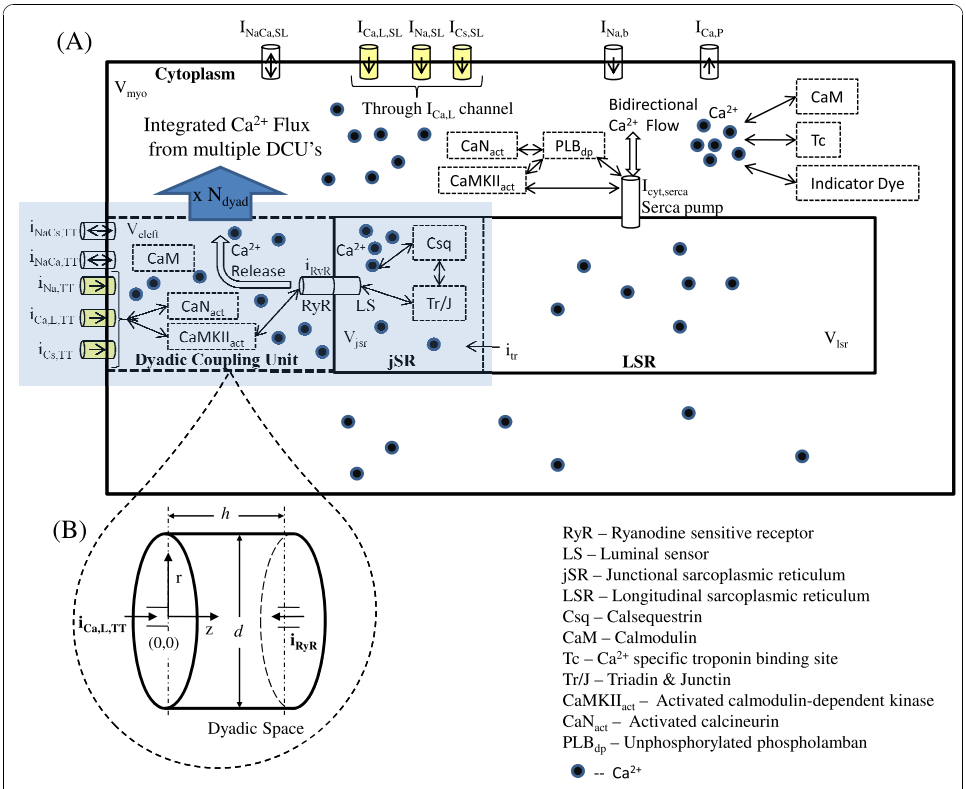

Figure 1 Cellular fluid compartments. Figure 1: Cellular fluid compartments. (a) Model configuration showing dyadic space, jSR, LSR, cytoplasm and SL; (b) Inset provides a more detailed description of the dyadic space showing the coupling of the two types of Ca^{2+} channels (trigger and Ca^{2+} release channels) via the dyadic fluid medium. Only one representative dyadic coupling unit is shown, however the whole model contains such 10,000 identical units lumped together.

Channel and Exchanger Distribution

Recent research has also shown that besides L-type Ca^{2+} channels, Na^{+}/Ca^{+} exchanger activity is also found predominantly in the T-tubules of rat ventricular myocytes [23]. Our model configuration reflects this finding in that the tubular fraction of $I_{Ca,L}$,I_{NaCa} and I_{NaCs} channels facing a unitary dyadic space are denoted as $i_{Ca,L,TT}$ (source of trigger Ca^{2+} into a unitary dyad), $i_{NaCa,TT}$ and $i_{NaCs,TT}$ respectively (Figure 2). The free sarcolemmal component of these same channels are denoted as $I_{Ca,L,SL}$, $I_{NaCa,SL}$ and $I_{NaCs,SL}$ respectively. $I_{Ca,L,TT}$ is the total current entering through L-type Ca^{2+} channels via all the dyadic units (N_{dyad}). We define the total L-type current $I_{Ca,L}$ as the combination of $I_{Ca,L,TT}$ and $I_{Ca,L,SL}$ (i.e., $I_{Ca,L} = I_{Ca,L,TT} + I_{Ca,L,SL}$). $I_{Ca,L}$ in our model is mostly (90%) from the L-type Ca^{2+} current in the T-tubules, since Kawai et al. [24], found L-type current to be highly concentrated (9-fold) in the T-tubules ($I_{Ca,L,TT}$) vs. the cell surface sarcolemma ($I_{Ca,L,SL}$) of rat ventricular myocytes. We described the $I_{Ca,L}$ channel using a 6-state Markovian model as shown in Figure 4A. The distribution of I_{NaCa} and I_{NaCs} correspond to that of $I_{Ca,L}$ channel in order to ensure Ca^{2+} and Na^{+} ion balance.

Since our study is focused on voltage clamp testing of Ca^{2+} transients in rat ventricular cells, we assume that the majority of Na^{+} and K^{+} channels are blocked by either the holding potential used (-40 mV) or appropriate blocking agents. Thus, these channels are not modeled, and we assume that only the dihy-dropyridine (DHP) -sensitive

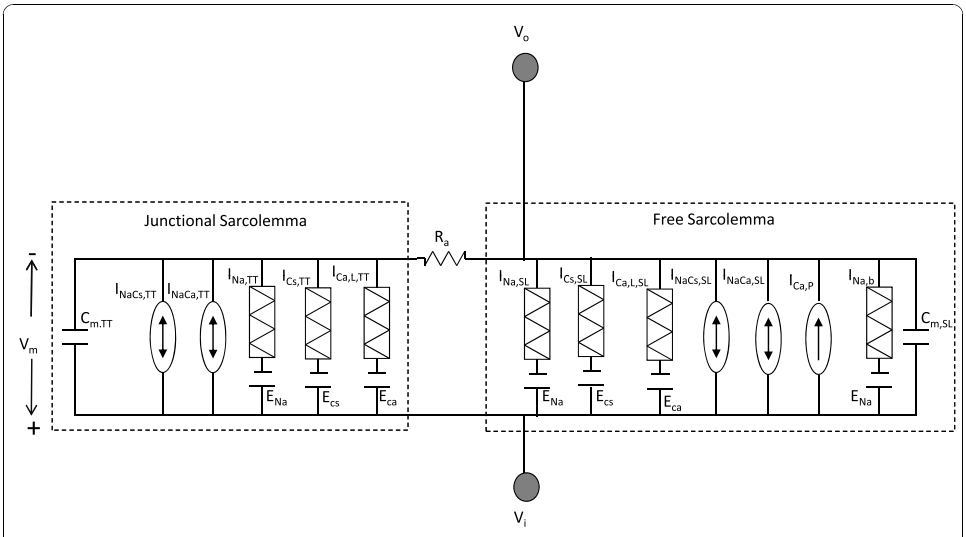

Figure 2 Electrical equivalent circuit for the plasma membrane of a rat ventricular cell. Figure 2: $C_{m,TT}$: membrane capacitance of the junctional SL membrane coupled with the dyadic space; $C_{m,SL}$: membrane capacitance of the uncoupled free SL membrane; Currents through the uncoupled free SL membrane are (a) $I_{Ca,L,SL}$: L-type calcium current, (b) $I_{Na,SL}$: sodium current through the DHPR channel, (c) $I_{Cs,SL}$: cesium current through the DHPR channel, (d) $I_{NaCa,SL}$: sodium-calcium exchanger current, (e) $I_{NaCs,SL}$: sodium-cesium exchanger current, (f) I_{PMCA}: calcium pump current, (g) $I_{Na,b}$: background sodium current; Currents through the junctional SL membrane coupled with a dyadic space are (h) $I_{Ca,L,TT}$: L-type calcium current; (i) $I_{Na,TT}$: sodium current through the DHPR channel, (j) $I_{Cs,TT}$: cesium current through the DHPR channel, (k) $I_{NaCa,TT}$: sodium-calcium exchanger current, (l) $I_{NaCs,TT}$: sodium-cesium exchanger current; V_o: potential in external medium; V_i: intracellular potential; The coupling resistance between the surface sarcolemma and the transverse tubules being very small is neglected in our model hence V_m: common transmembrane potential across both uncoupled and coupled membranes.

Ca^{2+} channels, the electrogenic pumps, Na^+/Ca^+ exchangers and Na^+/Cs^+ pumps expressed in the free and/or coupled SL membranes contribute to the voltage clamp response. Table 3 provides values for various parameters used to model the ion transport across the sarcolemmal membrane.

The SR Fluid Compartment

The SR is an intracellular organelle that consists of two lumped fluid compartments (the jSR and LSR) that communicate (Figure 1A; Figure 3). Like the sarcolemma, the bounding membranes of the jSR and LSR are differentiated regarding their ionic current content and degree of coupling with the sarcolemma. With regard to ionic currents, the LSR membrane has a thapsigargin-sensitive SERCA pump for pumping Ca^{2+} into the LSR lumen against a concentration gradient. In contrast, the jSR membrane contains an outwardly directed ryanodine (Ry)-sensitive channel for Ca^{2+} release from the jSR to the dyadic space. The jSR fluid compartment contains the Ca^{2+} binding protein calsequestin as well as the proteins triadin and junctin, which interact with the ryanodine receptor (RyR) and calsequestrin. This co-located configuration of the RyR receptor, along with the proteins calsequestrin, triadin and junctin which exist on the luminal side of the jSR membrane, constitutes a jSR Ca^{2+} release regulating mechanism called the luminal sensor (Figure 4B; Figure 5). The protein-protein interaction between them plays an important role in regulating the open-state of the RyR Ca^{2+} release channel [25]. A six-state Markovian scheme (Appendix A1, Equations 87-92) is used to describe the dynamics of this interaction and it is called the SR luminal Ca^{2+}

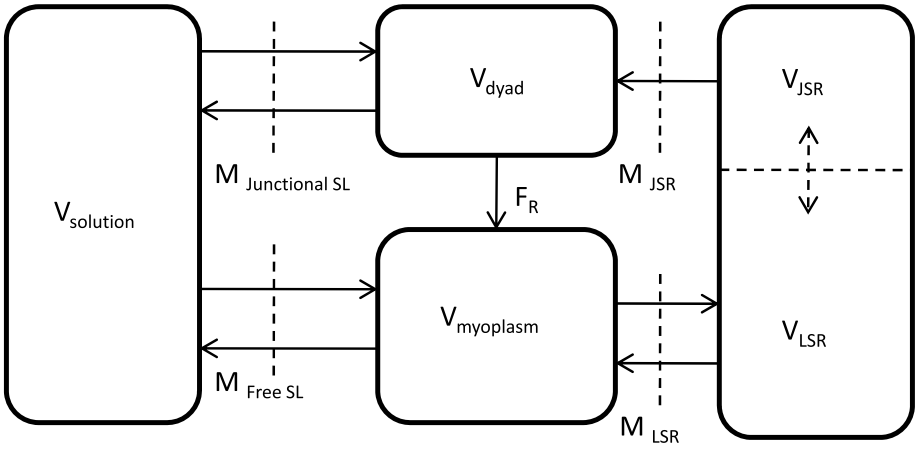

Figure 3 Fluid compartment model. Figure 3: Representative fluid compartment model, showing membrane surface area separating different compartments. M_{FreeSL}: free SL membrane; $M_{JunctionalSL}$: junctional SL membrane; M_{JSR}: junctional SR membrane; M_{LSR}: Longitudinal SR membrane.

sensor. Figure 4B shows a functional diagram of the luminal sensor and its output state is shown connected to the four-state RyR model. Specifically, the sensor adjusts Ca^{2+} dependent rate functions within the ryanodine receptor model, which affects the open probability P_o of the SR Ca^{2+} release channel.

With regard to coupling, the DHP and Ry-sensitive Ca^{2+} channels are assumed to be located on opposite sides of the small dyadic fluid space (nanodomain) as shown in Figure 6, and coupled functionally by a CICR mechanism. The dyadic space is assumed to be in fluid communication with the cell cytoplasm via a restricted diffusion region. In contrast, the LSR is not functionally coupled to the sarcolemma, but rather is in contact with the cytoplasm via the SERCA pump (as shown in Figure 3). Table 4 provides values for parameters used to model the intracellular ion transport.

The Dyadic Coupling Unit (DCU)

In describing this functional unit it is necessary to provide progressively more detailed descriptions of the component elements of the individual dyad, particularly the geometrically opposed DHP and Ry-sensitive Ca^{2+} channels, as well as the geometry and

Table 1 Surface area of various plasma membranes in the cell

Variable	Description	Value
$A_{Ext.SL}$	Surface area of external SL	$11.4 \times 10^3\ \mu m^2$
A_{TT}	Surface area of T-tubule	$5.52 \times 10^3\ \mu m^2$
A_{TotSL}	Surface area of total SL (including external SL and T-tubule)	$16.9 \times 10^3\ \mu m^2$ (*)
$A_{JunctExt.SL}$	Surface area of junctional external SL	$0.846 \times 10^3\ \mu m^2$
$A_{JunctTT}$	Surface area of junctional T-tubule	$2.54 \times 10^3\ \mu m^2$
$A_{TotJunct}$	Surface area of total junctional plasma membrane	$3.39 \times 10^3\ \mu m^2$
$A_{JunctSR}$	Surface area of junctional SR	$6.99 \times 10^3\ \mu m^2$
A_{LongSR}	Surface area of longitudinal SR	$36.8 \times 10^3\ \mu m^2$
A_{TotSR}	Surface area of total SR	$43.8 \times 10^3\ \mu m^2$

*Electrical capacitance of the cell membrane = 169 pF (using 1 $\mu F/cm^2$).

Table 1: Surface area of various plasma membranes in the cell. All the above parameters are derived from Bers [16].

Table 2 Parameters used to model sub-cellular morphology

Parameter	Definition	Value	References
N_{dyad}	Number of dyadic units	10000	[8]‡
V_{myo}	Myoplasmic volume	5.3581 × 10^{-2} *nL*	[16]†
V_{LSR}	Longitudinal SR volume	1.1776 × 10^{-3} *nL*	[16]*
$\sum_{N\,dyad} V_{jSR}$	Total junctional SR volume	1.104 × 10^{-4} *nL*	[16]*
Δr	Step size in the 'r' direction	10 *nm*	Numerical solution†
d	Diameter of the cylindrical cleft space in the 'r' direction	400 *nm*	[119,8,120,121,6]‡
Δz	Step size in the 'z' direction	0.76 *nm*	Numerical solution†
h	Length of the cylindrical cleft space in the 'z' direction	15.2 *nm*	[119,8,120,121,6]‡
V_{cleft}	Volume of a unit dyadic space	1.91 × 10^{-9} *nL*	–

Table 2: Parameters used to model sub-cellular morphology. Adopted (*), derived (†) or estimated (‡) from the cited sources.

buffering properties of the small dyadic space. As will be shown, we have described the dynamics of both types of Ca^{2+} channels using Markovian state models (Figure 4) which include features such as Ca^{2+} mediated channel inactivation, a graded CICR process with a "calcium gain" of approximately 6-7, and two-dimensional Ca^{2+} diffusion within the dyadic space. Crank [26] discusses diffusion problems in a two-phase heterogeneous medium and shows that diffusion through a system of barriers (RyR feet structures in the dyadic cleft space) can be approximated by diffusion in the same region without barriers but with a reduced effective diffusion coefficient. We hence take this approach in modeling the Ca^{2+} diffusion by solving the 2-D Laplacian

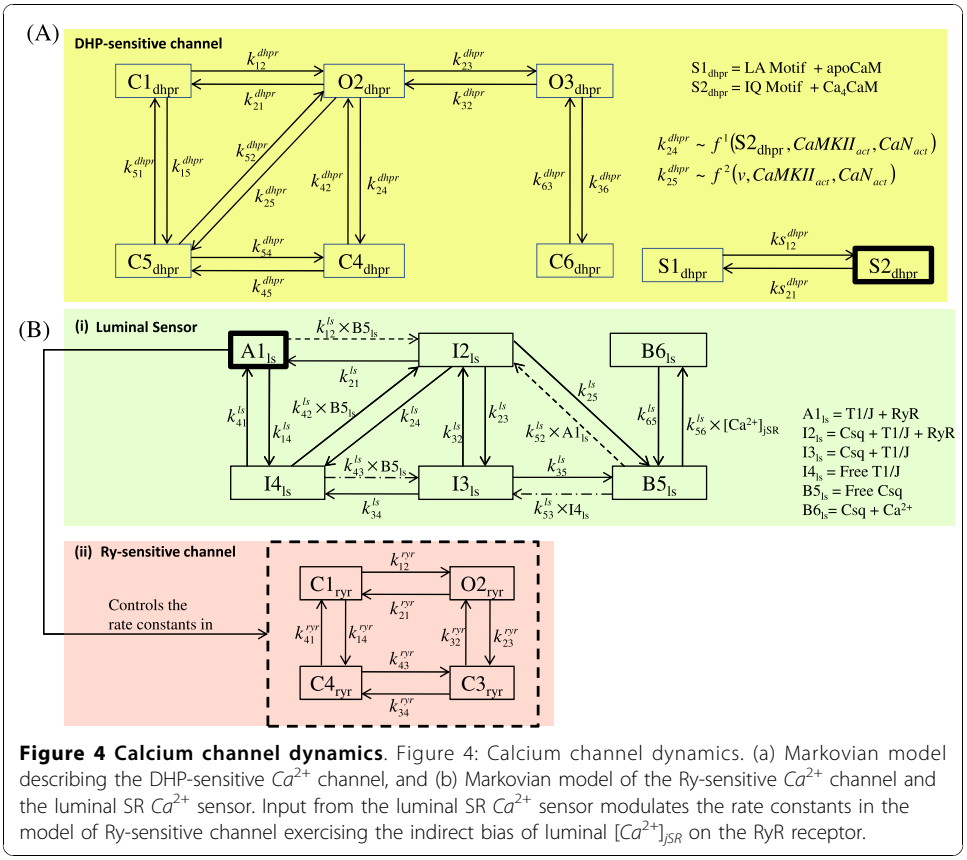

Figure 4 Calcium channel dynamics. Figure 4: Calcium channel dynamics. (a) Markovian model describing the DHP-sensitive Ca^{2+} channel, and (b) Markovian model of the Ry-sensitive Ca^{2+} channel and the luminal SR Ca^{2+} sensor. Input from the luminal SR Ca^{2+} sensor modulates the rate constants in the model of Ry-sensitive channel exercising the indirect bias of luminal $[Ca^{2+}]_{jSR}$ on the RyR receptor.

Table 3 Parameters used to model ion transport across the sarcolemmal membrane

Parameter	Definition	Value	References
F	Faraday's constant	96485 $coul \cdot mol^{-1}$	–
R	Ideal gas constant	8314 $mJ \cdot mol^{-1} \cdot K^{-1}$	–
T	Absolute temperature	290 K	Measured
$[Ca^{2+}]_o$	Extracellular Ca^{2+} concentration	1.0 mM	Measured
$[Na^{+}]_o$	Extracellular Na^{+} concentration	140.0 mM	Measured
$[Cs^{+}]_o$	Extracellular Cs^{+} concentration	3.0 mM	Measured
Z_{Na}, Z_{Cs}	Valence of Na^{+} and Cs^{+} ions	1.0	–
Z_{Ca}, Z_{Ba}	Valence of Ca^{2+} and Ba^{2+} ions	2.0	–
P_{Ca}	Permeability of L-Type calcium channel to Ca^{2+}	6.7367×10^{-9} $\mu L \cdot s^{-1}$	[30]*
P_{Na}	Permeability of L-Type calcium channel to Na^{+}	8.0355×10^{-11} $\mu L \cdot s^{-1}$	[30]*
P_{Cs}	Permeability of L-Type calcium channel to Cs^{+}	6.2088×10^{-11} $\mu L \cdot s^{-1}$	[30]*
K_{mAllo}	Dissociation constant for allosteric Ca^{2+} activation	125×10^{-6} mM	[85]*
K_{mCao}	Dissociation constant for extracellular Ca^{2+}	1.14 mM	[85]*
K_{mCai}	Dissociation constant for intracellular Ca^{2+}	0.0036 mM	[122]*
K_{mNao}	Dissociation constant for extracellular Na^{+}	87.5 mM	[83]*
K_{mNai}	Dissociation constant for intracellular Na^{+}	12.3 mM	[85]*
V_{max}	Maximum Na^{+}/Ca^{+} exchange current	776.2392 pA	[85]*
k_{mpca}	Half saturation constant for the SL Ca^{2+} pump	0.5 μM	[30]*
$\bar{I}_{PMCA}$	Maximum sarcolemmal Ca^{2+} pump current	1.15 pA	[30]*
K_{mcs}	Dissociation constant for extracellular Cs^{+}	1.5×10^{3} μM	[94,92,88,74]‡
K_{mna}	Dissociation constant for intracellular Na^{+}	2.14×10^{5} μM	[94,92,88,74]‡
$\bar{I}_{NaCs}$	Maximum Na^{+}/Cs^{+} pump current	147.3 pA	[94,92,88,74]‡
G_{Nab}	Maximum background Na^{+} current conductance	0.00141 nS	[30]*
R_a	Mean access resistance of the tubular system	20.0 $k\Omega$	[123]*

Table 3: Parameters used to model the transmembrane currents $I_{Ca,L}$, I_{NaCa}, I_{PMCA}, I_{NaCs} and the background sodium current $I_{Na,b}$. Adopted (*) or estimated (‡) from the cited sources.

equation Appendix A3 (Equations 147-150) in the DCU without explicitly accounting for local potential fields. The DHP-sensitive $i_{Ca,L,TT}$ channel brings in trigger Ca^{2+} (0.1 pA which is of the same order as measured by Wang et. al. [13]) causing a sparklet (a local increase in Ca^{2+} concentration at the mouth of the channel). This trigger Ca^{2+} causes a release from a cluster of opposing RyR channels, causing a spark. This combined release from a cluster of RyR channels causing a spark is represented as the release from a unitary RyR channel (i_{RyR}) in our model (shown in Figure 6). The characteristics of elemental Ca^{2+} release from a unitary RyR channel in our model agrees with data in terms of amplitude which is of the order of 3 pA (reported by Cheng et al. [27] and Blatter et al. [28]) and duration (full duration at half maximum (FDHM)) which is of the order of 50 ms (reported by Zima et al. [14]).

The single DCU in our model represents the lumped activity of a large number of individual dyads (e.g. 10,000), and it is charged with the task of forming the cytosolic Ca^{2+} transient (hence mechanical contraction) each beat of the cardiac muscle cell. In response to tonic application of voltage clamp pulses, the DCU strongly depends on an adequate supply of Ca^{2+} from the SR. The measurements of Diaz et al. [29] show that, although trigger current may be supplied regularly by tonic voltage clamp pulses, there is an inherent steady-state dependence of the magnitude of Ca^{2+} release on the particular value of SR Ca^{2+} content (i.e., there is a relationship between SR Ca^{2+} content

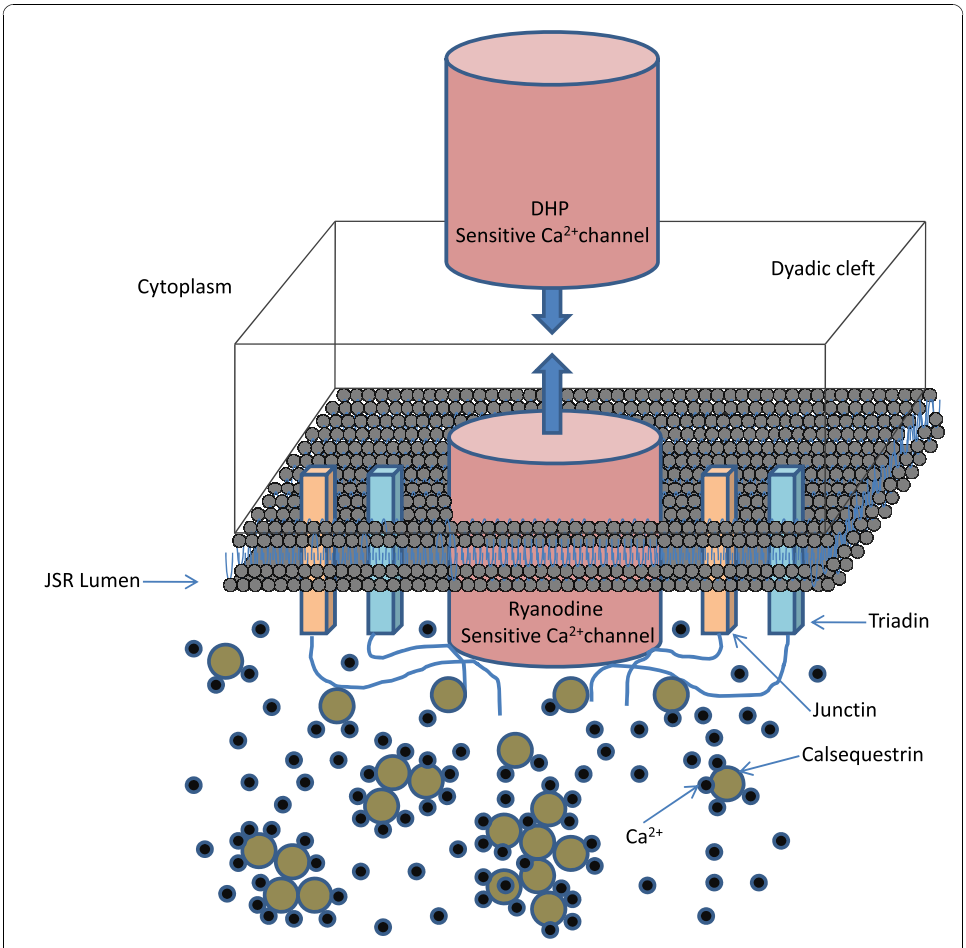

Figure 5 Schematic of the CICR subsystem. Figure 5: Schematic of the CICR subsystem. The dyadic coupling unit comprises of a DHP-sensitive Ca^{2+} channel opposing a Ry-sensitive Ca^{2+} channel. The transmembrane proteins triadin and junction along with calsequestrin mediate the interaction between the luminal Ca^{2+} and the RyR thus regulating the release of Ca^{2+} flux from the jSR into the dyadic space.

and peak $[Ca^{2+}]_{myo}$; Figure 4 Diaz et al. [29]). This plot gives us a glimpse of the input-output relationship of the dyadic coupling unit and indicates that SR Ca^{2+} content is an important controlling variable for the CICR process implemented by the DCU model.

L-Type Ca^{2+} Current

A multiple state characterization of $I_{Ca,L}$ in rat ventricular myocytes has been reported previously by our group [30]. The gating scheme used in this $I_{Ca,L}$ model has an additional high voltage state $C6_{dhpr}$ as shown in Figure 4A which is introduced to reproduce $I_{Ca,L}$ tail currents. Upon voltage-dependent activation, the channel achieves the primary open state $O2_{dhpr}$. The degree of opening is enhanced in the presence of activated calmodulin-dependent kinase ($CaMKII_{act}$) [31-33] which is known as Ca^{2+}-dependent facilitation (CDF). CaMKII has been shown to tether to the $I_{Ca,L}$ channel [34] functioning as a Ca^{2+} signalling sensor for facilitation. The open probability of the $I_{Ca,L}$ channel is also increased in the presence of activated calcineurin (CaN_{act}) [35]. These two effects are modeled as shown in Figure 4A, where k_{12}^{dhpr} is a function of

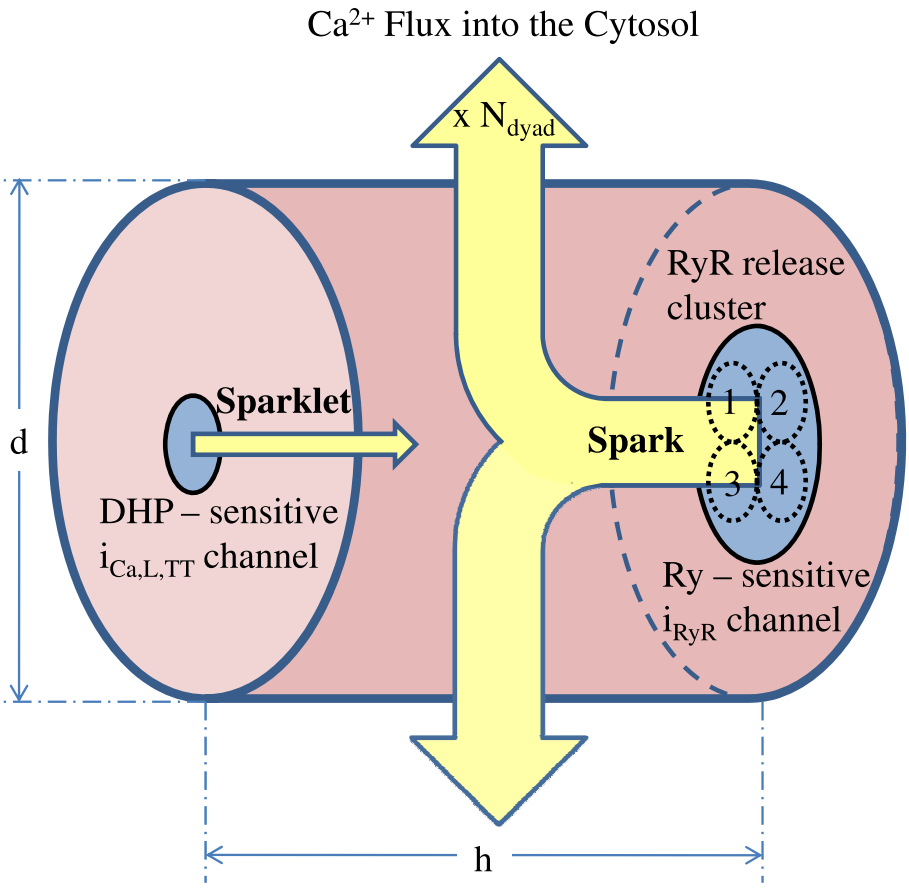

Figure 6 Schematic of the Dyadic nanodomain. Figure 6: Schematic of the LCC-RyR coupling. The dyadic cleft allows Ca^{2+} signaling between a DHP-sensitive Ca^{2+} channel opposing a cluster of Ry-sensitive Ca^{2+} channels (represented as the release channel i_{RyR} in our model). The trigger sparklet due to Ca^{2+} entering via DHP-sensitive $i_{Ca,L,TT}$ channel causes a spark as a result of release from a cluster of opposing RyR channels. The large amount of Ca^{2+} released subsequently diffuses into the cytosol.

both $CaMKII_{act}$ and CaN_{act} besides voltage. The gating scheme features two different pathways for inactivation of the open state. The pathway $O2_{dhpr} \leftrightarrow C5_{dhpr}$ accounts for voltage-dependent inactivation, whereas the pathway $O2_{dhpr} \leftrightarrow C4_{dhpr} \leftrightarrow C5_{dhpr}$ with Ca^{2+}-calmodulin (Ca_4CaM) dependent rate constant k_{24}^{dhpr} accounts for the fast and slow phases of Ca^{2+}-dependent inactivation (CDI) [36]. Transitions to the closed state via both the inactivation pathways are suppressed in the presence of $CaMKII_{act}$ and CaN_{act} to allow CDF. A 2-state Markovian model allows Ca^{2+} mediated interaction between calmodulin and the $I_{Ca,L}$ channel. As shown in Figure 4A, state $S2_{dhpr}$, which denotes Ca_4CaM bound to the IQ-motif of the $I_{Ca,L}$ channel, modulates calmodulin dependent Ca^{2+}-induced inactivation. This is in agreement with the findings of Nikolai M. Soldatov [37]. Our approach to modeling the effects of the proteins *CaM*, *CaMKII*, and *CaN* on the $I_{Ca,L}$ channel was based on the premise that they are co-localized with the channel itself [35]. Most of the beat-to-beat modulation is produced by *CaM* and *CaMKII*, whereas *CaN* is constitutively active in the dyad [38]. Tables 5, 6 and 7 provide values for the rate constants used to model Ca^{2+}/CaM binding, CaM buffering, Ca^{2+}/CaM/CaMKII as well as Ca^{2+}/CaM/CaN interactions.

Table 4 Parameters used to model intracellular ion transport

Parameter	Definition	Value	References
k_{12}^{PLB}	rate of PLB_{dp} phosphorylation	6800 s^{-1}	[77]*
k_{21}^{PLB}	rate of PLB_p dephosphorylation	1000 s^{-1}	[77]*
$K_{cyt,serca}$	Maximal binding/release rate of Ca^{2+} from cytosol to SERCA	6250 s^{-1}	[77]*
$K_{serca,sr}$	Maximal binding/release rate of Ca^{2+} from SERCA to LSR	6.25 s^{-1}	[77]*
$SERCA_{tot}$	Total amount of SERCA	47.0 μM	[77]*
PSR	Phospholamban to SERCA ratio	1.0	[77]*
PKA_{act}	Relative regulatory activity of PKA	0.1	[77]†
τ_{tr}	Time const. for transfer of Ca^{2+} from LSR to jSR	7.0×10^{-3} s	[30]‡
τ_{Na}	Time const. for transfer of Na^{+} from dyad to myoplasm	1.0×10^{-3} s	[30]‡
τ_{Cs}	Time const. for transfer of Cs^{+} from dyad to myoplasm	6.0×10^{-3} s	[30]‡
P_{ryr}	Permeability of the RyR channel	1.714×10^{-7} $\mu L \cdot s^{-1}$	[27,28,13]‡
D_{Ca}	Diffusion constant for Ca^{2+} in the dyadic space	100.0 $\mu m^2 s^{-1}$	[119]*
N_h	Density of high-affinity Ca^{2+} binding sites	200.0 μM	[119]‡
N_l	Density of low-affinity Ca^{2+} binding sites	16.0 μM	[119]‡
K_l	Half-saturation value of low-affinity Ca^{2+} binding site	1100.0 μM	[119]*
K_h	Half-saturation value of high-affinity Ca^{2+} binding site	13.0 μM	[119]*
$[Mg^{2+}]_{myo}$	Intracellular Mg^{2+} concentration	634 μM	[124]*
$[fluo3]_{tot}$	total concentration of indicator dye	100.0 μM	Measured
k_{fluo3}^{+}	association rate of Ca^{2+} binding to dye fluo-3	80 $\mu M^{-1} \cdot s^{-1}$	[125]*
k_{fluo3}^{-}	dissociation rate of Ca^{2+} binding to dye fluo-3	90 s^{-1}	[125]*

Table 4 Parameters used to model the intracellular ion transport $I_{cyt,serca}$, $I_{serca,sr}$, I_{tr}, I_{RyR}, and Ca^{2+} diffusion/buffering. Adopted (*), derived (†) or estimated (‡) from the cited sources.

Our previous study [30] was focused on the characterization of the $I_{Ca,L}$ channel under conditions of low $[Ca^{2+}]$ in the dyadic space and myoplasm. In fact, Ca^{2+}- release from the jSR was blocked by administering a relatively high dose of ryanodine (20 μM) in all experiments. Therefore, to study the additional influence of SR Ca^{2+} release on $I_{Ca,L}$, we modified the original $I_{Ca,L}$ model to better characterize the process of Ca^{2+}-dependent inactivation. In the modified $I_{Ca,L}$ model, majority of the structure for the 6-state dynamic scheme remains the same, however changes have been made to the voltage-dependent inactivation rate function (k_{25}^{dhpr}), and the Ca_4CaM dependent inactivation rate function (k_{24}^{dhpr}). The specific formulas for the Markovian state equations and the modified k_{25}^{dhpr} and k_{24}^{dhpr} functions used in this study are given in Appendix A1 (Equations 4-50). Our adjustments consist of reducing the contribution from voltage-dependent inactivation process and strengthening the Ca_4CaM-dependent inactivation process. The rate constants k_{36}^{dhpr} and k_{63}^{dhpr} are constructed in order to provide a re-excitation window during the return of the clamp voltage to the resting potential. With these adjustments, the Markovian state description for $I_{Ca,L}$ can provide good fits to measured $I_{Ca,L}$ data under both test conditions (presence and absence of ryanodine -sensitive Ca^{2+} release) as well as produce tail currents during repolarization from large clamp voltages (≥ 40 mv).

Calcium Buffering in the Dyadic Space

Previous modeling work by Post et al. [39], and Post and Langer [40] considered the effect of Ca^{2+} binding sites on the inner sarcolemmal leaflet. Following these authors, we included low-affinity (k_d = 1.1 mM) and high-affinity (k_d = 1.3 μM) Ca^{2+} binding sites on SL wall boundary of cylindrical dyadic space. The presence of these membrane

bound sarcolemmal Ca^{2+} binding sites in our model has significant physiological implications, in that it prevents local dyadic Ca^{2+} concentration near the "mouth" of DHP-sensitive $I_{Ca,L}$ channel from becoming excessively high. Allowing such a condition to occur can cause a reversal of the $I_{Ca,L}$ current, which does not occur physically during normal jSR release. Addition of these SL Ca^{2+} binding sites does not significantly slow the build-up of Ca^{2+} within the dyadic space, nor is the Ca^{2+}-induced Ca^{2+} release mechanism affected [41].

Ca^{2+} Release Channel

The gating characteristics of the Ry-sensitive release channel are not only modulated by the dyadic Ca^{2+} concentration at its mouth but also the jSR Ca^{2+} concentration via the luminal sensor. Several RyR gating schemes have been deduced from isolated RyR currents measured in lipid bilayers, including: (1) the 4-state scheme developed by Keizer and Levine [42] with 4 Ca^{2+} binding for activation and 3 Ca^{2+} binding for inactivation to explain the "adaptation" of the RyR observed by Gyorke and Fill [43]; (2) the 6-state scheme suggested by Zahradnikova and Zahradnik [44], which allowed opening the RyR channel upon binding of a single calcium ion; and (3) the Markov model proposed by Keizer and Smith [45], which can be dynamically switched among the six, five and four-state representations during the simulation as Ca^{2+} levels vary. Stern et al. [6] demonstrated that none of these schemes yielded stable local control of SR release, even with extensive adjustment of parameters. Stern et al. [6] further reported that all schemes resulted in models that manifested local instability, as indicated by failure of release to terminate after activation, or global instability caused by spontaneous activation by resting $[Ca^{2+}]_{myo}$. Since many of the kinetic gating schemes derived from lipid bi-layer data fail to support stable E-C coupling in simulations, he concluded that the RyR gating process in situ may differ considerably from that in bi-layers.

Our gating scheme is patterned after the release channel used in the model of Stern, Pizarro and Rios [46] (Figure 4B), where the channel is assumed to have four states: rest (closed), activated (open), inactivated (closed) and refractory (closed). The activation gate is opened by the simultaneous, cooperative binding of two Ca^{2+} ions, whereas inactivation depends on the binding of a single Ca^{2+} ion. Four additional features have been built into our model: (a) the crucial role of the luminal SR Ca^{2+} sensor (Figure 5) in assisting the inactivation of the RyR channel is modeled via the dependence of all

Table 5 Rate constants used to model Ca/CaM binding and CaM buffering

Rate Constant	Value	Rate Constant	Value
k_{02}^{CM}	4.8387‡	k_{42B}^{CM}	k_{42}^{CM}
k_{20}^{CM}	10.0*	k_{0Bon}^{CM}	3.5×10^{-4}‡
k_{24}^{CM}	3.4722‡	k_{0Boff}^{CM}	1.4×10^{-6}‡
k_{42}^{CM}	500.0*	k_{2Bon}^{CM}	k_{0Bon}^{CM}
k_{02B}^{CM}	k_{02}^{CM}	k_{2Boff}^{CM}	k_{0Boff}^{CM}
k_{20B}^{CM}	k_{20}^{CM}/100	k_{4Bon}^{CM}	k_{0Bon}^{CM}
k_{24B}^{CM}	k_{24}^{CM}	k_{4Boff}^{CM}	k_{0Boff}^{CM}

Table 5: Rate constants used to model Ca/CaM binding and CaM buffering. Adopted (*) or estimated (‡) from Saucerman et. al. [38].

Table 6 Rate constants used to model Ca/CaM/CaMKII interactions

Rate Constant	Value	Rate Constant	Value
k_{PP1}	1.72	k_{32}^{CK}	2.2
k_{mPP1}	11.5	k_{45}^{CK}	3.35×10^{-3}
k_{21}^{CK}	65.67164	k_{54}^{CK}	3.4722
k_{12}^{CK}	328.3582	k_{46}^{CK}	2.2×10^{-3}
k_{13}^{CK}	3.4722	k_{64}^{CK}	65.67164
k_{31}^{CK}	3.35	k_{56}^{CK}	328.3582
k_{23}^{CK}	65.67164	k_{65}^{CK}	65.67164

Table 6: Rate constants used to model Ca/CaM/CaMKII interactions. All the above parameters are adopted from Saucerman et. al. [38].

the rate constants in the 4-state RyR model, on the degree of interaction between the RyR and the proteins triadin and junctin (Figure 4B); (b) $CaMKII_{act}$ dependent enhancement in RyR release [47-50] is modeled via the rate functions k_{12}^{ryr}, k_{41}^{ryr}, k_{43}^{ryr} and k_{32}^{ryr}; (c) a stronger Ca^{2+} dependent inactivation of the RyR channel (at a fixed depolarization level), is adopted to reflect recent observations that the inactivation of the RyR depends on the high local Ca^{2+} concentration consequential to their own Ca^{2+} release [51]; and (d) inactivation of the RyR at different depolarization levels is made dependent on local Ca^{2+} concentration (i.e., $[Ca^{2+}]_{ryr}$ at the "mouth" of the RyR channel on the dyadic side) as per Wier et al. [52] and Zucchi et al. [53]. Our initial studies indicated that the repriming rate (k_{32}^{ryr}) in the RyR gating scheme of Stern et al. [46] was quite large, which can lead to a saturated open probability of the Ca^{2+} release channel. This occurs during the later phase of channel inactivation, where the large value of k_{32}^{ryr} tends to reactivate the channel, resulting in saturated Ca^{2+} release. Therefore, we utilized a value of k_{32}^{ryr} that is 10% of that used by Stern et al. [46], and further assumed that the unitary permeation flux of the jSR release channel is proportional to jSR luminal Ca^{2+} concentration ($[Ca^{2+}]_{jSR}$). The specific equations for the Ca^{2+} release model are given in Appendix A1 (Equations 73-92).

Luminal RyR sensor

The RyR Ca^{2+} release is modulated by a multi-molecular Ca^{2+} signalling complex which is localized to the junctional SR [54-56]. This complex consists of the ryanodine

Table 7 Rate constants used to model Ca/CaM/CaN interactions

Rate Constant	Value	Rate Constant	Value
k_{Caon}^{CN}	2.0	k_{0on}^{CN}	46.0
k_{Caoff}^{CN}	1.0	k_{0off}^{CN}	537.966
k_{02}^{CN}	4.8387	k_{2on}^{CN}	46.0
k_{20}^{CN}	0.0606	k_{2off}^{CN}	3.2604
k_{24}^{CN}	3.4722	k_{4on}^{CN}	46.0
k_{42}^{CN}	0.199362	k_{4off}^{CN}	1.3×10^{-3}

Table 7: Rate constants used to model Ca/CaM/CaN interactions. All the above parameters are adopted from Saucerman et. al. [38].

receptor (RyR) which functions as a Ca^{2+} conducting pore [57,58], calsequestrin (CS) which acts as the Ca^{2+} binding protein [59,60], and the junctional SR transmembrane proteins triadin [61] and junctin [62]. It was known previously that the proteins triadin and junctin anchor calsequestrin to the ryanodine sensitive receptor [61]. More recently, it has been observed that the protein-protein interactions between triadin, calsequestrin and RyR modulate sarcoplasmic reticulum calcium-release in cardiac myocytes [25]. Triadin and junctin are structurally homologous proteins [63], but the functional differences in their roles are unclear at present. Therefore we have refrained from modeling these proteins separately with unique roles, and will hereafter only mention triadin. The RyR model proposed by Shannon et al. [64] takes a heuristic approach towards free SR Ca^{2+} concentration dependent luminal control of the RyR channel. Our detailed biophysical model of the luminal sensor is strongly based on the recent findings of Terentyev et al. [25] which uncovers complex $[Ca^{2+}]_{jSR}$) dependent, CS mediated mechanistic interaction of the protein triadin with the RyR channel.

The triadin protein facilitates SR Ca^{2+} release by sensitizing the RyR to activation by the trigger current $I_{Ca,L,TT}$. This is incorporated in our model by allowing the rate constants in the 4-state Markovian model for the RyR (Figure 4B-ii) channel to be functions of the activated state $A1_{ls}$, which represents the degree of binding between triadin and RyR, in the 6-state model for the luminal sensor (Figure 4B-i).The degree of triadin assisted anchoring of CS to the RyR channel [61,62] is denoted by the state $I2_{ls}$. Triadin is also known to exist in a form bound to CS alone [25] denoted by the state $I3_{ls}$ and in its free unbound form represented as $I4_{ls}$ in the model. CS which is known to exist in a Ca^{2+} bound form modeled by $B6_{ls}$ also modulates SR Ca^{2+} release by influencing the open probability of the RyR channel [65-67], via interactions with Triadin [54,66,25]. The degree of unbound CS is denoted by $B5_{ls}$ in the model.

During the diastolic period the relatively large concentration of available free Ca^{2+} in the SR results in most of the CS being bound to Ca^{2+}, decreasing the degree of interaction between CS and triadin. This enables a strong interaction between the available unbound triadin and the RyR channel increasing its propensity for trigger Ca^{2+} induced SR release. Our model incorporates this property by facilitating movement of states towards $A1_{ls}$ and $B6_{ls}$ in the presence of large SR Ca^{2+} concentration. Following SR Ca^{2+} release, a reduced luminal Ca^{2+} concentration in the jSR causes an increase in the amount of free calsequestrin ($B5_{ls}$ in the model) available to bind with triadin. This results in a decrease in the extent of interaction between triadin and RyR ($A1_{ls}$ in the model), thus inhibiting the RyR channel and leading to robust termination of SR Ca^{2+} release in cardiac myocytes [66]. This release termination mechanism is incorporated in our combined RyR-Luminal sensor model (Figure 4B and Appendix A1, Equations 73-92).

Due to the lack of in-vivo measurements on individual state transitions, the rate constants in our novel luminal sensor model (Table 8) are chosen such that (i) the triadin mediated sensitization of the RyR channel (via $A1_{ls}$) provides adequate peak RyR release which translates into the upstroke velocity of the cytosolic Ca^{2+} transient; (ii) the luminal sensor mediated RyR channel inactivation (via $A1_{ls}$) causes timely release termination resulting in a cytosolic Ca^{2+} transient duration, physiological for a rat ventricular myocyte; (iii) the rate of post-release RyR recovery results in appropriate channel refractory characteristics. In the case of channels where there is an interaction

between ion flow (which is not at equilibrium) and its gating mechanism the microscopic reversibility criteria does not hold true [68,69]. The RyR channel which is solely modulated by $[Ca^{2+}]$ (both on the dyadic side ($[Ca^{2+}]_{ryr}$) as well as the luminal side ($[Ca^{2+}]_{jSR}$)) experiences a strong interaction of Ca^{2+} flow through itself and its gating mechanism described as $[Ca^{2+}]_{ryr}$ induced self-inhibition and the luminal sensor induced inactivation. Hence, the rate constants of the luminal sensor model (Figure 4B-i) are not constrained by microscopic reversibility criteria. However, a stability constraint in the form of, the sum of probabilities of all possible states corresponding to triadin ($A1_{ls}$, $I2_{ls}$, $I3_{ls}$, $I4_{ls}$) and CS ($I2_{ls}$, $I3_{ls}$, $B5_{ls}$, $B6_{ls}$) being equal to one is explicitly imposed Appendix A1, Equations 87-88) on the model of the luminal sensor in order to avoid run-off.

Ca^{2+} Buffering in Myoplasm and SR

Ca^{2+} buffers play an important role in sequestering a fraction of the total Ca^{2+} released during E-C coupling and contraction. These buffers include: (a) calmodulin (CaM), which is assumed to be uniformly distributed in the myoplasm and dyadic space; (b) troponin in the bulk myoplasm; and (c) calsequestrin (CS) in the jSR. The dyadic space has been shown to be accessible to calmodulin (CaM), but mostly inaccessible to fluorescent dyes [70,71]. Therefore, we consider the dyadic space filled with calmodulin, but not fluo-3. This provides a more direct calcium communication pathway between the DHP and Ry receptors. The rate constants for Ca^{2+} binding to calmodulin were based on a model from [22], whereas those for Ca^{2+} binding to troponin were taken from Potter and Zott [72]. Rate constants used to describe Ca^{2+} binding to calsequestrin were based on the study of Cannell and Allen [73], whereas those for Ca^{2+} binding to troponin-Mg complex were adopted from Lindblad et al. [74].

It is well recognized that fluorescent indicator dyes introduced into the cytosol also act as Ca^{2+} buffers [22], even at submillimolar concentrations [51]. In our simulations, we have used 100μM fluo-3. We assume that the quantity observed experimentally as a "calcium concentration" signal is actually the calcium complexed with fluo-3, or [CaF3]. The differential equation describing the change in [CaF3] with time is given in Appendix A2 (Eq. 138) which follows from Shannon et al. [75].

Ca^{2+}-Uptake

Cytosolic Ca^{2+} is pumped into the LSR (Figure 1A) by a Ca^{2+}-ATPase, which lowers $[Ca^{2+}]_{myo}$ and helps to induce relaxation in cardiac muscle. The transport reaction involves two Ca^{2+} ions and one ATP molecule [76], and it is represented by the description given for $I_{cyt,serca}$ and $I_{serca,sr}$ in Appendix A1 (Equations 51-63). The model used for the uptake pump is adopted from Koivumaki et al. [77] and takes into account both the forward flux of Ca^{2+} from the cytosol to the LSR lumen and the backward flux from the LSR to the cytosol along with the Ca^{2+} buffering action of the SERCA protein. The phospholamban (PLB) to SERCA ratio has been fixed to 1.0, assuming almost equal availability of both the proteins. $CaMKII_{act}$ affects the SERCA pump via direct phosphorylation assisting in enhancement of SR Ca^{2+} transport by increasing the pumping rate [78] and indirectly via phosphorylation of PLB [79] relieving the inhibition caused by PLB on the SERCA pump in turn increasing the sensitivity of the pump for Ca^{2+} uptake. These two effects are modeled by allowing the rate

Table 8 Parameters used in the luminal sensor model

Rate Constant	Value	Rate Constant	Value
k_{12}^{ls}	88.16	k_{23}^{ls}	57.9
k_{21}^{ls}	4.1	k_{32}^{ls}	2.42
k_{14}^{ls}	0.5	k_{35}^{ls}	150.3
k_{41}^{ls}	85.7	k_{53}^{ls}	25.5
k_{42}^{ls}	2.98	k_{52}^{ls}	88.16
k_{43}^{ls}	25.5	k_{56}^{ls}	1.2
k_{34}^{ls}	150.3	k_{65}^{ls}	401.7

Table 8: Static rate constants used in the model for the luminal sensor.

constants for Ca^{2+}+ binding to/release from the SERCA pump as well as the rate constant for phosphorylation of PLB to be a function of $CaMKII_{act}$ in the cytosol. The activating role of CaN in modulating the SERCA pump [80,81] is accounted for in our model by allowing the rate constant for phosphorylation of PLB to be dependent on available CaN_{act} in the cytosol. The relative regulatory role of the enzyme protein kinase A(PKA) is fixed at 0.1, as its modulatory effect is beyond the scope of this study. The current $I_{cyt,serca}$ dictates the transport of Ca^{2+} between the cytosol and the SERCA protein. Similarly, the current $I_{serca,sr}$ dictates the transport of Ca^{2+} between the SERCA protein and the LSR. The difference in these Ca^{2+} currents accounts for the Ca^{2+} buffered by the SERCA protein. The jSR is subsequently refilled by Ca^{2+} diffusion from the LSR. The differential equations describing the Ca^{2+} balance and particularly the transfer between two separate SR compartments (jSR and LSR) are provided in Appendix A1 (Eq. 72).

Ca^{2+}-Extrusion via Sarcolemmal Ca^{2+} Pump

Although the sarcolemmal Ca^{2+}-pump has a high affinity for $[Ca^{2+}]_{myo}$, its transport rate is far too slow for it to be an important factor in Ca^{2+} fluxes during the cardiac cycle. It might, however be more important in long-term extrusion of Ca^{2+} by the cell. Our model of the plasma membrane Ca^{2+} ATPase pump current is adopted from Sun et al. [30]. We have used a constant value of half activation constant k_{mpca} = 0.5μM in our model on the basis of measurements by Caroni et al [82].

Ca^{2+}-Extrusion via Na^{+}/Ca^{2+} Exchanger

In mammalian cardiac cells, it is generally accepted that the Na^{+}/Ca^{2+} exchanger has a stoichiometry of $3Na^{+}$:$1Ca^{2+}$ [83]. I_{NaCa} (again, the combination of $I_{NaCa,TT}$ and $I_{NaCa,SL}$) is important in removing Ca^{2+} during twitch relaxation, in competition with I_{up}. A simple thermodynamic Na^{+}/Ca^{2+} exchanger current model [84] may be sufficient to predict the direction of Ca^{2+} transport by Na^{+}/Ca^{2+} exchange and the driving force, however the amplitude is subject to kinetic limitations (depending on substrate concentrations). A more comprehensive Na^{+}/Ca^{2+} exchanger current equation [85] is adopted in our model, which includes factors for allosteric Ca^{2+} activation and the transport for Na^{+} and Ca^{2+} inside and out. The maximal flux through the exchanger V_{max} is estimated to ensure that the Ca^{2+} ion transport (which is voltage dependent) via the Na^{+}/Ca^{2+} exchanger matches the influx of Ca^{2+} via the $I_{Ca,L}$ channel [86,87], maintaining whole cell Ca^{2+} homeostasis.

Na^+/Cs^+ Pump

The Na^+/K^+ pump, helps in maintaining homeostasis of the intracellular Na^+ ion concentration. ATPase activity powers the pump, as it generates an outward Na^+ flux and an inward K^+ flux with a Na^+ to K^+ stoichiometry of 3 to 2 [88]. However, in our experimental protocol, external solution in the bath was normal Tyrode (1 mM Ca^{2+}) with Cs^+ substituted for K^+ in order to block the inward rectifier K^+ current. The internal solution in the pipette contained Cesium aspartate supplemented with 20 mM $CsCl$, 3 mM Na_2ATP , 3.5 mM $MgCl_2$ and 5 mM HEPES.

Activation of the electrogenic sodium pump in mammalian non-myelinated nerve fibres [89], skeletal muscle [90] and rat brain cells [91] by Cs^+ is reported in the literature. It is observed that the late effects of reducing extracellular K^+ concentration ($[K^+]_o$) to 0 mM in mammalian cardiac muscle can be prevented by including appropriate concentrations of other activator cations of the Na^+/K^+ pump such as Cs^+ in the 0 mM $[K^+]_o$ bathing solution [92]. Monovalent cations (including Cs^+) were also added to K^+ free bathing solution to reactivate the sodium pump in guinea-pig ventricular myocytes [93]. The effectiveness of Cs^+ as an external cation in activating the electrogenic sodium pump is known to be lesser than potassium [92].

We have represented I_{NaCs} in our model by the expression for Na^+/K^+ pump formulated by Linblad et al. [74] replacing K^+ ion concentrations with the Cs^+ ion concentration. While ensuring whole cell Na^+ ion balance, the peak Na^+/Cs^+ pump current is modified to be one-sixth to account for the decreased potency of the cation Cs^+ in activating the pump. The voltage-dependence of I_{NaCs} is adopted from the data on Na^+/K^+ pump from Hansen et al. [94].

Results

The DCU is a fundamental element in the mechanism of CICR. The sequence of events resulting in CICR is triggered by the Ca^{2+} entering through the $I_{Ca,L}$ channel. The characteristics of this channel are hence examined in detail to understand its voltage and Ca^{2+} dependent behavior. The ability of the $I_{Ca,L}$ channel to facilitate graded RyR release is noted. The high gain associated with RyR release is quantified. This is followed by a study of the properties of the RyR channel with a particular emphasis on its inactivation mechanism. The Ca^{2+} mediated interaction between these channels is investigated in detail. This is followed by an effort to understand the role of $[Ca^{2+}]_{jSR}$ in CICR. In particular, the relationship of the peak cytosolic calcium transient and the SR Ca^{2+} content is examined. The effect of modulatory agents like caffeine and thapsigargin on SR release/uptake is studied to understand the significance of these mechanisms in facilitating a normal CICR.

L-type Ca^{2+} current ($I_{Ca,L}$)

The L-type DHP-sensitive Ca^{2+} channel has a key role in initiating CICR. Hence a thorough analysis of its activation and inactivation mechanisms is considered here. Though the activation of the $I_{Ca,L}$ channel is solely voltage dependent once activated, the inactivation of the channel is influenced not only by the trans-membrane voltage but also the Ca^{2+} concentration in the vicinity of the channel [95]. The relative contribution of the voltage-dependent and Ca^{2+}-dependent inactivation pathways in the $I_{Ca,L}$ channel model can be studied by selectively blocking each pathway in the model.

Figure 7 shows the model-generated waveform for $I_{Ca,L}$ under three conditions; (i) control case with both voltage and calcium dependent in-activation pathways intact; (ii) ryanodine applied to allow only the voltage-dependent inactivation and the Ca^{2+}-dependent inactivation via $I_{Ca,L}$ self-inhibition in the absence of RyR release; and (iii) Ca^{2+} substituted with Ba^{2+} to facilitate only the voltage-dependent inactivation pathway and block all Ca^{2+} dependent inactivation pathways ($k24_{dhpr}$ set to zero). The protocol used in case (i) was a 50 ms pulse with clamp voltages ranging from 10 mv to 40 mv in steps of 10 mv from a holding potential of -40 mV. In case (ii) and (iii) the pulse duration was increased to 200 ms to replicate the data.

Measured data obtained using the same voltage clamp pulse under all three conditions (Control, Ryan-odine application and Barium substitution) is shown for comparison (data obtained from Dr. Palade's lab was pre-processed to eliminate transients produced by changing clamp voltage in order to obtain model fits using a non-linear least-squares method [18]). The degree of $I_{Ca,L}$ channel opening is known to be enhanced in the presence of $CaMKII_{act}$ [33] which is known as Ca^{2+}-dependent facilitation (CDF). According to Bers et al. [33] the positive regulation of the channel by $CaMKII_{act}$ requires Ca^{2+} influx (it is not seen when Ba^{2+} is the charge carrier as in Figure 7D and is more strongly apparent when local Ca^{2+} influx is amplified by SR Ca^{2+} release as in Figure 7A). Increase in $CaMKII_{act}$ seems to play an important function in enhancing $I_{Ca,L}$ peak amplitude [96], suggesting a critical role for Ca^{2+}-dependent facilitation. Our model generated results also indicate that a stronger CDF (in Figure 7A) in the presence of RyR Ca^{2+} release causes an enhancement in $I_{Ca,L}$ peak amplitude (compare the model fits to data in Figure 7A (presence of RyR release) with Figure 7B (no RyR release) and Figure 7C (Ca^{2+} substituted by Ba^{2+})). It is important to note that the peak of the $I_{Ca,L}$ current is reached after the RyR open probability reaches its maximum value owing to the faster dynamics of the RyR channel. Our simulations indicate that following the inward current peak, Ca^{2+}-dependent inactivation (CDI) is much faster and dominates the response for the duration of voltage clamp (30 ms <t <80 ms). In addition, a comparison of Figs. 7A and 7B shows that, Ca^{2+}-dependent inactivation (CDI) caused by Ca^{2+} release from Ry-sensitive channels is much more significant than the self-inhibition produced by Ca^{2+} influx via $I_{Ca,L}$ itself. The graded behavior of the cytosolic Ca^{2+} transient is shown in Figure 7C. Voltage dependent inactivation (VDI) is relatively slow compared with CDI and is best seen in Figure 7D where all Ca^{2+} inactivation effects have been blocked by Ba^{2+} substitution for Ca^{2+}. Under RyR blockade (Figure 7B), the relatively slow VDI has its major effect during the late phase of the long voltage clamp pulse (e.g., beyond 100 ms) and in a time range where CDI is relatively constant. Quantitative analysis of movement of states (during the depolarizing pulse duration of 50ms) via different pathways in the six state Markovian model shows that 68.24% of the total inactivation of $I_{Ca,L,TT}$ is via the calcium dependent $O2_{dhpr}$-$C4_{dhpr}$ pathway, owing to the large Ca^{2+} concentration which the channel is exposed to in the dyad. In contrast, only 19.21% of the total inactivation of $I_{Ca,L,SL}$ is via the calcium dependent $O2_{dhpr}$-$C4_{dhpr}$ pathway, because of the low cytoplasmic Ca^{2+} concentration in the vicinity of the channel. Considering the total $I_{Ca,L}$ current ($I_{Ca,L,TT}$ + $I_{Ca,L,SL}$), around 63.34% of the $I_{Ca,L}$ channel inactivation is via the Ca^{2+} dependent pathway.

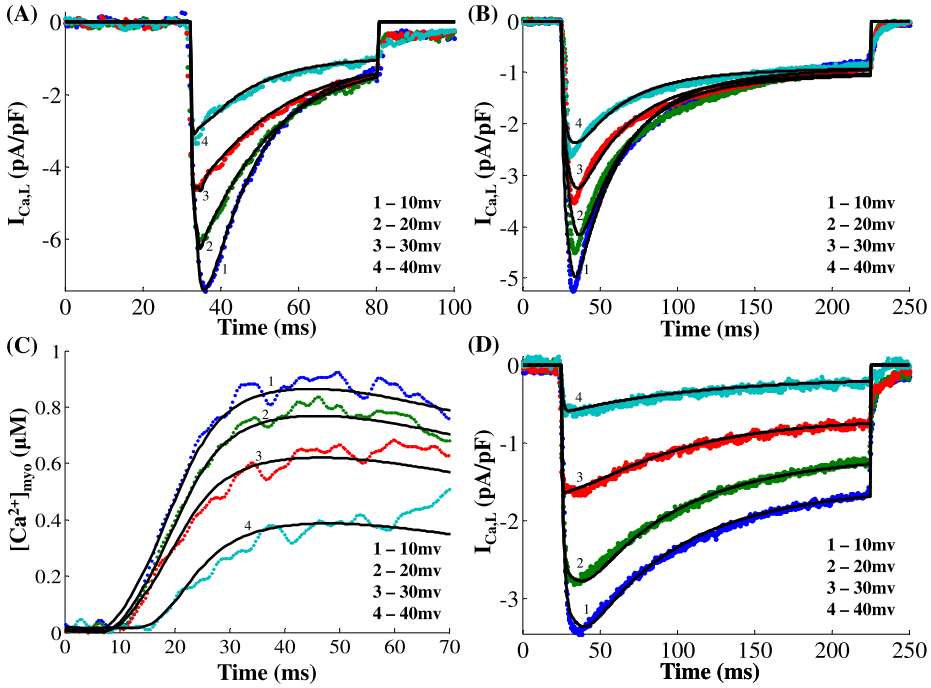

Figure 7 $I_{Ca,L}$ & $[Ca^{2+}]_{myo}$ - comparison of model generated and experimental data in the positive voltage range. Figure 7: Model generated and experimentally obtained data from a rat ventricular myocyte clamped to voltages between 10 and 40 mv in steps of 10 mv. The holding potential used is -40 mv. Data is obtained from Dr. Philip. T. Palade's lab. (A) $I_{Ca,L}$ in the presence of Ca^{2+} release from the Ry-sensitive channel. The pulse duration used is 50 ms. (B) $I_{Ca,L}$ with Ryanodine administered to block RyR release. The pulse duration used is 200 ms. (C) Global cytosolic calcium transients $[Ca^{2+}]_{myo}$ in the presence of RyR release. The pulse duration used is 50 ms (D) $I_{Ca,L}$ using Barium as the charge carrier in the absence of RyR. The pulse duration used is 200 ms. Solid traces are the model-generated results and dotted lines represent the data.

Figure 8A shows a comparison of model generated and experimentally obtained $I_{Ca,L}$ data (obtained from Dr. Palade's lab and pre-processed to eliminate transients produced by changing clamp voltage in order to obtain model fits using a non-linear least-squares method [18]) from a rat ventricular myocyte (different from the cell used to obtain data in Figure 7) at negative (-30 mv ≤ v ≤ 0 mv) clamp voltages. The corresponding graded behavior of the cytosolic Ca^{2+} transient is shown in Figure 8C. Figure 8B shows the well known [52] bell-shaped dependence of the peak $[Ca^{2+}]_{myo}$ on the clamp voltage.

Figure 9 shows model generated normalized $I_{Ca,L}$ obtained by a voltage clamp to 10 mv from a holding potential of -40 mv using the following protocols. Case 1: Normal release is allowed where, following CICR, a strong Ca^{2+} dependent inactivation inhibits the $I_{Ca,L}$ current as seen in the plot numbered 1 (data obtained from Dr. Palade's lab). Case 2: Ryanodine applied to block RyR release; Ca^{2+} entering via the $I_{Ca,L}$ channel causes Ca^{2+} induced inactivation, although the magnitude of inhibition is far less than in the control case. Case 3: Ba^{2+} substitution for Ca^{2+} to completely suppress the Ca^{2+} inactivation mechanism; the only inactivation pathway present is the slow voltage dependent pathway [97], which causes substantially reduced recovery compared to cases 1 and 2. Besides the inactivation, it can be seen from Figure 9 that the rate of channel activation, which is evident in the slope of the individual plots during the

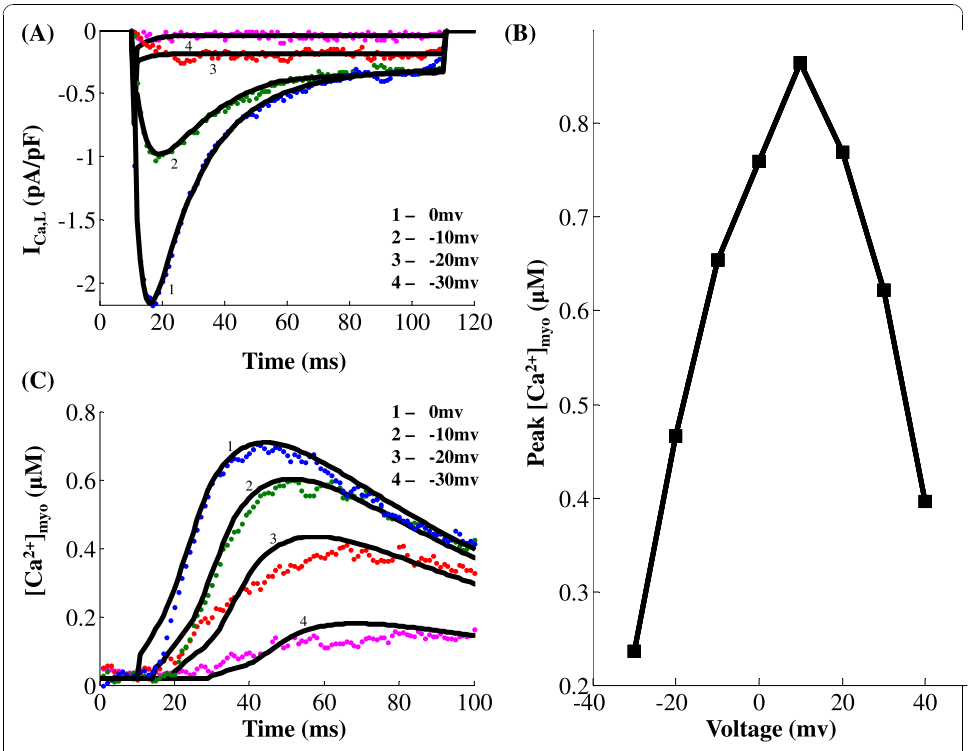

Figure 8 $I_{Ca,L}$ & $[Ca^{2+}]_{myo}$ - comparison of model generated and experimental data in the negative voltage range. Figure 8: Model generated and experimentally obtained data from a rat ventricular myocyte clamped to voltages between -30 and 0 mv in steps of 10 mv. The holding potential used is -40 mv. Data is obtained from Dr. Philip. T. Palade's lab. (A) $I_{Ca,L}$ invoked by negative clamp voltages in the range of -30 mv to 0 mv in steps of 10 mv. The pulse duration used is 100 ms. (B) Peak $I_{Ca,L}$ dependance on clamp voltage. (C) Global cytosolic calcium transients $[Ca^{2+}]_{myo}$ at negative (-30 mv ≤ v ≤ 0 mv) clamp voltages. The pulse duration used is 100 ms (D) Peak cytosolic calcium transients ($[Ca^{2+}]_{myo}$) dependence on clamp voltages. Solid traces are the model-generated results and dotted lines represent the data.

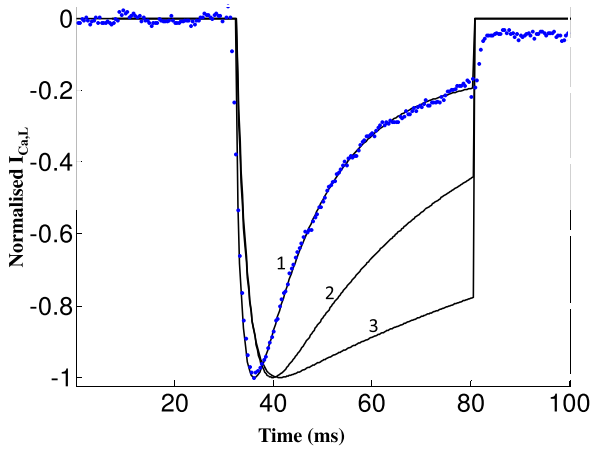

Figure 9 $I_{Ca,L}$ inactivation pathways. Figure 9: $I_{Ca,L}$ inactivation pathways. Voltage clamp protocol used is a 50 ms step pulse to 10 mv from a holding potential of -40 mv. Both model generated results and the data are normalized for easy comparison (1) Control case where both voltage and calcium dependent inactivation pathways are intact. Solid trace is the model-generated result and the dotted line represents the data obtained from Dr. Philip. T. Palade's lab; (2) voltage-dependent inactivation exists however Ca^{2+}-dependent inactivation is only via $I_{Ca,L}$ self-inhibition without RyR release; (3) Only voltage-dependent inactivation pathway preserved by blocking all Ca^{2+} dependent pathways.

initial activation phase, is faster in the presence of RyR Ca^{2+} release (a result of enhanced CDF in the presence of elevated Ca^{2+} levels). This highlights the important role of Ca^{2+} in regulating $I_{Ca,L}$ channel opening and thus controlling the amount of extracellular Ca^{2+} entering the cell.

$I_{Ca,L,TT}$ - dependent Graded SR-release

One of the most important characteristics of the CICR mechanism is the modulation of the RyR Ca^{2+} release based on the amount of trigger calcium delivered via the DHPR channel. The voltage-controlled $I_{Ca,L}$ channel is the link between the extracellular excitation and the intracellular Ca^{2+} release. As shown in Figure 10A, our model reproduces graded release. It is important to note that the onset of the Ca^{2+} transient is also modulated based on the magnitude of the trigger calcium available to initiate release, as shown in Figure 10A-iii. This is due to the fact that the rate of increase in the open probability of the Ry-sensitive Ca^{2+} release channel is controlled by the amount of trigger Ca^{2+} present at the 'mouth' of this channel, which in-turn is graded by the amount of trigger Ca^{2+} entering the DCU by means of the DHP-sensitive $I_{Ca,L,TT}$ channel. This mechanism is incorporated in our model by allowing the rate constants in the 4-state Markovian model of the Ry-sensitive Ca^{2+} release channel (Figure 4) to be $[Ca^{2+}]_{ryr}$ dependent. Small changes in $i_{Ca,L,TT}$ cause modulation of pre-release $[Ca^{2+}]_{ryr}$, which dictates the propensity of the RyR channel for a Ca^{2+} release. The pre-release values of the rate constants in the 4-state Markovian model of the RyR channel (nonlinear dependence on $[Ca^{2+}]_{ryr}$ as shown in Appendix A1, Equations 79-84) along with the diastolic $[Ca^{2+}]_{jSR}$ (which is kept constant in Figure 10) set the peak RyR open probability achieved by the RyR channel as well as the peak $[Ca^{2+}]_{myo}$. The use-dependent adaptation of the RyR channel [13] is reflected in its non-linear response to trigger Ca^{2+}. As shown in Figures 10B-iii, iv, the delay in the onset of cytosolic Ca^{2+} transient closely follows the modulation of the onset of RyR release. Though occurring in separate compartments, the peak of cytosolic Ca^{2+} transient also tracks the maximum value attained by the open probability of the Ry-sensitive Ca^{2+} release channel. Here, the clamp voltage was held constant at 10 mv to avoid the interference of voltage dependent Ca^{2+} transport via the Na^{+}/Ca^{2+} exchanger which is co-located [98] with the $I_{Ca,L}$ channel in the dyad and the scaling down of $I_{Ca,L,TT}$ corresponds to a fast flicker block of the channels by dihydropyridine.

The slow rising foot that precedes the rapid upstroke (trace at position 0 in Figure 10B-i and B-ii) is the contribution from a single sparklet (Figure 6), which is the result of Ca^{2+} release from a single $i_{Ca,L,TT}$ channel in our model (0.1 pA), which is of the same order as reported by Wang et. al. [13] bringing trigger Ca^{2+} into a unitary dyad. This L-type Ca^{2+} channel (LCC) triggers release from a cluster of RyR channels causing a Ca^{2+} spark (Figure 6), which results in the rapid increase in $[Ca^{2+}]_{dyad}$ that follows the foot (shown in Figure 10B-i and B-ii). As shown in Figure 10B, the latency from the onset of the sparklet foot to the triggered Ca^{2+} spark increases with decrease in the magnitude of $i_{Ca,L,TT}$ [13]. The SR Ca^{2+} release flux underlying a typical Ca^{2+} spark corresponds to approximately 2 pA [27,28,13]. From RyR single channel conductance measurements in lipid bilayer studies [99], a Ca^{2+} spark translates into a release from around 4 RyR channels (also reported by Blatter et. al. [28]). This single Ca^{2+} spark corresponds to a unitary RyR release (2 pA) in our model. Our model does not

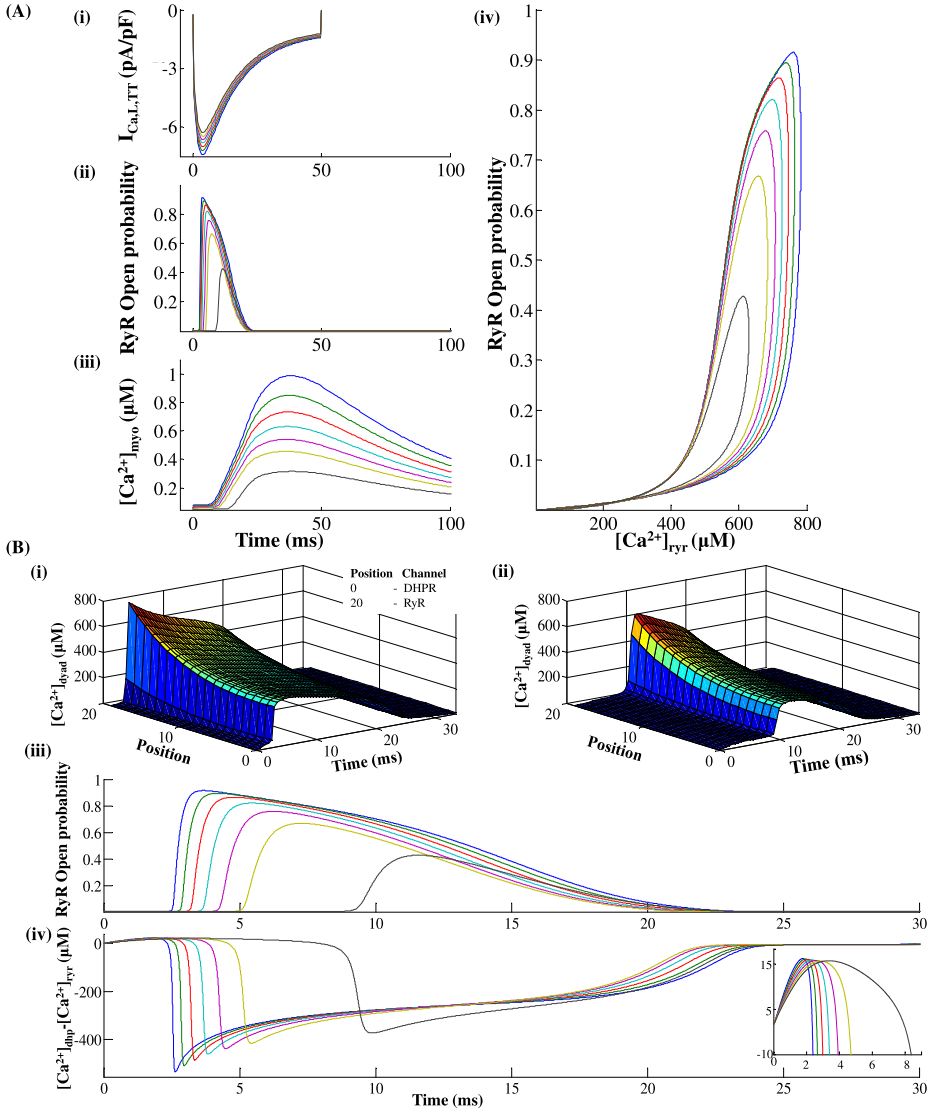

Figure 10 Graded CICR. Figure 10: SR calcium release graded by the trigger current $I_{Ca,L,TT}$. (A) - (i) Decreasing trigger current $I_{Ca,L,TT}$ (ii) With decreasing trigger current, RyR open probability shows a graded decrease in its peak as well as an increasing delay in its onset (iii) Cytosolic calcium transient follows the trend shown by the RyR release channel (a graded decrease in peak and increasing delay in onset) (iv) RyR open probability vs $[Ca^{2+}]_{nyr}$ for increasing trigger current $I_{Ca,L,TT}$. (B)- (i)Concentration profile in the dyad as a result of RyR release caused by a largest trigger current (see part A(i)) (ii)Concentration profile in the dyad as a result of RyR release caused by a smallest trigger current (see part A(i)) (iii) With decreasing trigger current, RyR open probability shows a graded decrease in its peak as well as an increasing delay in its onset (shown on an expanded time scale) (iv)Difference in concentration between the mouth of the DHP and Ry-sensitive Ca^{2+} channels. (Inset shows the cross-over when this difference becomes negative indicating trigger current dependent latency involved in release).

attempt to reproduce the stochastic kinetics of the single channel LCC-RyR coupling; however it mimics accurately the average behavior of this stochastic process which is the net Ca^{2+} release flux into the cytosol causing the Ca^{2+} transient. This on/off stochastic nature of the coupling was used earlier to explain the release termination via stochastic attrition. However, it is now known [25] that the luminal sensor plays a fundamental role in an active extinguishing mechanism [51] that effects a robust $[Ca^{2+}]_{jSR}$

- dependent closure of the RyR channel. This mechanism for inactivation of the Ry-sensitive Ca^{2+} release channel is accounted for in our model.

Cytosolic Ca^{2+} transient is also graded by the duration of the $I_{Ca,L,TT}$ trigger current controlled by the voltage clamp pulse duration. Our model also shows that triggered release can be prematurely stopped by rapid repolarization [100-102]. The effect of depolarization duration on the time course of the cytosolic Ca^{2+} transient is indicated in Figure 11 where the duration of the voltage clamp pulse is decreased from 80 ms to 5 ms (while keeping the clamp voltage constant at 10 mv) resulting in premature stoppage of release and thus a decrease in peak cytosolic Ca^{2+} transient. This effect is a combined result of (i) the modulation of release due to pulse duration dependent change in the amount of trigger Ca^{2+} entering the dyadic coupling unit (DCU) and (ii) the pulse duration dependent change in the relative role of the Na^{+}/Ca^{2+} exchanger co-located in the DCU.

High Gain of Ca^{2+} Release

Besides the graded release, an extremely valuable characteristic of the CICR process is the high gain associ-ated with it. A small amount of Ca^{2+} entering the DCU via the $I_{Ca,L,TT}$ channel causes a large release of Ca^{2+} from the sarcoplasmic stores via the Ry-sensitive Ca^{2+} release channel on the jSR lumen that interacts with the DCU. This high gain is essential in producing physiological cytosolic Ca^{2+} transients when 10000 of these DCU's operate in tandem. Two different definitions of the gain or amplification factor due to CICR have been adopted in our model simulations, namely the ratio of:

1. average integrated RyR flux to average integrated DHPR flux [7]; and
2. the peak Ca^{2+} transient in the presence of CICR to the peak calcium transient in its absence, con-tributed by the trigger calcium alone [3].

Thus, criterion (1) measures calcium gain observed in the dyadic space, whereas criterion (2) measures gain observed in the cytosolic space.

With regard to the dyadic space, Figure 12A shows the Ca^{2+} flux through DHPR and RyRs, respectively. Figure 12B shows cytosolic calcium transients under conditions of ryanodine blockade and with RyR Ca^{2+} release. Based on our measurements, there is approximately a 2 ms delay from the onset of the DHPR influx to the initiation of the RyR release flux.

At a clamp voltage of 10 mv, criterion (1) applied to our simulation yields an integrated flux ratio of 6.39, whereas a gain of 5.75 is calculated using criterion (2). By either method, a CICR amplification factor of approximately 6 is calculated, which is similar to that reported by Stern [3]. This result is also consistent with gain calculations from the measured data of Fan and Palade [17] on rat ventricular cells. They estimated a gain of approximately 7 using comparisons of the rates of rise of Ca^{2+} transients in the presence and absence of ryanodine. The model generated results are obtained by using a voltage clamp protocol of a 50 ms step pulse to 10 mv from a holding potential of -40 mv.

The inset in Figure 12A shows the voltage dependence of CICR gain formulated using criterion (1). Our model shows a decline in gain as the clamp voltage is

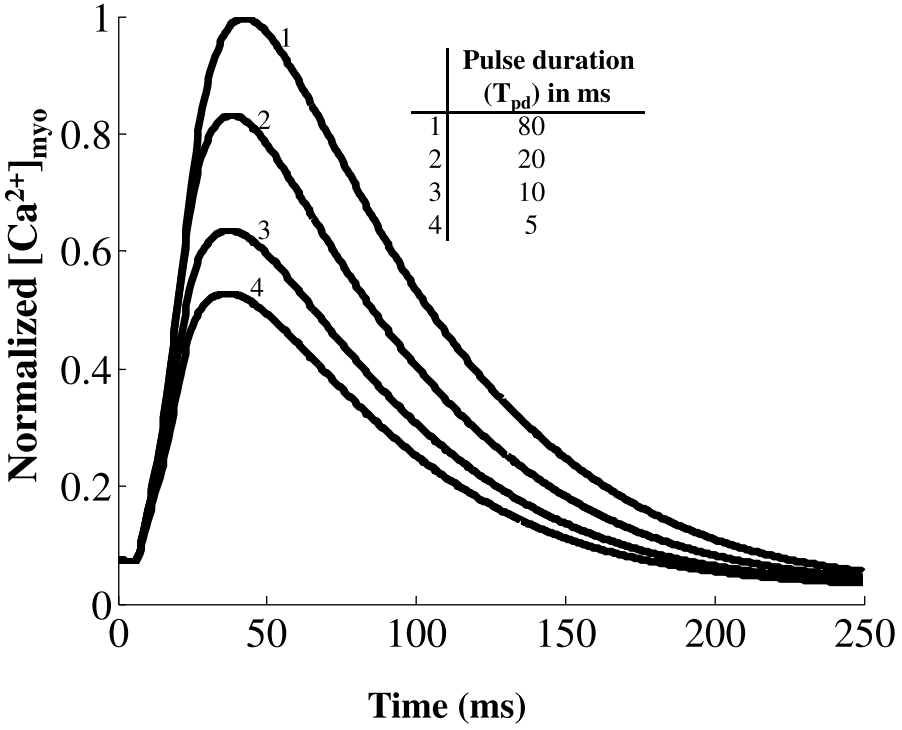

Figure 11 Effect of depolarization duration on $[Ca^{2+}]_{myo}$. Figure 11: The effect of changing the duration of depolarizing pulses T_{pd} on the time course of the $[Ca^{2+}]_{myo}$ transient. Voltage clamp protocol used is a step pulse to 10 mv from a holding potential of -40 mv. Normalized $[Ca^{2+}]_{myo}$ transient corresponding to depolarizing pulses of 5, 10, 20, and 80 ms duration. This model-generated result shows similarity to data in Figure 2, Cannell et al. [100] showing pulse-duration dependent changes in cytosolic Ca^{2+} concentration.

increased from -30 mv to 20 mv [52,103]. However, any further increase in clamp voltage results in a small increase in gain (Figure 1C, Altamirano et al. [104]). It is important to note that, with increasing clamp voltage, the decreased ability of the Na^{+}/Ca^{2+} exchanger (which is co-located [98] in the dyad) to extrude Ca^{2+} partially compensates for the declining trigger current, in facilitating SR release and hence assists in increasing CICR gain.

RyR Refractory Characteristics

Given the fact that the CICR mechanism has a high gain associated with it, it could be prone to unstable behavior if not for the refractory characteristics of the Ry-sensitive release channel [105]. It is now known [25] that the luminal sensor plays a fundamental role in an active extinguishing mechanism [51] effecting a $[Ca^{2+}]_{jSR}$ dependent robust closure of the RyR channel which is accounted for in our model. The RyR release fails to become regenerative due to the role of the luminal sensor which after a release occurs, forces the RyR channel into an absolute refractory state followed by a relative refractory state as shown in Figure 13C. When the RyR channel is in the absolute refractory period, $[Ca^{2+}]_{ryr}$ drops to a level much below what is caused by a sparklet (trigger Ca^{2+}) hence it robustly avoids re-excitation. This extremely critical refractory feature of the channel enabled by the RyR luminal sensor acts as a protective mechanism against premature Ca^{2+} release in the wake of a secondary excitation that

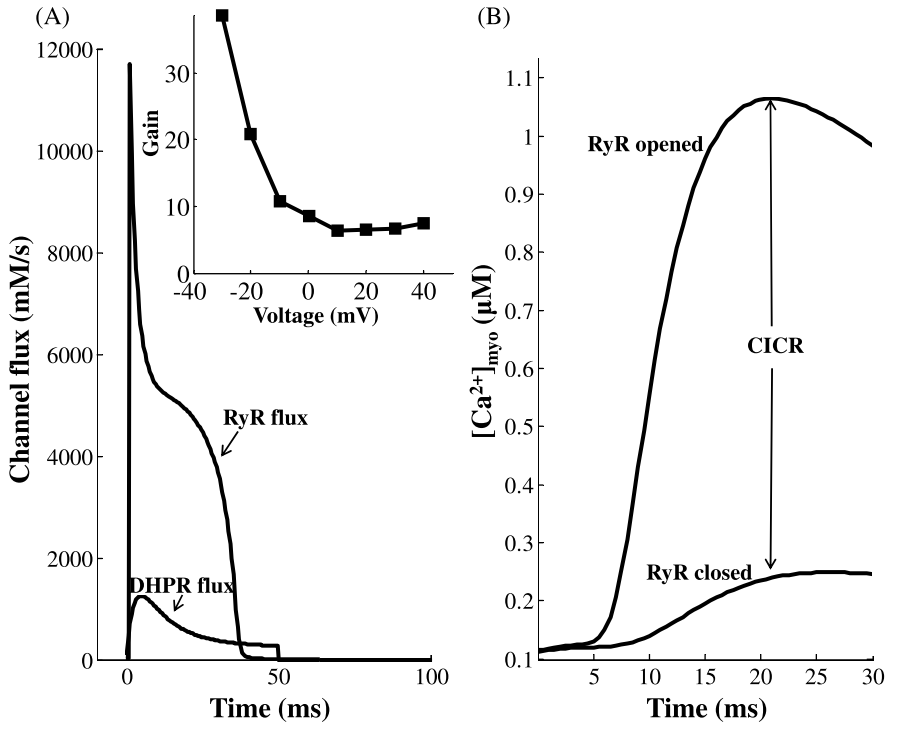

Figure 12 CICR Ca^{2+} gain. Figure 12: High gain associated with CICR. Voltage clamp protocol used is a 50 ms step pulse to 10 mv from a holding potential of -40 mv. (A) Gain formulation by comparison of Ca^{2+} flux through the DHP sensitive and RyR sensitive Ca^{2+} channels. The voltage dependence of gain measured using this method is shown in the inset. (B) Gain formulation by comparison of cytosolic calcium transient formed in the presence and absence of RyR Ca^{2+} release.

occurs before jSR can be filled back to the control level. The refractory nature of the channel is caused by the $[Ca^{2+}]_{jSR}$ dependent inhibition induced by the protein triadin from the luminal side of the RyR channel. This restraining lock on the RyR channel assists in reloading the jSR.

A dual stimulus protocol (S1-S2) was employed to study RyR refractoriness. The RyR channel was stimulated initially by stimulus trigger current S1, followed after an interval (T_2 in Figure 13A) by an identical stimulus current S2. Each of the two stimuli directed into the dyadic coupling unit is the dyadic component ($I_{Ca,L,TT}$) of trace 1 ($I_{Ca,L}$ evoked by a 10 mv clamp pulse) in Figure 7A with a peak amplitude of 6.657 pA/pF and a duration (T_1 in Figure 13A) of 50 ms. The stimuli S1 & S2 were kept identical to delineate the effects of RyR refractoriness on CICR. The time interval between the two stimuli (T_2) was gradually reduced from 250 ms to 50 ms in steps of 25 ms to observe the effects of partial recovery of the RyR channel.

As seen in Figure 13, the decrease in interval between stimuli causes partial recovery of $[Ca^{2+}]$ level in the jSR which manifests in increasing levels of unbound version of the protein calsequestrin, which tends to bind with triadin. As more triadin binds to calsequestrin, there is less left to bind to the luminal side of RyR to activate the channel for CICR. This signaling sequence mediated by the luminal sensor via the interaction of proteins calsequestrin and triadin, allows only a partial SR Ca^{2+} release based on the degree of SR Ca^{2+} content recovery. This is an important feature that helps

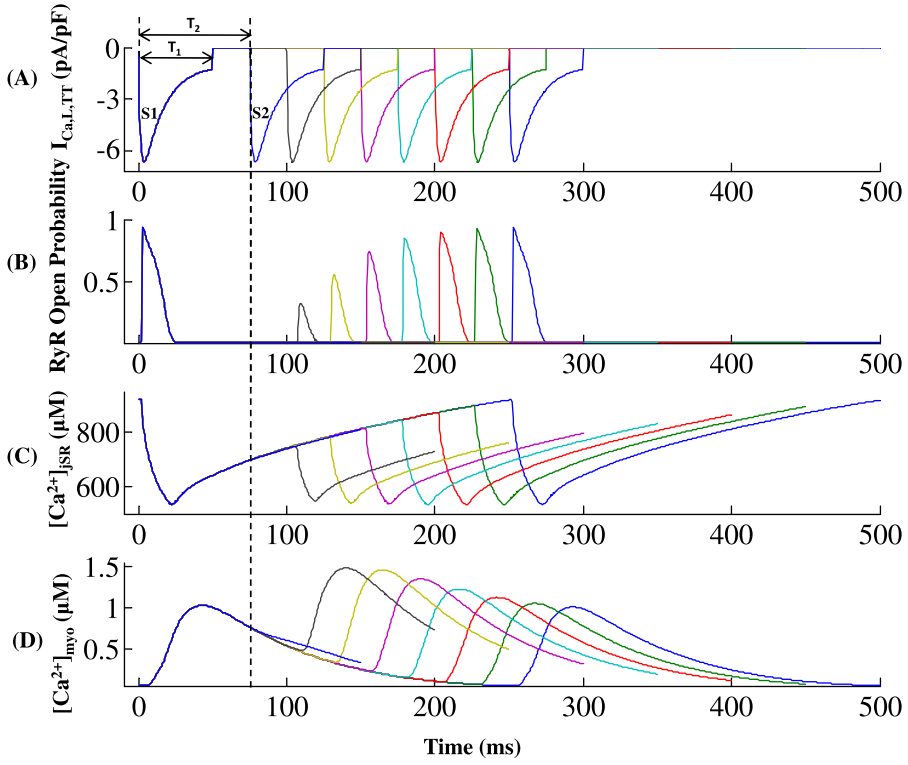

Figure 13 RyR refractory characteristics. Figure 13: RyR refractory characteristics. (A) The stimulation protocol comprises of two consecutive stimuli S1 & S2, both of which are identical to the dyadic component ($I_{Ca,L,TT}$) of trace 1 ($I_{Ca,L}$ evoked by a 10 mv clamp pulse) in Figure 7A with a peak amplitude of 6.657 pA/pF and a duration (T_1) of 50 ms. These are applied with their separation in time (T_2) increasing from 50ms to 250 ms in steps of 25 ms. (B) The RyR sensitive Ca^{2+} release channel shows refractory characteristics with an absolute refractory period of 50 ms and a relative refractory period of 250 ms. (C) The corresponding $[Ca^{2+}]_{jSR}$ traces reflect partial RyR recovery. (D) Cytosolic calcium transient recovers completely after 250 ms. The dotted line indicates lack of RyR release when T_2 = 75 ms due to insufficient RyR recovery.

restore the jSR Ca^{2+} content at the end of every cycle. The RyR channel in our model has an absolute refractory period of 75 ms and a relative refractory period of 250 ms (Figure 13C). These results are consistent with the refractory period measurements by Sobie et al [106] on rat ventricular myocytes. When the RyR channel is in the absolute refractory period, $[Ca^{2+}]_{RyR}$ drops to a level much below what is caused by a sparklet (trigger Ca^{2+}) and hence robustly avoids re-excitation. However, when the RyR channel is in the relative refractory period, a partial release (Figure 13C) is possible, despite the RyR receptors affinity for release being low.

Figures 14A and 14B show the steady state $[Ca^{2+}]_{myo}$ and $[Ca^{2+}]_{jSR}$ predicted by the model, with and without a functioning luminal sensor, respectively. The stimulation protocol used is a pulse train of amplitude (-40 mv to 10 mv), duration (50 ms) and frequency of 4.0 Hz which is applied for a period of 2.5 sec. The value of the luminal control of the RyR channel in allowing adequate SR filling can be seen in Figure 14 where, in the presence of the luminal sensor the cell maintains a normal cytosolic Ca^{2+} transient (Figure 14A-i). This is made possible due to sufficient SR filling (Figure 14A-ii) as a result of RyR refractoriness. However, inactivation of the RyR channel is also known to depend on the high local Ca^{2+} concentration consequential to its own

Ca^{2+} release [51]. The lack of a luminal sensor forces the RyR channel to solely rely on Ca^{2+} dependent inactivation mechanism. The resulting inadequate RyR inactivation depletes diastolic $[Ca^{2+}]_{jSR}$ level (Figure 14B-ii) causing the cytosolic Ca^{2+} transient to diminish to new lowered steady state values (shown in Figure 14B-i). The absence of the luminal sensor is modeled by setting the value of the luminal sensing variable ('var' in the model) to a level consistent with it's normal value under 4 Hz, voltage clamp stimulation. This mimics the case where the luminal sensor is insensitive to changes in $[Ca^{2+}]_{jSR}$ and hence non-functional. It is important to note that the decrease (37.07%) in diastolic SR level (as indicated in Figure 14B-ii) is due to the lack of a luminal control on the RyR channel resulting in a reduced rate of RyR recovery which in turn reflects in a compromised SR filling rate. Hence, the presence of a luminal sensor which monitors the SR Ca^{2+} content, is key to long term Ca^{2+} stability in the cell.

CICR modulation by the jSR Ca^{2+} content

From the refractory characteristics of the RyR channel, it is evident that the RyR release is strongly dependent on the jSR Ca^{2+} content. In fact, the SR Ca^{2+} release through the RyR channel depends on: (a) the amount of trigger Ca^{2+} entering by means of the $I_{Ca,L,TT}$ channel (b) the concentration gradient of Ca^{2+} between the jSR and the mouth of the RyR channel in the dyadic space and (c) the open probability of the RyR channel modulated by the interaction between the luminal sensor and the

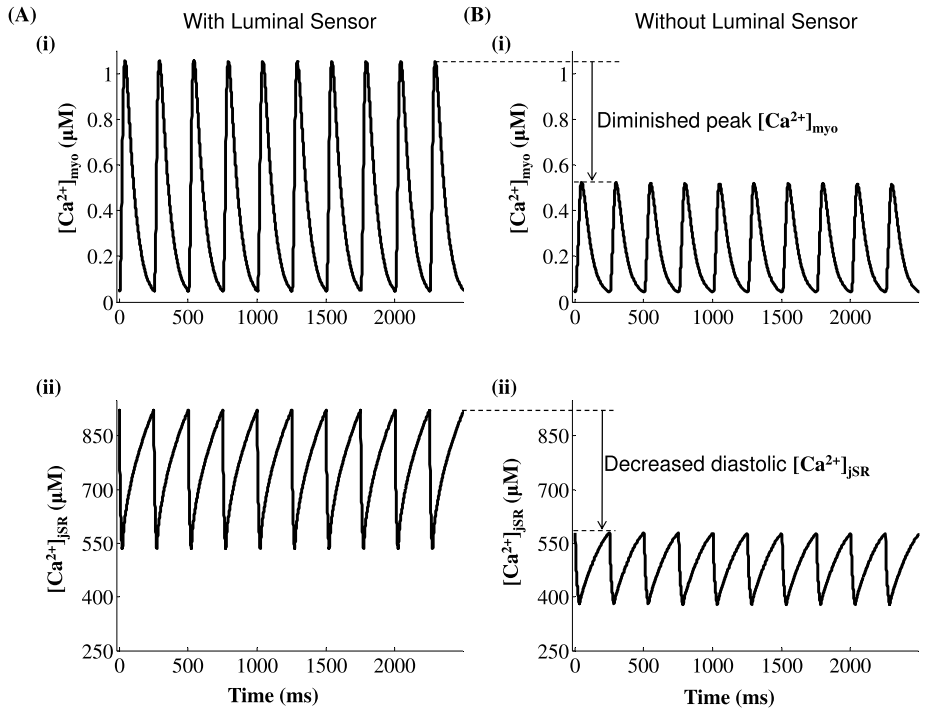

Figure 14 Role of Luminal sensor. Figure 14: Application of a train of voltage clamp pulses (amplitude -40 to 10 mV; duration 50 ms) for a period of 2.5 sec. Pulse repetition rate is 4.0 Hz. Luminal sensor is intact in A and removed in B. Both A and B are steady state responses to voltage clamp stimulation. A-(i) $[Ca^{2+}]_{myo}$ transients with normal amplitude. A-(ii) Sustained SR filling due to robust RyR inactivation. B-(i) Diminishing $[Ca^{2+}]_{myo}$ transients indicate poor SR filling. B-(ii) Lowered $[Ca^{2+}]_{jSR}$ levels indicating inadequate refilling of SR stores due to lack of RyR refractoriness.

RyR protein. The SR Ca^{2+} released also inactivates the trigger current $I_{Ca,L,TT}$ (as shown in Figure 7), hence causing an indirect self-inhibition of RyR release.

Figure 15 shows a phase plot of RyR open probability ($O2_{ryr}$) versus the Ca^{2+} concentration at the mouth of the RyR channel in the dyadic space $[Ca^{2+}]_{ryr}$ constructed from model-generated data for a pulse of amplitude -40 mv to 10 mv and a duration of 50 ms. The pre-release diastolic $[Ca^{2+}]_{jSR}$ is 918 μM. Following excitation by the trigger current during phase A, the RyR channel begins to open, allowing Ca^{2+} flux into the dyad and elevating $[Ca^{2+}]_{ryr}$ at the mouth of the RyR channel. The rate of opening of the channel is Ca^{2+} dependent; hence as $[Ca^{2+}]_{ryr}$ increases, RyR open probability increases first slowly and then ever more rapidly. With this onrush of Ca^{2+}, $[Ca^{2+}]_{ryr}$ rapidly equilibrates with the $[Ca^{2+}]_{jSR}$, reducing and eventually abolishing the concentration gradient across the channel. $[Ca^{2+}]_{ryr}$ soon reaches its maximum value (T1 in Figure 15) and begins to track the decrease in $[Ca^{2+}]_{jSR}$, there being no further significant concentration gradient existing between $[Ca^{2+}]_{jSR}$ and $[Ca^{2+}]_{ryr}$ at the mouth of the RyR channel. During phase B, the rate of rise in RyR open probability decreases due to decreasing $[Ca^{2+}]_{ryr}$ and the onset of self-inhibition due to the large values of Ca^{2+} concentration at the mouth forcing the RyR open probability to attain its maximum value (T2 in Figure 15). This is followed by phase C, where the RyR open probability begins to decrease slowly, initiating channel recovery due to decreasing overall $[Ca^{2+}]_{dyad}$ levels as a result of (a) Ca^{2+} fluxing out of the dyad into the cytosol, (b) lack of a drive from SR release due to drastically diminished Ca^{2+} gradient

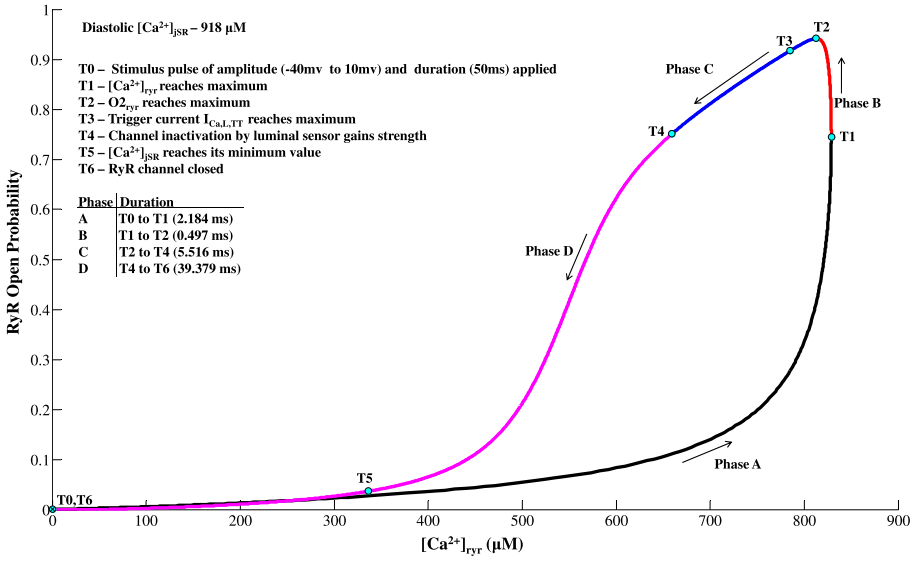

Figure 15 Ryanodine receptor open probability. Figure 15: RyR open probability modulation by concentration at the mouth. The pre-release diastolic $[Ca^{2+}]_{jSR}$ is 918 μM. The stimulation protocol used is a pulse of amplitude (-40 mv to 10 mv) and duration (50 ms). Phase A - As a result of excitation by the trigger current, $[Ca^{2+}]_{ryr}$ initially increases rapidly with a small accompanying rise in RyR open probability followed by steeper increase to peak $[Ca^{2+}]_{ryr}$ with a large increase in RyR open probability.; Phase B - RyR open probability increases to its maximum value at a declining rate reflecting a falling $[Ca^{2+}]_{ryr}$ level and onset of Ca^{2+} induced self-inhibition; Phase C - Decreasing $Ca^{2+}{}_{dyad}$ and continued Ca^{2+} induced self-inhibition, begins the channel recovery process; Phase D - Decreasing $[Ca^{2+}]_{jSR}$ forces a strong RyR inactivation via the luminal sensor hence robustly closing the channel.

at the mouth of the RyR channel and (c) continued Ca^{2+} induced self-inhibition. Decreasing levels of free Ca^{2+} in the jSR force a strong RyR inactivation via the luminal sensor (beginning at T4 and continuing throughout phase D; Figure 15), which in turn causes a sharp decline in RyR open probability. The minimum value of $[Ca^{2+}]_{jSR}$ occurs at T5, and the channel is ultimately closed at T6 (Figure 15). The luminal sensor mediated inactivation assists in robust $[Ca^{2+}]_{jSR}$ recovery.

Cytosolic peak [Ca^{2+}] dependence on SR Ca^{2+} content

Figure 16A shows three characteristic regions in the plot of the peak $[Ca^{2+}]_{myo}$ vs $[Ca^{2+}]_{jSR}$. In Region I, where the jSR load is small, two things occur: (a) RyR release is reduced, as is the basal intracellular Ca^{2+} concentration, and (b) Ca^{2+} dependent inactivation of the $I_{Ca,L,TT}$ channel is reduced due to the lowered dyadic Ca^{2+} concentration, which allows for greater Ca^{2+} entry into the dyadic space via the $I_{Ca,L}$ channel. This increase in trigger current results only in a very small increase in Ca^{2+} release, because of the inhibition of the Ry-sensitive channel caused by the luminal sensor in

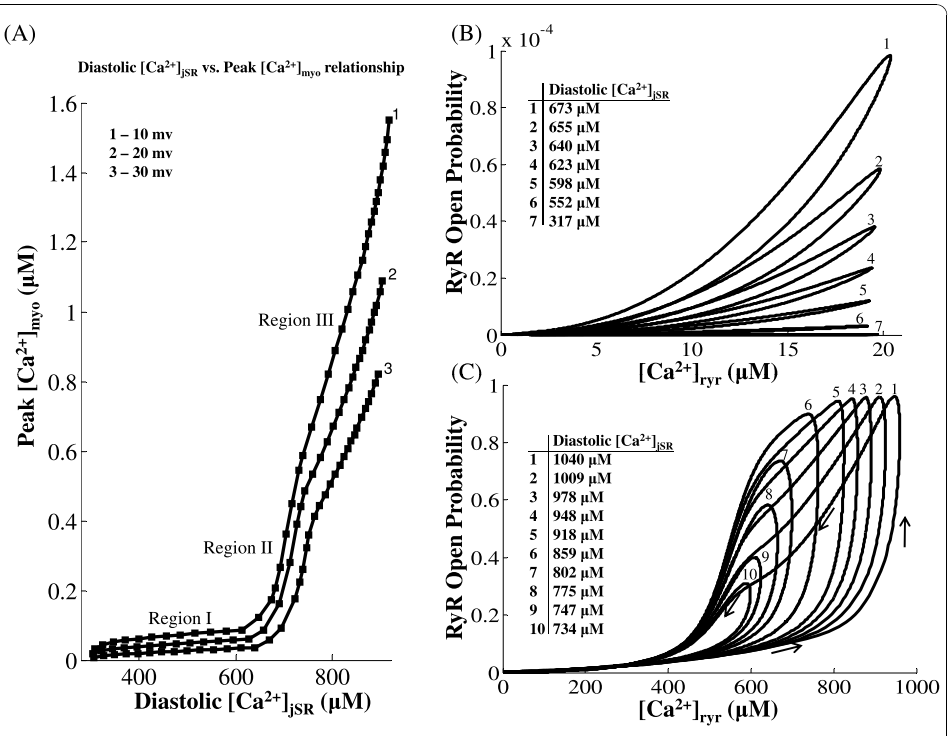

Figure 16 Peak $[Ca^{2+}]_{myo}$ vs $[Ca^{2+}]_{jSR}$. Figure 16: (A) Relation between the peak of the cytosolic Ca^{2+} transient and the diastolic $[Ca^{2+}]_{jSR}$. Region I: The peak RyR open probability is very small owing to the low SR Ca^{2+} content. This causes the peak Ca^{2+} transient to be very small. Region II: Increasing SR Ca^{2+} content causes an increase in the peak RyR open probability and hence in the peak of the cytosolic Ca^{2+} transient. Region III: A large rapid increase in the peak $Ca^{2+}{}_{myo}$ is observed due to the large RyR Ca^{2+} release associated with the high SR Ca^{2+} content and saturation of RyR open probability. This model-generated result shows similarity to data in Figure 4, Diaz et al. [29].(B) Dependence of RyR open probability ($O2_{RyR}$) on diastolic $Ca^{2+}{}_{jSR}$. Increasing pre-release diastolic $Ca^{2+}{}_{jSR}$ results in increasing peak $O2_{RyR}$. However, owing to the low SR Ca^{2+} levels the peak open probability is very small. The stimulation protocol used is a pulse of amplitude -40 mv to 10 mv with a duration of 50 ms. (C) Dependence of RyR open probability ($O2_{RyR}$) on diastolic $Ca^{2+}{}_{jSR}$. Increasing diastolic $Ca^{2+}{}_{jSR}$ results in a linearly increasing peak $O2_{RyR}$. In the open probability saturation region the increase in peak cytosolic Ca^{2+} transient is sustained by increasing the area contained by each loop as seen in traces numbered 5 to 1. The progress in time occurs along the arrow indicated on trace 1. The stimulation protocol used is a pulse of amplitude -40 mv to 10 mv with a duration of 50 ms.

response to low SR Ca^{2+} content. Thus, these factors cumulatively result in only a small linear increase in the peak $[Ca^{2+}]_{myo}$ with increasing SR Ca^{2+} content in Region I. The behavior in Region I corresponds to traces 7-1 in Figure 16B (shows phase plots of $O2_{ryr}$ vs $[Ca^{2+}]_{ryr}$ for different steady state $[Ca^{2+}]_{jSR}$ concentrations), where the peak RyR open probability shows very small gradual increase with increasing levels of diastolic pre-release $[Ca^{2+}]_{jSR}$ for a constant trigger Ca^{2+} input via $I_{Ca,L}$. The steady state diastolic $[Ca^{2+}]_{jSR}$ levels being low, the maximum RyR open probability values attained are low. Although the peak $[Ca^{2+}]_{ryr}$ does not increase substantially as the diastolic $[Ca^{2+}]_{jSR}$ levels increase from 317μM to 673μM, the area enclosed by the $[Ca^{2+}]_{ryr}$ - $O2_{ryr}$ loop (which indicates the amount of SR Ca^{2+} released into the dyad) increases exponentially due to increasing peak RyR open probability combined with the increasing difference between rate of activation and inactivation with rate of activation increasing faster than the rate of channel inactivation. In Region II of Figure 16A, increasing SR Ca^{2+} content begins to translate into a substantial increase in peak $[Ca^{2+}]_{myo}$. This is because increasing diastolic $[Ca^{2+}]_{jSR}$ causes a significant increase in the peak RyR open probability, as shown in Figure 16C, which translates into a commensurate increase in the peak of the cytosolic Ca^{2+} transient. The inhibiting role of the luminal sensor is relieved with building $[Ca^{2+}]_{jSR}$ levels. The nonlinearity observed between the diastolic $[Ca^{2+}]_{jSR}$ levels 673μM (Figure 16B) and 734μM (Figure 16C) at the transition between Regions I and II corresponds to the existence of a threshold characteristic for RyR release [107,108]. As the diastolic $[Ca^{2+}]_{jSR}$ levels increase beyond 734μM, the area enclosed by the $[Ca^{2+}]_{ryr}$ - $O2_{ryr}$ loop increases substantially reaching a maximum value at $[Ca^{2+}]_{jSR}$ level of 948μM not only due to a significant increase in both peak $[Ca^{2+}]_{ryr}$ and peak $O2_{ryr}$ but also due to a rapid increase in rate of RyR activation resulting in a much larger difference in rate of activation and inactivation. Region III exhibits a large rapid increase in peak $[Ca^{2+}]_{myo}$ due to the large RyR Ca^{2+} release associated with the high SR Ca^{2+} content. However, it is important to note that this is not a result of increasing peak RyR open probability, which begins to plateau for steady state $[Ca^{2+}]_{jSR}$ values larger than 850μM (traces 6-1 in Figure 16C). The continuing rapid increase in peak cytosolic Ca^{2+} concentration in region III is a combined result of: (a) increased release owing to large SR Ca^{2+} content; (b) large values for saturated RyR open probability supported by an increase in the area contained by each loop as seen in traces 6-1 of Figure 16C; and (c) saturated operation of the SERCA pump which acts as a predominant buffer in restoring the Ca^{2+} concentration levels in the cytosol after RyR release [77]. As the diastolic $[Ca^{2+}]_{jSR}$ levels increase beyond 948μM, the area enclosed by the $[Ca^{2+}]_{ryr}$ - $O2_{ryr}$ loop begins to decrease despite increasing peak $[Ca^{2+}]_{ryr}$ due to saturation of the peak RyR open probability and increasing rate of RyR channel inactivation due to large values of local Ca^{2+} concentration ($[Ca^{2+}]_{ryr}$) assisting in faster recovery [51]. This model generated relationship between the peak $[Ca^{2+}]_{myo}$ and the pre-release $[Ca^{2+}]_{jSR}$ agrees with Figure 4 in Diaz et. al. [29].

As seen in traces 1-10 of Figure 16C, during the initial activation of a RyR channel (linear region of phase A in Figure 15), at any specific $[Ca^{2+}]_{ryr}$ the RyR open probability takes a lower value despite a higher steady state diastolic $[Ca^{2+}]_{jSR}$ level. This decreasing slope with increasing diastolic, pre-release $[Ca^{2+}]_{jSR}$ reflects a faster rate of rise in $[Ca^{2+}]_{ryr}$ for a larger pre-release SR content with a very small accompanying increase in the RyR open probability.

Ca^{2+} Release and its Effect on $I_{Ca,L}$

Caffeine

Adachi-Akahane et al. [71] investigated $I_{Ca,L}$-induced Ca^{2+} release in rat ventricular myocytes in the presence and absence of caffeine, which altered $[Ca^{2+}]_{myo}$. Using their protocols and data as a guide, we modeled the effect of caffeine on jSR Ca^{2+} release and its subsequent effect on $I_{Ca,L}$. Specifically, a Boltzman relationship was adopted to simulate the binding of caffeine to the ryanodine receptor increasing channel conductance, which in turn enhances jSR Ca^{2+} release. The process is assumed to be dose-dependent, with an open probability of 0.5 at a caffeine concentration of 5 mM (Appendix A1, Eq. 86).

Figures 17A and 17B show model-generated $[Ca^{2+}]_{myo}$ responses in myocytes dialyzed with 2 mM Fura-2, where a simple voltage clamp pulse (-40 mV to 0 mV) is applied in the presence and absence of caffeine. $I_{Ca,L}$ waveforms associated with these two protocols are shown in Figure 17C. In protocol A, conducted at normal rest levels of $[Ca^{2+}]_{myo}$ (10 nM), the depolarizing test pulse to 0 mV from the holding potential of -40 mV for 0.1 sec fully activates $I_{Ca,L}$, which in turn triggers a rapid but small amplitude Ca^{2+} transient (a rise from 30 nM to 95 nM as shown in Figure 17A. Protocol B starts with an application of 5 mM caffeine for a period of 1.0 sec (open state probability of RyR channel is 0.5), followed by the same depolarizing test pulse applied at 1.0 sec. The conditioning caffeine pulse induces a $[Ca^{2+}]_{myo}$ transient rising from a resting value of 30 nM to a peak value of 110 nM (Figure 17B, first peak -note the different timescale). The short depolarizing pulse activates $I_{Ca,L}$, which triggers a much

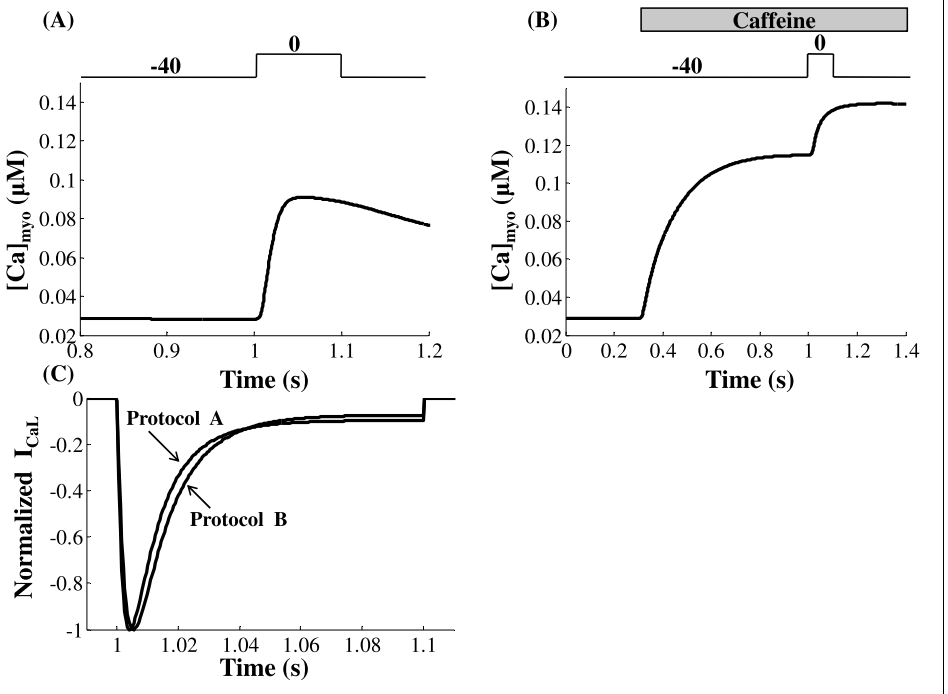

Figure 17 Effects of the application of caffeine. Figure 17: Model-simulated effects of the application of caffeine on $I_{Ca,L,TT}$ and $[Ca^{2+}]_i$ in a cell dialyzed with 2 mM Fura-2. Changes in $[Ca^{2+}]_{myo}$ resulting from: (A) application of a simple depolarizing pulse from -40 mV to 0 mV, and (B) the same depolarizing pulse following pre-exposure to caffeine (5 mM). Panel (C) compares the $I_{Ca,L}$ waveforms associated with these protocols. This model-generated result shows similarity to data in Figure 3, Adachi-Akahane et al. [71].

smaller $[Ca^{2+}]_{myo}$ transient via CICR (30 nM, Figure 17B, second peak). This $I_{Ca,L}$-evoked Ca^{2+} transient in response to the voltage pulse is smaller in amplitude than control (Figure 17A), due to: (a) reduction in RyR release due to depletion in $[Ca^{2+}]_{jSR}$ ($[Ca^{2+}]_{jSR}$ drops from 1.25 mM to 0.25 mM with caffeine application).; and (b) the strong competing role of the luminal RyR sensor in inactivating the RyR channel in response to the post-caffeine, low SR content. The $I_{Ca,L}$-inactivation characteristics undergo a change as shown in Figure 17C, where trace B inactivates more slowly compared to the control $I_{Ca,L}$ (trace 1). After exposure to caffeine, the overall amplitude of $[Ca^{2+}]_{dhp}$ during release does not increase as much as in the control case, since jSR Ca^{2+} release is reduced. Consequently, Ca^{2+} dependent inactivation (during release) of $I_{Ca,L}$ after caffeine application is not as strong as that in the control case. However, the baseline level of Ca^{2+} concentration at the mouth of the DHP channel ($[Ca^{2+}]_{dhp}$) is elevated following caffeine application, causing sustained inactivation resulting in the crossover of the current trace in Figure 17C. This is consistent with the observation of Cens et al. [41], that Ca^{2+} induced inactivation is a result of calmodulin mediated sensing of the local Ca^{2+} concentration.

Thapsigargin

Analogous to the experimental protocol of Adachi-Akahane et al. [71] dealing with thapsigargin blockade of the SERCA pump (their Figure 9), we apply a series of voltage pulses (-40 mV to 0 mV, duration 0.1 sec, frequency 0.05 Hz) to our cell model, modified by blockade of the SERCA pump and addition of 2 mM Fura-2. Figure 18 shows that when Ca^{2+} uptake is blocked, SR Ca^{2+} content declines, as does the jSR Ca^{2+} release with each voltage pulse (Figure 18A). Considerable time is consumed after thapsigargin application, before SR Ca^{2+} content is finally exhausted (8-10 beats at 0.05 Hz; Figure 18A). As the magnitude of the $[Ca^{2+}]_{myo}$ transient decreases, the $[Ca^{2+}]_{dhp}$ dependent inactivation of $I_{Ca,L}$ slows (Figure 18B), resulting in an enhanced peak.

For a given clamp amplitude, a decrease in jSR Ca^{2+} content decreases Ca^{2+} release, producing decreased Ca^{2+} concentration at the dyadic side of the DHP-sensitive channel. Consequently, a smaller amount of calcium-calmodulin complex (Ca_4CaM) is activated, leading to a lower degree of Ca^{2+} dependent inactivation. Thus, $I_{Ca,L}$ peak is enhanced, as shown in Figure 18B, increasing the area under the waveform, corresponding to an increased amount of Ca^{2+} entering the cell. This inverse relationship between jSR Ca^{2+} content and the amount of trigger Ca^{2+} entering the dyadic space for a given clamp voltage is the essence of the feedback mechanism maintaining the efficacy of CICR. This mechanism is operational even in the presence of high concentrations of cytoplasmic Ca^{2+}-buffers, since the small dimensions of the dyadic space allow jSR released Ca^{2+} to reach its destination (i.e., the DHP receptor) before being captured by the buffers [109].

Effect of modulation of $[Ca^{2+}]_o$

Increase in $[Ca^{2+}]_o$ causes an increase in entry of extracellular Ca^{2+} into the cell via the $I_{Ca,L}$ channel. This results in an increase in SR Ca^{2+} content, as shown in Figure 19B. Aided by an increase in trigger Ca^{2+} as well as a larger SR Ca^{2+} content, the RyR release is enhanced. This increase in SR release assisted by impaired Na^+/Ca^{2+} exchange due to elevated $[Ca^{2+}]_o$ manifests in an increase in the peak Ca^{2+} concentration levels in the cytosol, as shown in Figure 19A. Similarly, a decrease in extracellular

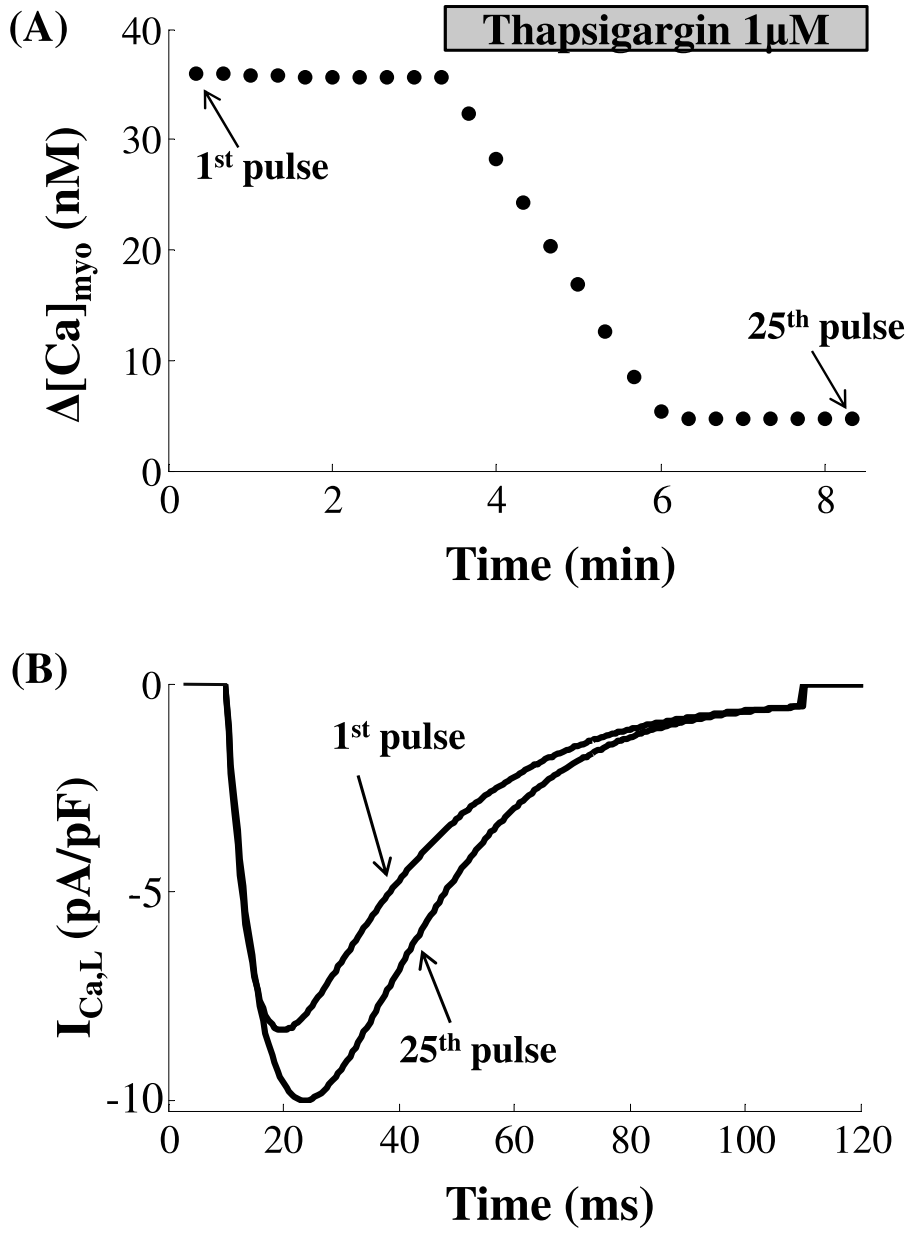

Figure 18 Effects of the application of Thapsigargin. Figure 18: In rat ventricular myocytes dialyzed with 2 mM Fura-2, thapsigargin gradually abolishes $[Ca^{2+}]_{myo}$ transients and decreases the rate of inactivation of $I_{Ca,L}$. This result is generated by the model, in response to a pulse train of amplitude (-40 mV to 0 mV), duration (0.1 sec) and frequency of 0.05 Hz. (A) Time course of the effect of thapsigargin on $\Delta[Ca^{2+}]_i$. (B) L-type Ca^{2+} currents at the times indicated in (A). This model-generated result shows similarity to data in Figure 11, Adachi-Akahane et al. [71]

Ca^{2+} levels causes a decrease in trigger Ca^{2+} available to cause CICR, which results in a decrease in peak $[Ca^{2+}]$ levels in the cytosol, as shown in Figure 19C. Reduced Ca^{2+} entry into the cell via $I_{Ca,L}$, translating into decreased availability of post-release Ca^{2+} in the cytosol, causes reduction in SR filling via the bi-directional SERCA pump. The corresponding drop in the SR Ca^{2+} content is evident in Figure 19D. Although, our model-generated results show similarity to data in Figure 2, Diaz et al. [110], our result

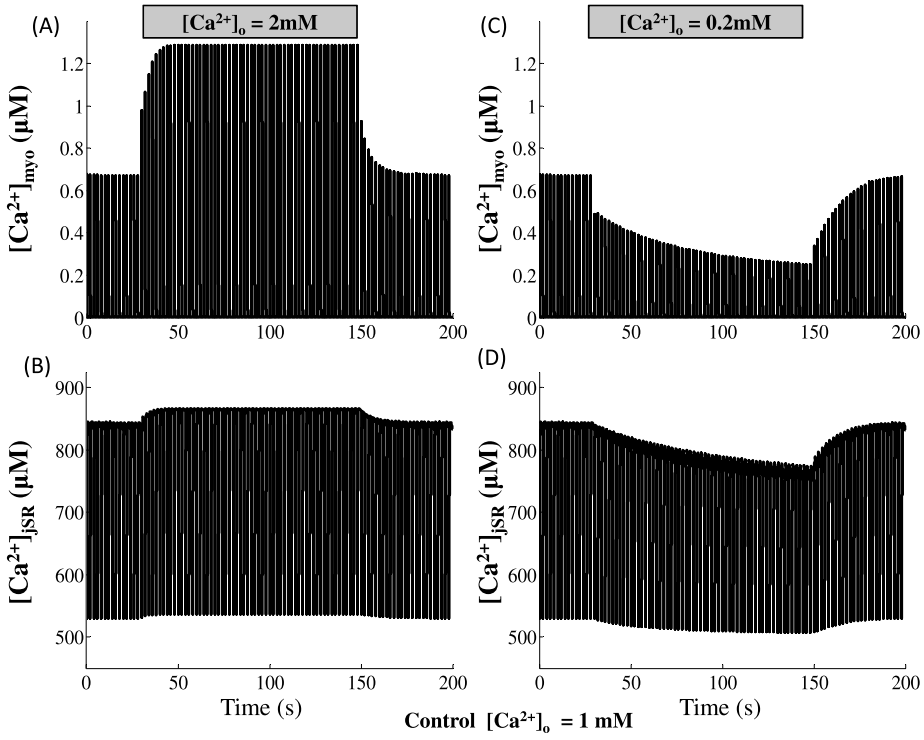

Figure 19 Effects of modulating $[Ca^{2+}]_o$. Figure 19: The effects of changing external Ca^{2+} concentration on cytoplasmic Ca^{2+} and SR Ca^{2+} content. The stimulation protocol used is a pulse train of amplitude (-40 mv to 0 mv), duration (100 ms) and frequency of 0.5 Hz. (A) Following sudden rise in $[Ca^{2+}]_o$ the instantaneous increase in $[Ca^{2+}]_{myo}$ occurs due to more Ca entry, followed by a gradual staircase rise due to the the change in SR content; (B) Changes in $[Ca^{2+}]_{myo}$ forced by a sudden decrease in $[Ca^{2+}]_o$; (C) Changes in $[Ca^{2+}]_{jSR}$ due to increased $[Ca^{2+}]_o$; (D) Changes in $[Ca^{2+}]_{jSR}$ due to reduced $[Ca^{2+}]_o$. This model-generated result shows similarity to data in Figure 2, Diaz et al. [110].

in Figure 19D does not confirm an increase in SR Ca^{2+} content with a decrease in $[Ca^{2+}]_o$ as reported in Figure 2B, Diaz et al. [110]. On the contrary, they agree with the data in Figure 5, Diaz et al. 1997 which shows a decrease in free diastolic steady-state SR Ca^{2+} content with decrease in $[Ca^{2+}]_o$ in cells not showing spontaneous release. In this study, we have attempted to isolate the effects of changes in $[Ca^{2+}]_o$ on intracellular Ca^{2+} levels by ensuring that there are no voltage dependent effects on Ca^{2+} transport via the $I_{Ca,L}$ channel, Na^+/Ca^{2+} exchanger or the plasma membrane Ca^{2+} ATPase pump. The simulation protocol used in our study (reproduced from Diaz et al. [110]), is a pulse train of amplitude (-40 mv to 0 mv), duration (100 ms) and a frequency of 0.5 Hz. However, it is important to note that, for any constant extracellular Ca^{2+} concentration, in response to a voltage clamp pulse train, increasing clamp potential (>10 mv) results in a decrease in steady state SR Ca^{2+} content as a result of the dominating effect of reduced Ca^{2+} entry via the $I_{Ca,L}$ channel despite a decrease in net Ca^{2+} extrusion via the Na^+/Ca^{2+} exchanger per cycle.

Calcium balance under conditions of repetitive stimulation

Our model exhibits long term Ca^{2+} stability. Analogous to the experimental protocols of Negretti el al. [111], we studied the dynamic aspects of the calcium balance in the cell model by subjecting it to repetitive voltage clamps of different durations. For stable

steady-state operation, Ca^{2+} entry into the cytosol via $I_{Ca,L}$ must exactly balance Ca^{2+} efflux. Changing the rate or pattern of stimulation can have significant effects on the cell's cytosolic Ca^{2+} balance and subsequent contractile response [16]. To demonstrate Ca^{2+} balance in our model, long (Figure 20A) or short (Figure 20B, C and 20D) voltage clamp pulses were applied at a selected repetition frequency, and the resultant changes in $[Ca^{2+}]_{myo}$ were correlated with sarcolemmal and SR Ca^{2+} fluxes. Analogous to the protocol of Negretti et al. [111], pulse trains were applied from a holding potential of -40 mV to +10 mV, with durations of either 800 ms (long-pulse) or 100 ms (short-pulse) at a frequency of 0.33 Hz, for a total test duration of 2 minutes (40 pulses). In analyzing the Ca^{2+} balance, the amount of electric charge Q transferred per pulse was calculated according to the equation: $\int_0^T \mathrm{I}(\mathrm{t})\,\mathrm{dt}$, where I(t) can be $I_{Ca,L}$, I_{NaCa}, I_{PMCA}, I_{ryr}, $I_{cyt,serca}$, and T is 1 cycle duration (3 ms for 0.33 Hz stimulation).

Numerical integration was carried out with respect to steady-state levels, hence only activating currents and leakage currents were considered (background Ca^{2+} current is neglected). The results of the Ca^{2+} balance are presented in a manner where relative Ca^{2+} fluxes can be easily compared. We note that in evaluating the integral of the combined exchanger current I_{NaCa}, the integral is multiplied by a factor of 2 to account for the fact that the exchanger stoichiometry is $3Na^{+}$ per Ca^{2+} (the exchanger

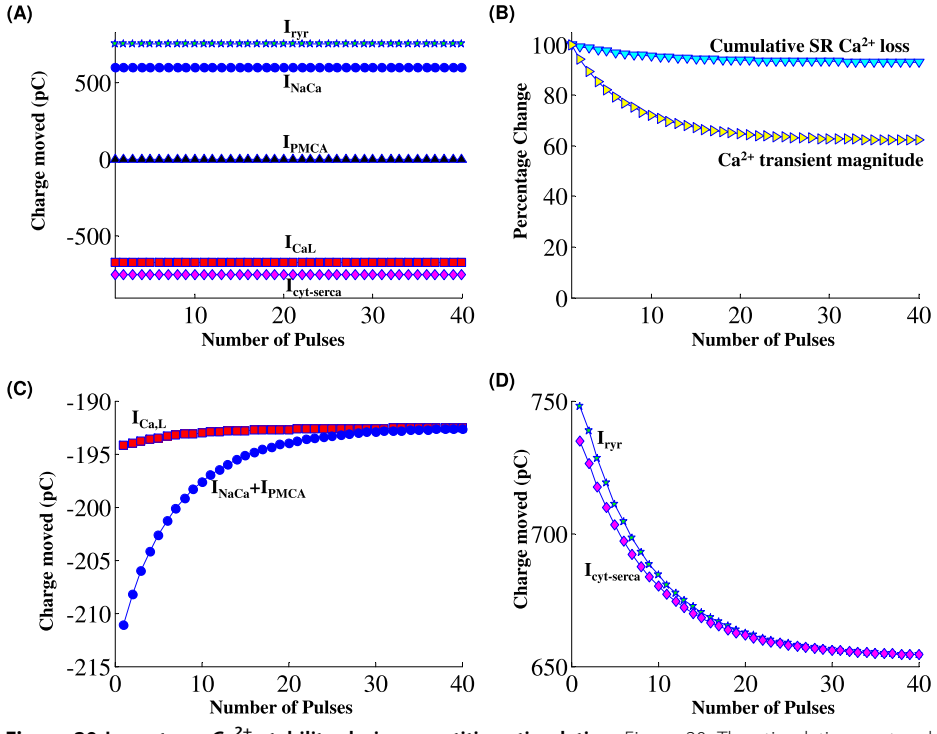

Figure 20 Long term Ca^{2+} stability during repetitive stimulation. Figure 20: The stimulation protocol used is a pulse train of amplitude (-40 mv to 10 mv) and frequency of 0.33 Hz.(A) Integrals of external and internal Ca^{2+} currents on stimulation with repetitive long pulses (800 ms); (B) Percentage of changes in $[Ca^{2+}]_{myo}$ peak magnitude and cumulative SR Ca^{2+} loss on stimulation with repetitive short pulses (100 ms); (C) Integrals of external Ca^{2+} currents with short-pulse stimulations (100 ms); (D) Integrals of internal Ca^{2+} currents with short-pulse stimulations (100 ms). This model-generated result shows similarity to data in Figure 3 and Figure 5, Negretti et al. [111].

transports 1 net charge per Ca^{2+}, whereas all other Ca^{2+} currents transport 2 charges per Ca^{2+}).

Long-pulse protocol

During repetitive long-pulse (800 ms) stimulation, transient Ca^{2+} fluxes cross the sarcolemmal and SR membranes in both directions (inward (into the cytoplasm) and outward). However, $[Ca^{2+}]_{myo}$ returns to control levels by the end of the long-pulse stimulation protocol. The long-pulse stimulation protocol thus serves as a means of studying the steady-state balance of Ca^{2+} influx and efflux to and from the cytoplasm, under control conditions. In contrast, this Ca^{2+} balance is not present in the short-pulse protocol, and $[Ca^{2+}]_{myo}$ is elevated at pulse termination. Our long-pulse simulations show that: (1) the magnitude of individual Ca^{2+} transients do not change during the 40 pulse sequence; (2) the peak calcium release current (I_{ryr}) has a constant magnitude; and (3) the occupancy of the calsequestrin Ca^{2+} buffer in the jSR compartment is reduced by 15% as a result of Ca^{2+} release during each cycle. Although Ca^{2+} fluxes cross the sarcolemma and SR membranes in either direction, the integral of each of these currents (indicating charge transfer) over the pulse repetition interval is a constant. Figure 20A shows this well, in that, the charge transfer for each model current (large or small) is a constant, indicating no net loss of Ca^{2+} nor consecutive-pulse Ca^{2+} depletion (or augmentation) in the jSR compartment under the long-pulse protocol. In Figure 20, we refer to Ca^{2+} influx and efflux through the bounding cell membrane (sarcolemma (SL) and T-tubule) as "external fluxes" (i.e., $I_{Ca,L}$, I_{NaCa}, and I_{PMCA}), whereas SR membrane Ca^{2+} fluxes (I_{ryr}, $I_{cyt,serca}$) are called "internal fluxes." By convention, inward fluxes are negative (e.g. $I_{Ca,L}$) and outward positive (e.g., I_{NaCa} and I_{PMCA}). Figure 20A shows that the integrated external fluxes sum to zero. The average Ca^{2+} charge entering the cell via $I_{Ca,L}$ is 603.28 pC (pico-coulomb), and the sum of averaged Ca^{2+} charges extruded from the cell via I_{NaCa} and I_{PMCA} is 603.28 pC (602.2 pC by I_{NaCa} and 1.08 pC by I_{PMCA}. Figure 20A also shows the magnitudes of the integrated internal fluxes, which sum to zero as well. In calculating inward and outward Ca^{2+} fluxes relative to the SR lumen, we consider an inward flux (e.g., $I_{cyt,serca}$) negative and an outward flux positive (e.g., I_{ryr}). The integral of I_{ryr} is 751.8 pC, compared with integral of the $I_{Ca,L}$ trigger current (603.28 pC). The calcium gain of CICR calculated in this way is low owing to the increased entry of Ca^{2+} via the trigger current $I_{Ca,L}$ for a prolonged duration of 800 ms compared to 50 ms previously. The integral of SR Ca^{2+} uptake is 751.8 pC. These two internal component currents yield flat integral values during long-pulse stimulations and sum to zero.

Short-pulse protocol

Decreasing the length of the depolarizing pulse to 100 ms (short pulse) has a pronounced effect on the recovery of contraction (Figure 20B, C and 20D). Compared with the relatively flat amplitude of $[Ca^{2+}]_{myo}$ observed with stimulation by long pulses, short pulse stimulation produces a negative staircase (Figure 20B) in agreement with the data (Negretti et al. [111]), wherein the peak magnitude decays exponentially to a steady state level of 60% of the initial value. Figure 20B also shows that the model predicts a similar exponential decay in jSR Ca^{2+} concentration $[Ca^{2+}]_{jSR}$. Both of these indicators show a net loss of Ca^{2+} from the cell. Figure 20C and 20D show the transient charge movements associated with the external and internal Ca^{2+} currents respectively during application of the short-pulse train, which are indicative of an elevated

Ca^{2+} load and resultant Ca^{2+} imbalance when the pulse train is first applied. Balance is achieved, but at new lower values of $[Ca^{2+}]_{myo}$ and $[Ca^{2+}]_{jSR}$. For convenient comparison, all internal fluxes are made positive and all external fluxes negative. Figure 20C shows that I_{NaCa} plays a significant role in forming the transient response seen in the short-pulse protocol in extrusion of excess Ca^{2+} load on the cell. The decreasing amplitude of the Ca^{2+} transient causes a decreased LSR uptake current ($I_{cyt,serca}$), which in turn causes a decrease in $[Ca^{2+}]_{jSR}$ resulting in decreased release (I_{ryr}). With successive pulses, $I_{cyt,serca}$ and I_{ryr} decline further, mirroring the exponential decline in I_{NaCa} toward balance. At steady state, the external and internal fluxes reach the new equilibrium, where the sum of the integrals of external currents and the sum of the integrals of internal currents are zero.

Long-term calcium stability at higher pacing rates

Most VC experiments on cardiac cells are usually conducted at low stimulation rates. Our simulations of typical VC experiments at these low rates all exhibit long term calcium stability (Figures 17, 18, 19 and 20). However, our model can also exhibit sustained calcium balance at higher pacing rates. Figure 14A shows steady state cytosolic Ca^{2+} transients in response to a repetitive 4 Hz (which is more physiological for a rat ventricular myocyte) voltage clamp stimulation lasting for 2.5 seconds. The sustained peak and basal Ca^{2+} levels of $[Ca^{2+}]_{myo}$ over this prolonged time frame are indicative of long tern Ca^{2+} stability in the model. The corresponding $[Ca^{2+}]_{jSR}$ profile over 2.5 seconds is also shown in Figure 14A, which indicates sustained SR filling owing to the luminal sensor mediated control of the RyR channel. The stimulation protocol used is a pulse train of amplitude (-40 mv to 10 mv), duration (50 ms) and frequency of 4.0 Hz. Tables 9 and 10 provide values for the initial conditions used in our model.

Secondary $[Ca^{2+}]_{myo}$ transients induced by "tail currents"

Our voltage clamp simulations have dealt with clamp voltages in the range -30 mV ≤ V ≤ 40 mV. Some experimental studies [100,2,112] however have employed even larger clamp voltages (40 mV ≤ V ≤ 60 mV) to explore the high voltage behavior of the DHP-sensitive calcium channel. Such large clamp voltages elicit a brief Ca^{2+} influx called a "tail current", which has been shown to trigger RyR release and hence cause contraction during repolarization [100,2]. The secondary Ca^{2+} transient induced by the "tail current" is a critical argument in favor of CICR as these "tail currents" are not observed in skeletal muscle where the membrane potential directly controls SR Ca^{2+} release [112]. Our model reproduces this secondary Ca^{2+} transient observed during the return to resting potential from a large clamp voltage (≥ 40 mV). Figure 21A shows a cartoon depicting the voltage clamp stimulation protocol used in our study where a pulse of amplitude (-40 mV to +50 mV) is employed with the pulse duration (T_p; Figure 21A) increasing from 50 ms (trace 1) to 200 ms (trace 7) in steps of 25 ms. The clamp potential transition time (T_t) is fixed at 1 ms. The peak of the "tail current" at the end of the pulse is 25 times larger than the peak of the $I_{Ca,L}$ current observed at the beginning of the pulse. This is in agreement with model generated VC data reported by Geenstein et al.([8]; Figure 8). Figure 21B shows that, with an increase in clamp pulse duration, there is a corresponding increase in the peak of the trail current (see traces 1-7) until the effect ultimately saturates. Corresponding to this increase in peak $I_{Ca,L}$ tail current, there is an increase in the open probability of the RyR Ca^{2+}

Table 9 Initial Conditions

State variable	Definition	Initial Value
$[Ca^{2+}]_{myo}$	Ca^{2+} concentration in the myoplasm	8.1027×10^{-5} *mM*
$[Ca^{2+}]_{jSR}$	Ca^{2+} concentration in jSR	1.2677 *mM*
$[Ca^{2+}]_{LSR}$	Ca^{2+} concentration in LSR	1.3346 *mM*
$[Na^{+}]_{myo}$	Na^{+} concentration in myoplasm	16.746 *mM*
$[Na^{+}]_{dyad}$	Na^{+} concentration in dyadic space	16.321 *mM*
$[Cs^{+}]_{myo}$	Cs^{+} concentration in myoplasm	140.2154 *mM*
$[Cs^{+}]_{dyad}$	Cs^{+} concentration in dyadic space	140.2157 *mM*
O_c	Fractional occupancy of Calmodulin by Ca^{2+}	0.033091
O_{tc}	Fractional occupancy of Troponin by Ca^{2+}	0.016049
O_{tmgc}	Fractional occupancy of Troponin by Mg^{2+} and Ca^{2+}	0.321764
O_{tmgmg}	Fractional occupancy of Troponin by Mg^{2+}	0.598385
[*CaF* 3]	Concentration of Fluo3-Ca^{2+} complex	21.88721 μM
$C1_{ryr}$	Closed (resting) state of RyR channel	0.9990953
$O2_{ryr}$	Open (activated) state of RyR channel	1.03668×10^{-9}
$C3_{ryr}$	Inactivated state of RyR channel	9.38711×10^{-13}
$C1_{dhpr}$	Closed (resting) state of DHPR sensitive Ca^{2+} channel	0.1673614
$O2_{dhpr}$	Open (activated) state of DHPR sensitive Ca^{2+} channel	1.499173×10^{-3}
$O3_{dhpr}$	Open (activated) state of DHPR sensitive Ca^{2+} channel	3.300291×10^{-3}
$C4_{dhpr}$	Closed (resting) state of DHPR sensitive Ca^{2+} channel	7.478058×10^{-8}
$C6_{dhpr}$	Closed (resting) state of DHPR sensitive Ca^{2+} channel	7.478058×10^{-8}
$A1_{ls}$	Fraction of Tr/J bound to RyR	0.6709816
$I2_{ls}$	Fraction of Tr/J bound to RyR and Calsequestrin	0.155258
$I3_{ls}$	Fraction of Tr/J bound only to Calsequestrin	0.0623695
$B6_{ls}$	Fraction Calsequestrin bound to Ca^{2+}	0.619346
$[Ca^{2+}]_{serca}$	Ca bound to the serca protein	$36.0637 \times 10^{-5} \mu M$
$S2_{dhpr}$	Fraction of IQ Motif bound to Ca_4CaM	6.816729×10^{-2}
PLB_{dp}	Fraction of unphosphorylated Phospholamban	7.684160×10^{-2}
Ca_2CaM	2 Ca^{2+} ions bound to C-terminus of CaM	34.56529
Ca_4CaM	4 Ca^{2+} ions bound to C & N terminus of CaM	8.635052×10^{-2}
CaMB	Buffered CaM	7.563836×10^{-2}
Ca_2CaMB	Buffered Ca_2CaM	2.035086
Ca_4CaMB	Buffered Ca_4CaM	1.288455×10^{-6}
Ca_4CaN	CaN bound to 4 Ca^{2+} ions	$2.606246 \times 10^{-4} \mu M$
CaMCaN	CaN bound to CaM	$4.348535 \times 10^{-3} \mu M$
$Ca_2CaMCaN$	CaN bound to 2 Ca^{2+} ions and CaM	$1.419613 \times 10^{-1} \mu M$
$Ca_4CaMCaN$	CaN bound to 4 Ca^{2+} ions and CaM	$3.473412 \mu M$
$[Ca^{2+}]_{dyad}$	Ca^{2+} concentration in the dyadic space	9.012×10^{-5} *mM*

Table 9: Initial conditions used for the state vector in order to solve the linearized system of ordinary differential equations.

channel, with RyR Ca^{2+} release indicated by the corresponding decrease in $[Ca^{2+}]_{jSR}$ (panel C) and increase in $[Ca^{2+}]_{myo}$ (panel D). We note from Figure 21C that for a shorter 50 ms VC pulse, there is no RyR Ca^{2+} release although an $I_{Ca,L}$ tail current is produced. This tail current produced with the 50 ms pulse slightly augments the $[Ca^{2+}]_{myo}$ transient just after its peak (trace 1, panel E), but there is no corresponding decrease in the $[Ca^{2+}]_{jSR}$ transient (trace 1, panel D) indicating no RyR Ca^{2+} release.

Table 10 Initial Conditions

State variable	Definition	Initial Value
P_1	Fraction of inactive dephosphorylated CaMKII in Ca_2CaM bound state	5.527608×10^{-1}
P_3	Fraction of active dephosphorylated CaMKII in Ca_4CaM bound state	3.661260×10^{-1}
P_6	Fraction of active Thr^{287}-autophosphorylated but CaM autonomous CaMKII	1.314410×10^{-3}
P_5	Fraction of active Thr^{287}-autophosphorylated but Ca2CaM bound CaMKII	6.277911×10^{-7}
$P4$	Fraction of active Thr^{287}-autophosphorylated but Ca4CaM trapped CaMKII	9.121920×10^{-8}

Table 10: Initial conditions used for the state vector in order to solve the linearized system of ordinary differential equations.

At the end of this short pulse (50 ms), the RyR channel is in fact in its absolute refractory period. The small secondary increase in $[Ca^{2+}]_{myo}$ transient as seen in data corresponding to trace 4 of Figure 7C is a result of the large Ca^{2+} influx via the $I_{Ca,L}$ "tail current". During this phase, the Na^+/Ca^{2+} exchanger is biased to extrude Ca^{2+} out of the dyad, and hence cannot be responsible for this secondary rise in the cytosolic Ca^{2+} transient. As pulse duration is increased beyond 100 ms the "tail current" causes a

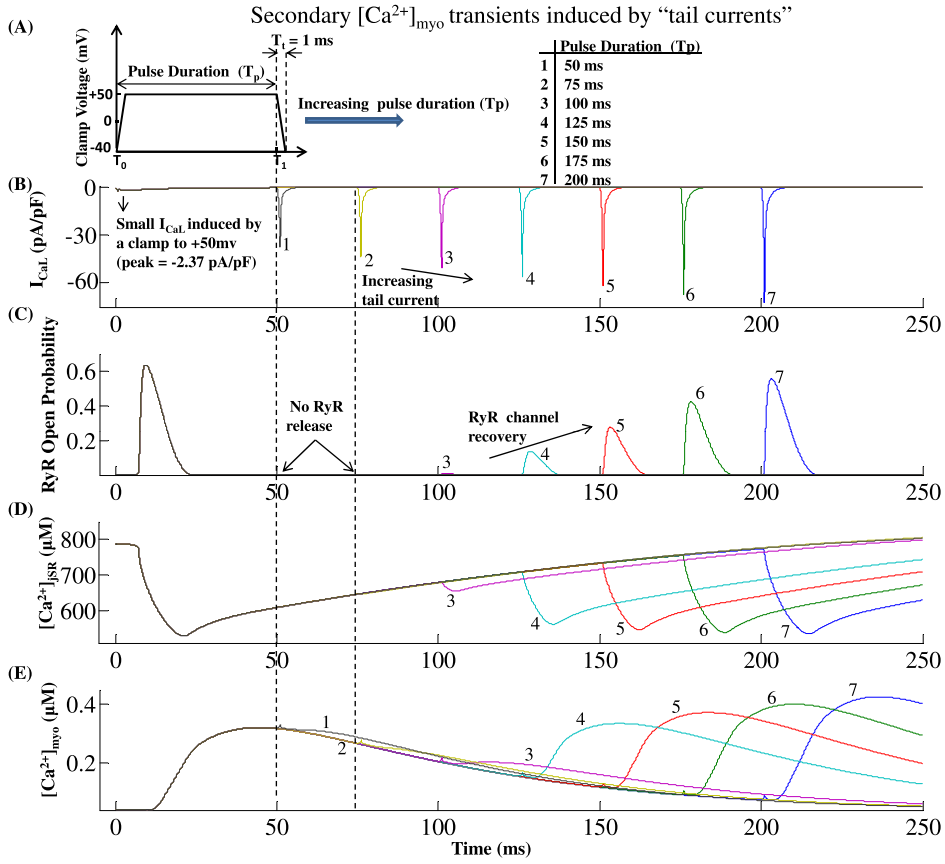

Figure 21 Secondary $[Ca^{2+}]_{myo}$ transients induced by "tail currents". Figure 21: The stimulation protocol used is a pulse of amplitude (-40 mv to +50 mv) with pulse duration T_p increasing from 50 ms (trace 1) to 200 ms (trace 7) in steps of 25 ms. (A) A cartoon depicting the voltage clamp stimulus protocol where, pulse duration (T_p) is varied to obtain traces 1-7 and the clamp potential transition time (T_t) fixed at 1 ms. (B) $I_{Ca,L}$ tail currents elicited during repolarization from +50 mv to -40 mv. (C) Open probability of the RyR channel indicating gradual recovery from the refractory period (D) $[Ca^{2+}]_{jSR}$ traces show increase in RyR release with increasing pulse duration as a result of adequate RyR channel recovery. (E) Cytosolic calcium transients indicate secondary RyR release caused by tail currents.

gradual increase in RyR open probability (traces 3-7 in Figure 21) indicating progressive recovery from the refractory period. Minimum value of $[Ca^{2+}]_{jSR}$ in traces 3-7 of Figure 21D show increase in SR Ca^{2+} release with increasing pulse duration as a result of adequate RyR channel recovery and increasing $I_{Ca,L}$ "tail current". Cytosolic Ca^{2+} transients shown in Figure 21E indicate "tail current" induced secondary RyR release for pulse duration ≥ 100 ms. It has also been previously reported [113] that recruitment of an additional population of previously 'silent' Ca^{2+} channels could cause facilitation of tail currents at increasingly large clamp voltages with a time-dependence associated with the recruitment process. Our model not only accounts for the contribution of the already open channels (in states $O2_{dhpr}$ &$O3_{dhpr}$) to the tail current during repolarization but also allows for the voltage- and time-dependent recruitment of 'silent' Ca^{2+} channels modeled using a high voltage state $C6_{dhpr}$. This study proves to be an adjunct to the study presented in Figure 13 in establishing the refractory nature of the RyR channel.

Cytosolic Buffering

In our model, cytosolic buffering is attributed to several factors including: (a) calmodulin (CaM); (b) the Ca^{2+}-specific (Tc) troponin binding site; (c) the Ca^{2+} - Mg^{2+} competitive troponin binding site; and (d) the fluorescent indicator dye Fluo3 used to detect changes in $[Ca^{2+}]_{myo}$. The effects of the component buffers in helping to maintain a low $[Ca^{2+}]_{myo}$ are shown in Figure 22 in terms of occupancy functions, such as O_C

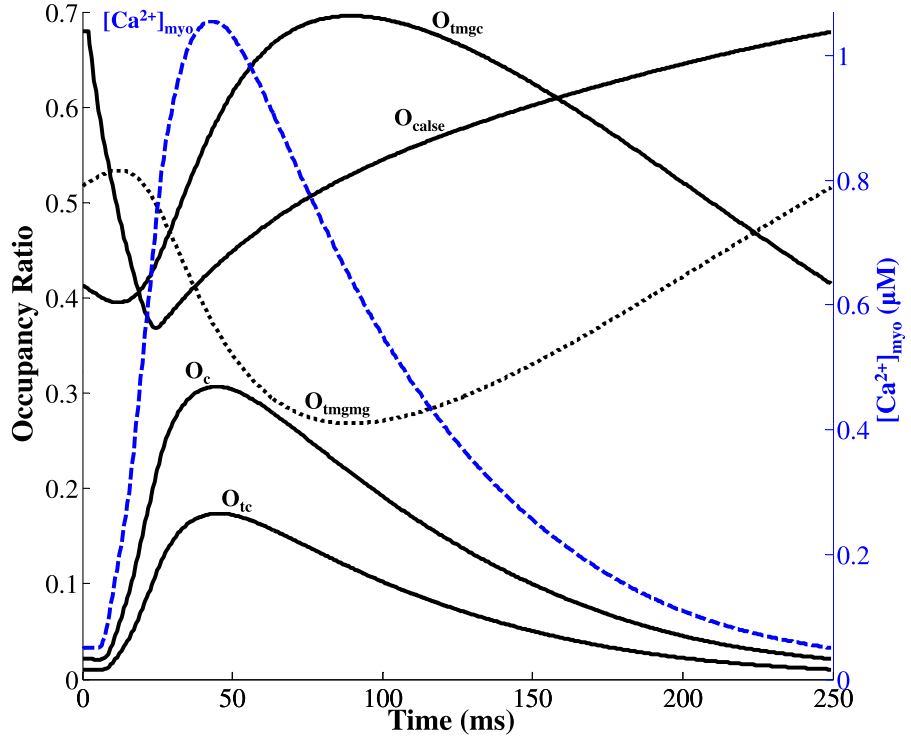

Figure 22 Occupancy of Ca^{2+} buffers. Figure 22: Contributions of fractional occupancy of Ca^{2+} buffers in SR and cytoplasm. Transfer from O_c and O_{tc} to O_{tmgc} occurs as a result of the pulse stimulation. O_{tmgmg} is shown as a dotted line as it does not reflect Ca^{2+} binding. The corresponding $[Ca^{2+}]_{myo}$ is overlayed (note the different axis)

(fractional occupancy of calmodulin by Ca^{2+}), O_{tc} (fractional occupancy of troponin-Ca sites by Ca^{2+}), O_{tmgc} (fractional ocupancy of troponin-Mg sites by Ca^{2+}), O_{tmgmg} (fractional occupancy of troponin-Mg sites by Mg^{2+}) in the cytosol, and O_{calse} (fractional occupancy of calsequestrin by Ca^{2+}) in the jSR Ca^{2+} release compartment. Figure 22 shows that when the Ry-sensitive Ca^{2+} release channel is triggered, the jSR releases Ca^{2+} and the occupancy O_{calse} in the jSR, declines from 68% to 37%. Ca^{2+} release from the jSR induces fast Ca^{2+} binding by calmodulin and troponin in the cytosol, as represented by the increases of O_c (0.29) and O_{tc} (0.16) in Figure 22. Interactions between Ca^{2+} and the troponin-Mg sites result in an increase in occupancy of these sites by Ca^{2+} (O_{tmgc}), and a decrease in occupancy by Mg^{2+} (O_{tmgmg}).

Discussion

It is well-established that mammalian cardiac excitation-contraction coupling is mediated by calcium-induced calcium release (CICR). We have developed a comprehensive mechanistic model of CICR under voltage clamp conditions in the rat ventricular myocyte, which includes electrical equivalent circuit models for both the free sarcolemma and that portion involving junctional transmission, as well as, fluid compartment models for several fluid media within the cell (dyadic cleft space, longitudinal sarcoplasmic reticulum (LSR or Ca^{2+} uptake compartment), junctional sarcoplasmic reticulum (jSR or release compartment), and the cytosolic fluid compartment). An external bathing medium completes our fluid compartment description of the cell Figure 1. The multiple component model is referred to as the "whole-cell model" (Figures 1 and 2). We have probed the mechanisms regulating Ca^{2+} in the cell. In particular, we have focused on the dyadic mechanisms effecting CICR.

The dyadic controller is a finely tuned coupling device consisting of two opposed Ca^{2+} channels separated by a small dyadic space (Figure 1B): the sarcolemmal DHP-sensitive "trigger" channel and the Ry-sensitive jSR Ca^{2+} release channel. The trigger channel is voltage-activated and is driven in our simulations by a voltage clamp pulse which opens the channels, admitting Ca^{2+} influx (trigger current) to the dyadic space. After diffusion within the dyadic space, trigger Ca^{2+} affects the Ca^{2+} dependent open probability of the jSR Ca^{2+} release channel over a small range of Ca^{2+} concentrations. Clamp voltage magnitude strongly affects the $I_{Ca,L}$ current and hence the amount of Ca^{2+} delivered to the dyadic space, but the range over which the Ca^{2+} concentration at the mouth of the Ca^{2+} release channel changes (in the absence of RyR release) is quite small (23.42μM to 8.82μM for a change in VC from 10 mv to 40 mv). The RyR-mediated Ca^{2+} release is activated by trigger current, but the release itself is affected by the concentration gradient between the jSR and the dyadic space, and the temporal and refractory properties of the ryanodine receptor (Figure 13). The four-state RyR model is informed regarding supply Ca^{2+} content by the jSR luminal sensor, a novel feature in our model which characterizes the important protein-protein interactions between calsequesterin, triadin/junctin and the RyR receptor. Triadin/junctin strongly regulates the sensitivity of RyR to trigger Ca^{2+}. Hence the luminal sensor, which is a key element responsible for robust post-release RyR inactivation and refractoriness of the Ry-sensitive Ca^{2+} release channel, is critical in providing realistic fits to cytosolic Ca^{2+} transients and an adequate refilling time for the SR Ca^{2+} stores. Ca^{2+} release is thus graded with Ca^{2+} concentration at

the mouth of Ca^{2+} channel in a very sensitive manner with a gain of approximately 7, as is shown in Figure 12.

The sarcolemmal portion of the dyadic membrane defining the dyadic space contains voltage-sensitive Ca^{2+} channels and deals with changes in the external environment of the ventricular cell (e.g., membrane response to changes in transmembrane potential and chemical signaling agents). It integrates these various stimuli and delivers a trigger current to the small dyadic space. In contrast, the jSR membrane lining the opposite boundary of the dyadic space is concerned with the adequacy of Ca^{2+} release in CICR. It contains Ry-sensitive Ca^{2+} channels that require a Ca^{2+} concentration gradient directed across the channel and into the dyadic space for their operation. Thus, jSR Ca^{2+} concentration must be maintained within an acceptable range so that calcium is always available for ready release. The relationship between jSR Ca^{2+} content and peak $[Ca^{2+}]_{myo}$ is shown in Figure 16A. The LSR compartment connects the jSR compartment with the cytosolic compartment. It feeds make-up calcium to the jSR, by using a SERCA pump to actively draw in Ca^{2+} from the myoplasm. Pumping rate is controlled by the cytosolic Ca^{2+} concentration $[Ca^{2+}]_{myo}$ as well as the LSR Ca^{2+} concentration $[Ca^{2+}]_{LSR}$ as part of a mechanism for replenishing and maintaining jSR Ca^{2+} stores. Our model also incorporates the Ca^{2+} induced CaM mediated effects of CaMKII and CaN on targets such as the DHP-sensitive $I_{Ca,L}$ channel, Ry-sensitive Ca^{2+} release channel, as well as the SR Ca^{2+} ATPase pump. Provision for the effects of phospholamban on SERCA has also been included.

The voltage-gated and chemically gated channels of the dyad are tightly coupled by feedback mechanisms that involve Ca^{2+} signaling. Although physically separated, the voltage-sensitive Ca^{2+} channel (Figure 9) as well as the Ry-sensitive release channel (Phase C in Figure 15) are inhibited by increased Ca^{2+} levels in the dyadic space [53]. In earlier models which lacked the luminal sensor, RyR self-inhibition by dyadic Ca^{2+} was the only mechanism besides stochastic attrition (both of which are inadequate in effecting a robust RyR channel closure) that was given the role of initiating RyR recovery. This has been tested in our model by artificially clamping all the variables (including concentration at the mouth of the RyR channel) to the levels reached at T2 in Figure 15 despite which the RyR open probability, begins to decline in phase C of Figure 15 showing the self-inhibitory role of high dyadic Ca^{2+} concentration. Our model predicts (data not shown) that this Ca^{2+} signaling continues even in the presence of high concentrations of Ca^{2+} buffering agents in the cytosol (in agreement with the data of Adachi-Akahane et al. [71] and Diaz et al. [110]). Tight coupling between the DHP and Ry-sensitive Ca^{2+} channels within the dyadic space thus preserves the mechanism of CICR under these extreme conditions.

Regulation of cytosolic Ca^{2+} concentration $[Ca^{2+}]_{myo}$ is evident at the cellular level. It is affected strongly by the voltage and $[Ca^{2+}]_{myo}$-dependent properties of the sarcolemmal currents I_{NaCa} and $I_{Ca,L}$, as well as the $[Ca^{2+}]_{myo}$-dependent properties of the I_{PMCA} and SERCA pumps. We demonstrate a model-generated whole-cell Ca^{2+} balance, which shows the importance of the Na^{+}/Ca^{+} exchanger in extruding the Ca^{2+} that has entered the cell under normal activity, and also any excess that might occur when cytosolic Ca^{2+} levels rise. The variety of experiments emulated in this study demonstrates quantification of Ca^{2+} balances for all external and internal Ca^{2+} fluxes and shows that the model has long-term stability in regulating cytosolic Ca^{2+}, as

shown in the 120-sec duration experiments of Negretti et al. (Figure 20) at a pulse repetition rate of 0.33 Hz., and the faster paced stimulation at 4 Hz shown in Figure 14A.

We have examined the dyadic component of the $I_{Ca,L}$ with regard to its Ca^{2+} -dependent inactivation as a function of jSR Ca^{2+} content (Figure 17C). Trigger current is voltage-dependent and therefore parameterized by clamp pulse amplitude (Figure 7A). In addition, its inactivation is Ca^{2+} dependent, especially during Ca^{2+} release. At a constant depolarizing voltage pulse, the pre-release jSR Ca^{2+} content dictates the peak of the cytosolic Ca^{2+} transient (Figure 16A), by controlling peak Ca^{2+} concentration in individual dyads. As jSR Ca^{2+} content increases, so does the peak dyadic Ca^{2+} concentration, and the amount of sarcolemmal Ca^{2+} influx declines due to greater Ca^{2+} dependent inactivation. This autoregulatory feedback mechanism helps to establish a stable operating point for jSR Ca^{2+} content. Transient *increases* in jSR Ca^{2+} content bring about increases in Ca^{2+} release, but reflexly, decrease sarcolemmal Ca^{2+} influx via $I_{Ca,L}$. Coupled with other dyadic and extra-dyadic mechanisms (I_{NaCa}) that decrease $[Ca^{2+}]_{myo}$ and hence Ca^{2+}-uptake via the SERCA pump, jSR Ca^{2+} content decreases. For *decreases* in jSR Ca^{2+} content, the opposite occurs, so that regardless of the sign of the perturbation in jSR Ca^{2+} content, it tends to stay constant in the steady-state. This is an important feature of the dyadic mechanism that preserves the integrity of CICR. The gain of this feedback system about the operating point is visualized as the slope of the peak Ca^{2+} transient vs SR Ca^{2+} content characteristic (Figure 16A) for a given voltage pulse level. Observing this figure, we note that there is a linear operating range beyond which the system gain increases dramatically. Our model results also show that a decrease of jSR Ca^{2+} content (simulated either by a decrease of Ca^{2+} uptake into the LSR by thapsigargin or an increase of Ca^{2+} leak out of the jSR by caffeine) decreases systolic $[Ca^{2+}]_{myo}$, and hence the model might serve as a useful adjunct in a study of heart failure, where decreased contractility as a result of diminished Ca^{2+} transients are commonly observed [114].

Model Limitations

(a) This model of a rat ventricular myocyte is limited to Ca^{2+} related channel, exchanger and pumps ($I_{Ca,L}$, I_{NaCa}, I_{PMCA} and SERCA pump), while lacking exclusive Na^{+} or K^{+} related channels and transporters and is based on data at positive potentials in the range 10 mV ≤ V ≤ 40 mV. It is aimed at mimicking voltage clamp conditions where channels other than calcium are blocked, and it cannot be used to study experiments involving the generation of action potentials. However, its focus on the Ca^{2+} dynamics allows one to comprehend more clearly the important role of Ca^{2+} signalling pathways and feedback control systems in maintaining whole cell homeostasis over a prolonged period of time.

(b) A single dyadic space in our model has one representative, lumped DHP-sensitive and Ry-sensitive Ca^{2+} channel, on opposing sarcolemmal and SR surfaces respectively. This simplified configuration does not conform to detailed structural information regarding the geometrical relationships between DHP and RyR-sensitive Ca^{2+} channels [115,55,116] and thus cannot be used to draw conclusions about this part of the EC coupling process. However, our lumped abstraction forms a functional model of the dyadic coupling unit that can produce accurate predictions of cytosolic

Ca^{2+} transients. The effectiveness of this model is further demonstrated by its ability to accurately characterize the interaction between the DHP and Ry-sensitive Ca^{2+} channels, including pulse duration dependent termination of release (Figure 11), Ca^{2+} dependent inactivation of $I_{Ca,L}$ (Figures 7, 9), as well as the wide variety of whole-cell voltage clamp protocols (Figures 17, 18, 19 and 20).

(c) Although our model provides secondary Ca^{2+} tail transients elicited by $I_{Ca,L}$ "tail currents" (Figure 21), this aspect of the model has not been verified extensively due to paucity of measured VC data showing tail transients over the high voltage range ($40 \leq V \leq 60$) in rat ventricular myocytes. Our $I_{Ca,L}$ tail currents are in general agreement with model generated data at a clamp voltage of 50 mV reported by Greenstein et al. ([8]; Figure 8). The restitution time for the RyR channel in rat ventricular myocytes is believed to be at least 25 ms [117] and as fast as 150 ms [118] indicating the wide range of values reported in the literature. We demonstrate model-generated RyR refractoriness by changing the duration of the simulated VC pulse and obtain RyR recovery characteristics that are consistent with measured data for Ca^{2+} spark restitution in rat ventricular myocytes reported by Sobie et al. [106]. However, our results on this important phenomena, particularly the onset of tail transients with increasing inter-stimuli interval are preliminary and further modeling investigations would benefit considerably from the availability of additional measured data.

Conclusion

We have developed a mathematical model of Ca^{2+} dynamics under voltage clamp conditions in the rat ventricular myocyte, which is based solidly on experimental data and includes the most extensive description available of a novel feature, namely the luminal Ca^{2+} sensor in the junctional SR which models the protein-protein interaction between triadin/junctin, calsequestrin and the RyR channel. The luminal sensor imparts the much needed refractoriness to the Ry-sensitive Ca^{2+} release channel. This element is critical in providing realistic fits to cytosolic Ca^{2+} transients and an adequate refilling time for the SR Ca^{2+} stores. Our voltage-clamp simulations demonstrate graded Ca^{2+} transients with sufficient gain, as well as quantification of Ca^{2+} balances for all external and internal Ca^{2+} fluxes. Our model of the dyadic coupling unit (DCU) provides mechanistic explanations of the major input-output relationship for CICR (Figure 16), as well as its modulation by trigger current (clamp voltage). The variety of experiments emulated in this study demonstrates that the model has long-term stability in regulating cytosolic Ca^{2+}, as shown in the 120-sec duration experiments of Negretti et al. (Figure 20) at a pulse repetition rate of 0.33 Hz., and the faster (physiological) paced stimulation at 4 Hz shown in Figure 14A. It also provides biophysically based insights into the molecular mechanisms underlying whole-cell responses to the wide variety of testing approaches used in voltage clamp studies of myocytes that have appeared in the literature over the past two decades (Figures 17, 18, 19 and 20). Thus, the model serves as a platform for the predictive modeling of VC investigations in a number of areas. These include new hypotheses with regards to the under-expression of triadin/junctin resulting in a malfunctioning luminal sensor, which could affect long-term calcium stability of the cell (Figure

14B), and/or changes in the refractoriness of the RyR Ca^{2+} channel (Figures 13 and 21) affecting the integrity of CICR under a variety of conditions. These are fundamental issues that would benefit from a better mechanistic understanding of deranged calcium signalling in the rat ventricluar myocyte. This study is aimed at providing an initial step towards this goal.

Appendix

Below is the complete set of equations used in the model.

A1 - Equations for currents in the model

L-Type Ca^{2+} current

Ca^{2+} current through the DHP-sensitive $I_{Ca,L}$ channel

$$I_{Ca,L} = R_{Ca,L}(O2_{dhpr} + O3_{dhpr})P_{Ca}Z_{Ca}^2\frac{F^2V}{RT}\times \left(\frac{[Ca^{2+}]_{dhp}e^{\frac{2FV}{RT}} - 341.0[Ca^{2+}]_0}{e^{\frac{2FV}{RT}} - 1}\right) \quad (1)$$

Na^+ current through the DHP-sensitive $I_{Ca,L}$ channel

$$I_{Na} = \frac{1.056\times e^{\left(\frac{v-21.73}{21.23841}\right)}}{1.056\times e^{\left(\frac{v-21.73}{21.23841}\right)} + [Ca_o^{2+}]}P_{Na}Z_{Na}^2\frac{F^2V}{RT}\times \left(\frac{0.75[Na^+]_{dhp}e^{\frac{FV}{RT}} - 0.75[Na^+]_0}{e^{\frac{FV}{RT}} - 1}\right) \quad (2)$$

Cs^+ current through the DHP-sensitive $I_{Ca,L}$ channel

$$I_{Cs} = \frac{1.056\times e^{\left(\frac{v-21.73}{21.23841}\right)}}{1.056\times e^{\left(\frac{v-21.73}{21.23841}\right)} + [Ca_o^{2+}]}P_{Cs}Z_{Cs}^2\frac{F^2V}{RT}\times \left(\frac{0.75[Cs^+]_{dhp}e^{\frac{FV}{RT}} - 0.75[Cs^+]_0}{e^{\frac{FV}{k_{Cs}RT}} - 1}\right) \quad (3)$$

where k_{Cs} = 0.5 and $[Ca^{2+}]_{dhp}$, $[Na^+]_{dhp}$, $[Cs^+]_{dhp}$ are Concentrations at the mouth of the DHP-sensitive Ca^{2+} channel.

The corresponding unitary currents $i_{Ca,L}$, i_{Na}, i_{Cs} are obtained by dividing the above net channel currents by the number of dyadic units, N_{dyad}.

Gating scheme for the 2-state Markovian model used to allow Ca^{2+} mediated interaction of the DHP-sensitive $I_{Ca,L}$ channel and calmodilin:

$$S1_{dhpr} = 1 - S2_{dhpr} \quad (4)$$

$$\frac{dS2_{dhpr}}{dt} = ks_{12}^{dhpr} S1_{dhpr} - ks_{21}^{dhpr} S2_{dhpr} \tag{5}$$

Expressions for the rate constants:

$$ks_{12}^{dhpr} = 4.0 \times e^{\left(\frac{[Ca_4CaM]_{dhp} - 100.0}{90.0}\right)} \tag{6}$$

$$ks_{21}^{dhpr} = 18.0 \tag{7}$$

Gating scheme for the 6-state Markovian model for the DHP-sensitive L-type Ca^{2+} release channel:

$$\begin{aligned} C5_{dhpr} &= 1 - (C1_{dhpr} + O2_{dhpr} + O3_{dhpr}) \\ &\quad -(C4_{dhpr}) \end{aligned} \tag{8}$$

$$\begin{aligned} \frac{dC1_{dhpr}}{dt} &= k_{21}^{dhpr} O2_{dhpr} + k_{51}^{dhpr} C5_{dhpr} \\ &\quad -(k_{12}^{dhpr} + k_{15}^{dhpr}) C5_{dhpr} \end{aligned} \tag{9}$$

$$\begin{aligned} \frac{dO2_{dhpr}}{dt} &= k_{12}^{dhpr} C1_{dhpr} + k_{42}^{dhpr} C4_{dhpr} \\ &\quad + k_{32}^{dhpr} O3_{dhpr} + k_{52}^{dhpr} C5_{dhpr} \\ &\quad -(k_{21}^{dhpr} + k_{23}^{dhpr}) O2_{dhpr} \\ &\quad -(k_{24}^{dhpr} + k_{25}^{dhpr}) O2_{dhpr} \end{aligned} \tag{10}$$

$$\frac{dO3_{dhpr}}{dt} = k_{23}^{dhpr} O2_{dhpr} - k_{32}^{dhpr} O3_{dhpr} \tag{11}$$

$$\begin{aligned} \frac{dC4_{dhpr}}{dt} &= k_{54}^{dhpr} C5_{dhpr} + k_{24}^{dhpr} O2_{dhpr} \\ &\quad -(k_{45}^{dhpr} + k_{42}^{dhpr}) C4_{dhpr} \end{aligned} \tag{12}$$

$$\frac{dC6_{dhpr}}{dt} = k_{36}^{dhpr} O3_{dhpr} - k_{63}^{dhpr} C6_{dhpr} \tag{13}$$

The open state $O3_{dhpr}$ accounts for the increased tail current produced as the result of a large depolarization. Expressions for rate constants:

$$k_{42}^{dhpr} = 1000.0 \tag{14}$$

$$k_{45}^{dhpr} = 600000.0 \tag{15}$$

$$k_{54}^{dhpr} = \frac{k_{45}^{dhpr} k_{52}^{dhpr} k_{24}^{dhpr}}{k_{42}^{dhpr} k_{25}^{dhpr}} \tag{16}$$

$$k_{15}^{dhpr} = \frac{k_{51}^{dhpr} k_{12}^{dhpr} k_{25}^{dhpr}}{k_{52}^{dhpr} k_{21}^{dhpr}} \tag{17}$$

- **Case 1:** With CICR (control)

$$k_{12}^{dhpr} = \left(300.3808 - \frac{301.0817}{1 + e^{\left(\frac{v - 13.5918}{8.85} \right)}} \right) \tag{18}$$

$$k_{21}^{dhpr} = \left(3359.8754 + \frac{966.95}{1 + e^{\left(\frac{v - 1.66}{1.4585} \right)}} \right) \tag{19}$$

$$\xi = 550 + 6 \times CaMKII_{act} + CaN_{act} \tag{20}$$

$$k_{24}^{dhpr} = \left(\frac{336160 \times S2_{dhpr}}{\xi} \right) \tag{21}$$

$$k_{25}^{dhpr} = \left(\frac{5939.4 + \frac{306806.8}{1 + e^{\left(\frac{v + 1.8716}{1.3072} \right)}}}{\xi} \right) \tag{22}$$

$$k_{52}^{dhpr} = \left(0.02925 + \frac{0.48961}{1 + e^{\left(\frac{v + 12.2249}{0.974} \right)}} \right) \tag{23}$$

$$k_{23}^{dhpr} = \left(1352 - \frac{1350}{1 + e^{\left(\frac{v}{1.8} \right)}} + \frac{1700}{1 + e^{(v+5)}} \right) \tag{24}$$

$$k_{32}^{dhpr} = \left(1030.0575 - \frac{713.1966}{1 + e^{(v-5.0)}} \right) \tag{25}$$

$$k_{51}^{dhpr} = \frac{383.5435}{1+e^{-\left(\frac{v-8.3702}{7.047}\right)}} + \frac{0.16725}{1+e^{-\left(\frac{v-31.8252}{0.01075}\right)}} + \frac{378.7085}{1+e^{\left(\frac{v-7.8953}{6.7691}\right)}} - 373.015 \tag{26}$$

$$k_{36}^{dhpr} = \left(100 - \frac{100.0}{1+e^{\left(\frac{v-41.0}{1.0}\right)}} \right) \tag{27}$$

$$k_{63}^{dhpr} = \left(\frac{600.0}{1+e^{\left(\frac{v-41.0}{1.0}\right)}} \right) \tag{28}$$

- **Case 2:** With Ryanodine applied (no RyR release)

$$k_{12}^{dhpr} = \left(30392.87 - \frac{30394.73}{1+e^{\left(\frac{v-183.5975}{28.5662}\right)}} \right) \tag{29}$$

$$k_{21}^{dhpr} = \left(3568.74658 + \frac{21921.25344}{1+e^{\left(\frac{v+24.9838}{0.7372}\right)}} \right) \tag{30}$$

$$\xi = 550 + 6 \times CaMKII_{act} + CaN_{act} \tag{31}$$

$$k_{24}^{dhpr} = \left(\frac{336160 \times S2_{dhpr}}{\xi} \right) \tag{32}$$

$$k_{25}^{dhpr} = \frac{0.0893 + \frac{26.3268}{1+e^{\left(\frac{v+15.0}{1.0}\right)}}}{\xi} \tag{33}$$

$$+ \frac{\frac{32.6642}{1+e^{-\left(\frac{v-14.4897}{0.3131}\right)}} + \frac{63.808}{1+e^{\left(\frac{v-27.411}{0.0854}\right)}}}{\xi} \tag{34}$$

$$k_{52}^{dhpr} = 2.69 + \frac{0.74152}{1 + e^{\left(\frac{v+27.945}{1.46976}\right)}} - \frac{2.43098}{1 + e^{\left(\frac{v-40.25}{0.4034}\right)}} \tag{35}$$

$$k_{23}^{dhpr} = 1908 - \frac{2687.3087}{1 + e^{\left(\frac{v+15.0}{0.9998}\right)}} + \frac{879.543}{1 + e^{\left(\frac{v-11.1635}{0.3238}\right)}} \tag{36}$$

$$k_{32}^{dhpr} = 145107.50934 - \frac{150299.048}{1 + e^{\left(\frac{v-1037.5224}{312.91482}\right)}} + \frac{5537.7875}{1 + e^{\left(\frac{v-9.4649}{0.2893}\right)}} \tag{37}$$

$$k_{51}^{dhpr} = \frac{27.651}{1 + e^{-\left(\frac{v-59.48}{4.444}\right)}} + \frac{11.488}{1 + e^{-\left(\frac{v+15.1148}{0.9423}\right)}} - \frac{16.3777}{1 + e^{-\left(\frac{v+15.01}{0.6351}\right)}} + 5.3384 \tag{38}$$

$$k_{36}^{dhpr} = \left(100 - \frac{100.0}{1 + e^{\left(\frac{v-41.0}{1.0}\right)}}\right) \tag{39}$$

$$k_{63}^{dhpr} = \left(\frac{600.0}{1 + e^{\left(\frac{v-41.0}{1.0}\right)}}\right) \tag{40}$$

- **Case 3:** With Ca^{2+} substituted with Ba^{2+}

$$k_{12}^{dhpr} = 3028.7604 - \frac{6279.833}{1 + e^{\left(\frac{v-58.1484}{9.5348}\right)}} + \frac{3259.706}{1 + e^{\left(\frac{v-40.2856}{0.2272}\right)}} \tag{41}$$

$$k_{21}^{dhpr} = \frac{26296.0826}{1+e^{\left(\frac{v+17.40398}{0.22797}\right)}} + \frac{4718.8152}{1+e^{-\left(\frac{v+1.4892}{4.9581}\right)}} + \frac{1544.9745}{1+e^{-\left(\frac{v-132.7305}{3.6234}\right)}} - 808.0319 \tag{42}$$

$$k_{24}^{dhpr} = (0.0) \tag{43}$$

$$k_{25}^{dhpr} = -5883.3476 + \frac{5973.3014}{1+e^{\left(\frac{v-41.4221}{0.5703}\right)}} \frac{528.171}{1+e^{-\left(\frac{v-20.4274}{0.187}\right)}} \tag{44}$$

$$k_{52}^{dhpr} = 175.78742 - \frac{174.7872}{1+e^{\left(\frac{v-32.3072}{4.4783}\right)}} - \frac{229.8479}{1+e^{-\left(\frac{v-36.9508}{5.4521}\right)}} \tag{45}$$

$$k_{23}^{dhpr} = \frac{2601.9597}{1+e^{\left(\frac{v-19.882}{0.4459}\right)}} - \frac{2647.5114}{1+e^{\left(\frac{v+15.6872}{2.1947}\right)}} - \frac{2501.6394}{1+e^{\left(\frac{v-39.8404}{0.3926}\right)}} + 2647.2042 \tag{46}$$

$$k_{32}^{dhpr} = \frac{1683.7686}{1+e^{-\left(\frac{v-20.0452}{0.40326}\right)}} + \frac{2161.9699}{1+e^{\left(\frac{v-360.2862}{1879.441}\right)}} - \frac{5926.5225}{1+e^{-\left(\frac{v+1.7842}{13.43183}\right)}} + 4129.8882 \tag{47}$$

$$k_{51}^{dhpr} = \frac{11.1993}{1+e^{-\left(\frac{v-35.2478}{0.2466}\right)}} + \frac{36.2341}{1+e^{-\left(\frac{v+23.9615}{15.8653}\right)}} - \frac{12.163}{1+e^{-\left(\frac{v-27.1529}{0.9455}\right)}} + 37.7673 \tag{48}$$

$$k_{36}^{dhpr} = \left(100 - \frac{100.0}{1 + e^{\left(\frac{v-41.0}{1.0}\right)}} \right) \tag{49}$$

$$k_{63}^{dhpr} = \left(\frac{600.0}{1 + e^{\left(\frac{v-41.0}{1.0}\right)}} \right) \tag{50}$$

Uptake of Ca^{2+} from the cytosol into the LSR

Ca^{2+} fluxes from cytosol to SERCA and SERCA to LSR

$$\begin{aligned} J_{cyt,serca} &= k_{cyt,serca} \times [Ca^{2+}]_{myo}^2 \times SERCA_{tot} \\ &\quad - k_{cyt,serca} \times [Ca^{2+}]_{myo}^2 \times [Ca^{2+}]_{serca} \\ &\quad - k_{serca,cyt} \times [Ca^{2+}]_{serca} \end{aligned} \tag{51}$$

$$\begin{aligned} J_{serca,sr} &= k_{sr,serca} \times [Ca^{2+}]_{LSR}^2 \times [Ca^{2+}]_{serca} \\ &\quad - k_{sr,serca} \times [Ca^{2+}]_{LSR}^2 \times SERCA_{tot} \\ &\quad + k_{cyt,sr} \times [Ca^{2+}]_{myo} \end{aligned} \tag{52}$$

$$I_{cyt,serca} = J_{cyt,serca} \times 2FV_{serca} \tag{53}$$

$$I_{serca,sr} = J_{serca,sr} \times 2FV_{serca} \tag{54}$$

Differential equation for Ca^{2+} buffered by the SERCA protein:

$$\frac{d[Ca^{2+}]_{serca}}{dt} = J_{cyt,serca} - J_{serca,sr} \tag{55}$$

Expressions for the rate constants for Ca^{2+} binding to/release from SERCA:

$$k_{cyt,serca} = K_{cyt,serca}(1.07 + 5500 \times CaMKII_{act}) \tag{56}$$

$$K_{cyt,serca} = K_{cyt,serca}(\ EC_{50}^{fwd})^2 \tag{57}$$

$$k_{serca,sr} = K_{serca,sr}(1.07 + 5500 \times CaMKII_{act}) \tag{58}$$

$$k_{sr,serca} = \frac{K_{serca,sr}}{(EC_{50}^{bwd})^2} \tag{59}$$

Affinities for the forward and backward Ca^{2+} fluxes:

$$EC_{50}^{fwd} = 0.015(1 + PSR \times PLB_{dp}) \times \left(\frac{1.027}{1 + 5500 \times CaMKII_{act}} \right) \tag{60}$$

$$EC_{50}^{bwd} = 1250 - 1110 \times PSR \times PLB_{dp} \tag{61}$$

Differential equation for phospholamban

$$\frac{dPLB_{dp}}{dt} = k_{12}^{PLB} PLB_p - k_{21}^{PLB}(5500 CaMKII_{act} + 2.5 CaN_{act} + PKA_{act})^2 PLB_{dp} \tag{62}$$

$$PLB_p = 1 - PLB_{dp} \tag{63}$$

Ca^{2+} pump in SL

$$I_{PMCA} = \overline{I_{PMCA}} \left(\frac{[Ca^{2+}]_{myo}}{kmpca + [Ca^{2+}]_{myo}} \right) \tag{64}$$

Na^{+}/Ca^{2+} exchanger

$$I_{NaCa} = \frac{NUM1 \times (NUM2 - NUM3)}{\wp \left(1 + 0.27 e^{\frac{-0.65FV}{RT}} \right)} \tag{65}$$

$$NUM1 = R_{NaCa} \left(\frac{V_{\max}}{1 + \left(\frac{K_{mAllo}}{[Ca^{2+}]_{NaCa}} \right)^2} \right) \tag{66}$$

$$NUM2 = e^{\frac{0.35FV}{RT}} ([Na^{+}]_{NaCa})^3 [Ca^{2+}]_o \tag{67}$$

$$NUM3 = e^{\frac{0.65FV}{RT}} ([Na^{+}]_o)^3 [Ca^{2+}]_{NaCa} \tag{68}$$

$$\begin{aligned}\wp &= K_{mCao}([Na^+]_{NaCa})^3 + K^3_{mNao}[Ca^{2+}]_{NaCa} \\ &+K^3_{mNai}[Ca^{2+}]\left(1+\frac{[Ca^{2+}]_{NaCa}}{K_{mCai}}\right) \\ &+K_{mCai}([Na^+]_o)^3\left(1+\left(\frac{[Na^+]_{NaCa}}{K_{mNai}}\right)^3\right) \\ &+\left(\left[Na^+\right]_{NaCa}\right)^3\left[Ca^{2+}\right]_o \\ &+\left(\left[Na^+\right]_o\right)^3\left[Ca^{2+}\right]_{NaCa}\end{aligned} \tag{69}$$

where $[Ca^{2+}]_{NaCa}$, $[Na^+]_{NaCa}$ are Concentrations at the mouth of the NaCa-exchanger.

The corresponding unitary current i_{NaCa} is obtained by dividing the above net channel current I_{NaCa} by the number of dyadic units N_{dyad}.

Na^+/Cs^+ pump

$$\begin{aligned}I_{NaCs} &= R_{NaCs}\overline{I_{NaCs}}\left(\frac{[Cs^+]_0}{[Cs^+]_0+kmcs}\right) \\ &\times\left(\frac{100([Na^+]_{myo})^{1.5}}{([Na^+]_{myo})^{1.5}+kmna^{1.5}}\right) \\ &\times\left(\frac{0.65558}{0.18445+e^{-\left(\frac{v+53.353}{15.58}\right)}}\right)\end{aligned} \tag{70}$$

The corresponding unitary current i_{NaCs} is obtained by dividing the above net channel current I_{NaCs} by the number of dyadic units N_{dyad}.

Background Na^+ current

$$I_{Na,b} = G_{Nab}\left(v-\frac{RT}{F}\ln\left(\frac{[Na^+]_o}{[Na^+]_{myo}}\right)\right) \tag{71}$$

Ca^{2+} transfer from LSR to a single jSR

$$i_{tr} = \left(\frac{[Ca^{2+}]_{LSR}-[Ca^{2+}]_{jSR}}{\tau_{tr}}\right)2FV_{jSR} \tag{72}$$

Ca^{2+} release from a unit jSR into a single DCU

$$i_{ryr} = J_{ryr}\times(2F\times\pi\Delta_r^2\Delta_z) \tag{73}$$

where,

$$J_{ryr} = \frac{O2_{ryr}([Ca^{2+}]_{jSR} - [Ca^{2+}]_{ryr})P_{ryr}}{\pi\Delta_r^2\Delta_z} \tag{74}$$

Gating scheme for the 4-state Markovian model for the RyR-sensitive SR Ca^{2+} release channel:

$$C4_{ryr} = 1 - (C1_{ryr} + O2_{ryr} + C3_{ryr}) \tag{75}$$

$$\frac{dC1_{ryr}}{dt} = k_{41}^{ryr}C4_{ryr} + k_{21}^{ryr}O2_{ryr} - (k_{12}^{ryr} + k_{14}^{ryr})C1_{ryr} \tag{76}$$

$$\frac{dO2_{ryr}}{dt} = k_{12}^{ryr}C1_{ryr} + k_{32}^{ryr}C3_{ryr} - (k_{21}^{ryr} + k_{23}^{ryr})O2_{ryr} \tag{77}$$

$$\frac{dC3_{ryr}}{dt} = k_{23}^{ryr}O2_{ryr} + k_{43}^{ryr}C4_{ryr} - (k_{34}^{ryr} + k_{32}^{ryr})C3_{ryr} \tag{78}$$

$$k_{12}^{ryr} = [Ca^{2+}]_{ryr}^2\left(0.05 - \frac{3.7465\times10^{-2}}{1 + e^{\frac{[Ca^{2+}]_{ryr} - 2052.7}{5.983}}}\right)var + \left(\frac{CaMKII_{act}}{12000}\right) \tag{79}$$

$$k_{21}^{ryr} = \left(698.56 - \frac{618.56}{1 + e^{\frac{[ca^{2+}]_{ryr} - 2052.9}{4.35}}}\right) \times \left(1 + \frac{6.0}{[Ca^{2+}]_{ryr}}\right)\frac{1}{var} \tag{80}$$

$$k_{14}^{ryr} = 8.748\times10^{-2}[Ca^{2+}]_{ryr}var \tag{81}$$

$$k_{41}^{ryr} = \left(\frac{2.0}{var}\right) + \frac{CaMKII_{act}}{12000} \tag{82}$$

$$k_{43}^{ryr} = k_{12}^{ryr};\ k_{34}^{ryr} = k_{21}^{ryr}; \tag{83}$$

$$k_{23}^{ryr} = k_{14}^{ryr}; k_{32}^{ryr} = k_{41}^{ryr}; \tag{84}$$

$$var = \left[10.0 \times e^{\frac{A1_{ls} - 0.7013}{0.03}} \right]^2 \tag{85}$$

where $[Ca^{2+}]_{ryr}$ is the Ca^{2+} concentration at the mouth of the RyR channel on the dyadic side. In the presence of caffeine (CF, concentration in μM):

$$O2_{ryr} = \left(\frac{-0.522}{1 + e^{\frac{[CF] - 410}{264.9}}} \right) + 0.503 \tag{86}$$

Gating scheme for the 6-state Markovian model for the Luminal Calcium sensor.

$$I4_{ls} = 1 - (A1_{ls} + I2_{ls} + I3_{ls}) \tag{87}$$

$$B5_{ls} = 1 - (I2_{ls} + I3_{ls} + B6_{ls}) \tag{88}$$

$$\frac{dA1_{ls}}{dt} = k_{41}^{ls} I4_{ls} + k_{21}^{ls} I2_{ls} - (k_{12}^{ls} B5_{ls} + k_{14}^{ls}) A1_{ls} \tag{89}$$

$$\begin{aligned} \frac{dI2_{ls}}{dt} &= k_{12}^{ls} B5_{ls} A1_{ls} + k_{42}^{ls} B5_{ls} I4_{ls} + k_{32}^{ls} I3_{ls} \\ &\quad -(k_{21}^{ls} + k_{24}^{ls} + k_{23}^{ls} + k_{25}^{ls})\, I2_{ls} \end{aligned} \tag{90}$$

$$\frac{dI3_{ls}}{dt} = k_{43}^{ls} B5_{ls} I4_{ls} + k_{23}^{ls} I2_{ls} - (k_{34}^{ls} + k_{32}^{ls})\, I3_{ls} \tag{91}$$

$$\frac{dB6_{ls}}{dt} = k_{56}^{ls} [Ca^{2+}]_{jSR} B5_{ls} - k_{65}^{ls} B6_{ls} \tag{92}$$

$A1_{ls}$ Fractional occupancy of RyR by Triadin/Junctin
$I2_{ls}$ Fractional occupancy of RyR by Triadin/Junctin and Calsequestrin
$I3_{ls}$ Fractional occupancy of Triadin/Junctin by Calsequestrin
$I4_{ls}$ Free Triadin/Junctin, B5ls - Free Calsequestrin
$B6_{ls}$ Fractional Occupancy of Calsequestrin by Calcium

Ca^{2+} dependent CaM mediated activation of CaMKII and CaN

Ca^{2+} binding to CaM and CaM buffering

$$\begin{aligned} CaM = CaM_{tot} &- Ca_2CaM - Ca_4CaM - CaMB \\ &- Ca_2CaMB - Ca_4CaMB - CaMCaN \\ &- Ca_2CaMCaN - Ca_4CaMCaN \\ &- CaMKII_{tot}\, (P_1 + P_3 + P_5 + P_4) \end{aligned} \tag{93}$$

$$B = B_{tot} - (CaMB + Ca_2CaMB + Ca_4CaMB) \tag{94}$$

$$RO2 = k_{02}^{CM}[Ca^{2+}]^2 \times CaM - k_{02}^{CM} \times Ca_2CaM \tag{95}$$

$$R24 = k_{24}^{CM}[Ca^{2+}]^2 \times Ca_2CaM - k_{42}^{CM} \times Ca_4CaM \tag{96}$$

$$RO2B = k_{02B}^{CM}[Ca^{2+}]^2 \times CaMB - k_{20B}^{CM} \times Ca_2CaMB \tag{97}$$

$$\begin{aligned} R24B = {} & k_{24B}^{CM}[Ca^{2+}]^2 \times Ca_2CaMB \\ & -k_{42B}^{CM} \times Ca_4CaMB \end{aligned} \tag{98}$$

$$ROB = k_{0Bon}^{CM} \times CaM \times B - k_{0Boff}^{CM} \times Ca_2CaMB \tag{99}$$

$$R2B = k_{2Bon}^{CM} \times Ca_2CaM \times B - k_{2Boff}^{CM} \times Ca_2CaMB \tag{100}$$

$$R4B = k_{4Bon}^{CM} \times Ca_4CaM \times B - k_{4Boff}^{CM} \times Ca_4CaMB \tag{101}$$

$$\begin{aligned} \frac{dCa_2CaM}{dt} = {} & R02 - R24 - R2B - R2CaN \\ & +CaMKII_{tot} \times (RCK_{56} - RCK_{21}) \end{aligned} \tag{102}$$

$$\begin{aligned} \frac{dCa_4CaM}{dt} = {} & R24 - R4CaN - R4B \\ & -CaMKII_{tot} \times (RCK_{46} - RCK_{23}) \end{aligned} \tag{103}$$

$$\begin{aligned} \frac{dCa_4CaM}{dt} = {} & R24 - R4CaN - R4B \\ & -CaMKII_{tot} \times (RCK_{46} - RCK_{23}) \end{aligned} \tag{104}$$

$$\frac{dCaMB}{dt} = R0B - R02B \tag{105}$$

$$\frac{dCa_2CaMB}{dt} = R02B + R2B - R24B \tag{106}$$

$$\frac{dCa_4CaMB}{dt} = R24B - R4B \tag{107}$$

CaMKII activation:

$$P_2 = 1 - P_3 - P_1 - P_4 - P_5 - P_6 \tag{108}$$

$$T = P_3 + P_4 + P_5 + P_6 \tag{109}$$

$$k_{34}^{CK} = 0.055 \times T + 0.0074 \times T^2 + 0.015 \times T^3 \tag{110}$$

$$RCK_{34} = k_{34}^{CK} \times P_3 - \left(\frac{K_{PP1} \times PP1_{tot} \times P_4}{k_{mpp1} + (CaMKII_{tot} \times P_4)} \right) \tag{111}$$

$$RCK_{21} = k_{21}^{CK} \times Ca_2CaM \times P_2 - k_{12}^{CK} \times P_1 \tag{112}$$

$$RCK_{13} = k_{13}^{CK} \times [Ca^{2+}]^2 \times P_1 - k_{32}^{CK} \times P_3 \tag{113}$$

$$RCK_{23} = k_{23}^{CK} \times Ca_4CaM \times P_2 - k_{32}^{CK} \times P_3 \tag{114}$$

$$RCK_{45} = k_{45}^{CK} \times P_4 - k_{54}^{CK} \times [Ca^{2+}]^2 \times P_5 \tag{115}$$

$$RCK_{46} = k_{46}^{CK} \times P_4 - k_{64}^{CK} \times Ca_4CaM \times P_6 \tag{116}$$

$$RCK_{56} = k_{56}^{CK} \times P_5 - k_{65}^{CK} \times Ca_2CaM \times P_6 \tag{117}$$

$$RCK_{51} = \frac{k_{PP1} \times PP1_{tot} \times P_5}{k_{mPP1} + (CaMKII_{tot} \times P_5)} \tag{118}$$

$$RCK_{62} = \frac{k_{PP1} \times PP1_{tot} \times P_6}{k_{mPP1} + (CaMKII_{tot} \times P_6)} \tag{119}$$

$$\frac{dP_1}{dt} = RCK_{21} + RCK_{51} - RCK_{13} \tag{120}$$

$$\frac{dP_3}{dt} = RCK_{23} + RCK_{13} - RCK_{34} \tag{121}$$

$$\frac{dP_4}{dt} = RCK_{34} - RCK_{46} - RCK_{45} \tag{122}$$

$$\frac{dP_5}{dt} = RCK_{45} - RCK_{56} - RCK_{51} \tag{123}$$

$$\frac{dP_6}{dt} = RCK_{46} - RCK_{56} - RCK_{62} \tag{124}$$

$$CaMKII_{act} = 100 \times (P_3 + P_4 + P_5 + P_6) \tag{125}$$

CaN activation:

$$\begin{aligned} Ca_2CaN = {} & CaN_{tot} - Ca_4CaN - CaMCaN \\ & - Ca_2CaMCaN - Ca_4CaMCaN \end{aligned} \tag{126}$$

$$\begin{aligned} RCN_{Ca4} = {} & k^{CN}_{Caon} \times [Ca^{2+}]^2 \times Ca_2CaN \\ & - k^{CN}_{Caoff} \times Ca_4CaN \end{aligned} \tag{127}$$

$$\begin{aligned} RCN_{02} = {} & k^{CN}_{02} \times [Ca^{2+}]^2 \times CaMCaN \\ & - k^{CN}_{20} \times Ca_2CaMCaN \end{aligned} \tag{128}$$

$$\begin{aligned} RCN_{24} = {} & k^{CN}_{24} \times [Ca^{2+}]^2 \times Ca_2CaMCaN \\ & - k^{CN}_{42} \times Ca_4CaMCaN \end{aligned} \tag{129}$$

$$\begin{aligned} RCN_0 = {} & k^{CN}_{0on} \times CaM \times Ca_4CaN \\ & - k^{CN}_{0off} \times CaMCaN \end{aligned} \tag{130}$$

$$\begin{aligned} RCN_2 = {} & k^{CN}_{2on} \times Ca_2CaM \times Ca_4CaN \\ & - k^{CN}_{2off} \times Ca_2CaMCaN \end{aligned} \tag{131}$$

$$\begin{aligned} RCN_4 = {} & k^{CN}_{4on} \times Ca_4CaM \times Ca_4CaN \\ & - k^{CN}_{4off} \times Ca_4CaMCaN \end{aligned} \tag{132}$$

$$\frac{dCa_4CaN}{dt} = RCN_{Ca4} - RCN_0 - RCN_2 - RCN_4 \tag{133}$$

$$\frac{dCaMCaN}{dt} = RCN_0 - RCN_{02} \tag{134}$$

$$\frac{dCa_2CaMCaN}{dt} = RCN_2 + RCN_{02} - RCN_{24} \tag{135}$$

$$\frac{dCa_4CaMCaN}{dt} = RCN_4 + RCN_{24} \tag{136}$$

$$\begin{aligned} CaN_{act} &= 100(Ca_4CaMCaN + 0.1\,Ca_2CaMCaN) \\ &+10\,Ca_4CaMCaN \;+ 0.1\,CaMCaN \\ &+0.1Ca_4CaN \end{aligned} \tag{137}$$

A2 - Differential equations for buffers used in the model

Fluorescent indicator dye

$$\begin{aligned} \frac{d[CaF3]}{dt} &= k^{+}_{fluo3}[Ca^{2+}_{myo}]([fluo3]_{tot} - [CaF3]) \\ &-k^{-}_{fluo3}[CaF3] \end{aligned} \tag{138}$$

Intracellular Ca^{2+} buffering:
calmodulin (bulkmyoplasm):

$$\frac{dO_c}{dt} = 200[Ca^{2+}]_{myo}(1 - O_c) - 476.0 \times O_c \tag{139}$$

Troponin
(Fractional occupancy of troponin-Ca complex by Ca^{2+}):

$$\frac{dO_tc}{dt} = 78.4[Ca^{2+}]_{myo}(1 - O_{tc}) - 392.0 \times O_{tc} \tag{140}$$

(Fractional occupancy of troponin-Mg complex by Ca^{2+}):

$$\begin{aligned} \frac{dO_c}{dt} &= 200[Ca^{2+}]_{myo}(1 - O_{tmgc} - O_{tmgmg}) \\ &-6.6 \times O_{tmgc} \end{aligned} \tag{141}$$

(Fractional occupancy of troponin-Mg complex by Mg^{2+}):

$$\begin{aligned} \frac{dO_{tmgmg}}{dt} &= 2.0[Mg^{2+}]_{myo}(1 - O_{tmgc} - O_{tmgmg}) \\ &-666.0 \times O_{tmgmg} \end{aligned} \tag{142}$$

A3 - Differential equations for ion concentrations used in the model

Intracellular Ca^{2+} concentration:

1. *Ca^{2+} concentration in the cytosol*

$$\begin{aligned} \frac{d[Ca^{2+}]_{myo}}{dt} &= \frac{I_{dyad} - I_{PMCA} - I_{Ca,L,SL}}{2FV_{myo}} \\ &+ \frac{-I_{cyt,serca} + 2I_{NaCa,SL}}{2FV_{myo}} \\ &- \frac{dO}{dt} - \frac{dCaF1}{dt} \end{aligned} \tag{143}$$

where I_{dyad} is the net integrated Ca^{2+} flux diffusing out of all the dyadic units into the cytosol

$$\frac{dO}{dt} = 3.2\frac{dO_{TC}}{dt} + 6.4\frac{dO_{TMgC}}{dt} + 1.8\frac{dO_c}{dt} \tag{144}$$

2. *Ca^{2+} concentration in the jSR*

$$\frac{d[Ca^{2+}]_{jSR}}{dt} = \frac{i_{tr} - i_{ryr}}{2FV_{jSR}} - 31000\frac{dB6_{ls}}{dt} \tag{145}$$

3. Ca^{2+} concentration in the LSR

$$\frac{d[Ca^{2+}]_{LSR}}{dt} = \frac{I_{cyt,serca} - N_{dyad}i_{tr}}{2FV_{LSR}} \tag{146}$$

4. Diffusion equation for Calcium in the dyadic space

$$\begin{aligned}\frac{\partial[Ca^{2+}]_{dyad}}{\partial t} &= D_{Ca}\nabla^2[Ca^{2+}]_{dyad} + J_{ryr} \\ &+ J_{dhpr} + J_{Naca} + J_{bnd}\end{aligned} \tag{147}$$

$$J_{dhpr} = \left(\frac{i_{Ca,L,TT}}{N_{dyad}}\right)\left(\frac{5.1821\times10^3}{\pi\Delta_r^2\Delta_z}\right) \tag{148}$$

$$J_{NaCa,TT} = \left(\frac{i_{NaCa,TT}}{N_{dyad}}\right)\left(\frac{2\times5.1821\times10^3}{\pi\Delta_r^2\Delta_z}\right) \tag{149}$$

$$\begin{aligned}J_{bnd} &= \left(\frac{N_hK_h}{(K_h + [Ca^{2+}]_{dyad})^2}\right) \\ &\times\left(\frac{N_lK_l}{(K_l + [Ca^{2+}]_{dyad})^2}\right)\frac{\partial[Ca^{2+}]_{dyad}}{\partial t}\end{aligned} \tag{150}$$

Intracellular Na^+ concentration:

1. *Na^+ concentration in the cytosol*

$$\begin{aligned}\frac{d[Na^+]_{myo}}{dt} &= N_{dyad}\left[\frac{[Na^+]_{dyad} - [Na^+]_{myo}}{\tau_{Na}}\right] \\ &-\left[\frac{I_{Na,b} + 3I_{NaCa,SL}}{F\times V_{myo}}\right] \\ &+\left[\frac{3I_{NaCs,SL}}{F\times V_{myo}}\right]\end{aligned} \tag{151}$$

2. Na^+ *concentration in the dyadic space*

$$\frac{d[Na^+]_{dyad}}{dt} = \left(\frac{[Na^+]_{myo} - [Na^+]_{dyad}}{\tau_{Na}} \right) - \left(\frac{3i_{NaCa,TT} + 3i_{NaCs,TT}}{F \times V_{cleft}} \right) \tag{152}$$

Intracellular Cs^+ concentration:

1. Cs^+ *concentration in the cytosol*

$$\frac{d[Cs^+]_{myo}}{dt} = N_{dyad} \left(\frac{[Cs^+]_{dyad} - [Cs^+]_{myo}}{\tau_{Cs}} \right) + \left(\frac{2I_{NaCs,SL}}{F \times V_{myo}} \right) \tag{153}$$

2. Cs^+ *concentration in the dyadic space*

$$\frac{d[Cs^+]_{dyad}}{dt} = \left(\frac{[Cs^+]_{myo} - [Cs^+]_{dyad}}{\tau_{Cs}} \right) + \left(\frac{2i_{NaCs,TT}}{F \times V_{cleft}} \right) \tag{154}$$

Abbreviations

ATP: Adenosine triphosphate; $[Ca^{2+}]$: calcium ion concentration; $[Ca^{2+}]_{dhp}$: Ca^{2+} concentration at the mouth of the DHP-sensitive $I_{Ca,L}$ channel; $[Ca^{2+}]_{dyad}$: spatial Ca^{2+} concentration in the dyad; $[Ca^{2+}]_{jSR}$: luminal Ca^{2+} concentration in the jSR; $[Ca^{2+}]_{LSR}$: Ca^{2+} concentration in the LSR; $[Ca^{2+}]_{myo}$: cytosolic Ca^{2+} concentration; $[Ca^{2+}]_{serca}$: Ca^{2+} concentration buffered by the SERCA protein; $[Ca^{2+}]_o$: extracellular Ca^{2+} concentration; $[Ca^{2+}]_{ryr}$: Ca^{2+} concentration at the "mouth" of the RyR channel on the dyadic side; CaCM: Ca^{2+} bound calmodulin; CaF3: Ca^{2+} bound to the buffer Fluo3; CaM: calmodulin; CaMKII: Ca^{2+}/calmodulin-dependent protein kinase II; $CaMKII_{act}$: activated Ca^{2+}/calmodulin-dependent protein kinase II; CaN: calcineurin; C_aN_{act} : activated calcineurin; CDF: calcium dependent facilitation; CDI: calcium dependent inactivation; CF: caffeine; CICR: calcium-induced calcium-release; CS: calsequestrin; $[Cs^+]_{myo}$: Cs^+ concentration in the cytosol; $[Cs^+]_{dyad}$: Cs^+ concentration in the dyadic space; DCU: dyadic coupling unit; DHP: dihydropyridine; DHPR: dihydropyridine receptor; E-C: excitation contraction; EC50bwd: affinity of backward Ca^{2+} flux from LSR to cytosol; EC50fwd: affinity of forward Ca^{2+} flux from cytosol to LSR; $I_{Ca,L}$: L-type Ca^{2+} current; $I_{Ca,L,SL}$: sarcolemmal component of the $I_{Ca,L}$ channel current; $I_{Ca,L,TT}$: $I_{Ca,L}$ channel facing the dyadic space; I_{Cs} : cesium current through the $I_{Ca,L}$ channel; $I_{cyt,serca}$: Ca^{2+} uptake current directed from the cytosol to the SERCA; I_{Na} : sodium current through the $I_{Ca,L}$ channel; $I_{Na,b}$: background sodium current; I_{NaCa} : sodium calcium exchanger current; $I_{NaCa,SL}$: sarcolemmal component of the I_{NaCa} exchanger current; $I_{NaCa,TT}$: I_{NaCa} exchanger facing the dyadic space; I_{NaCs} : sodium cesium pump current; I_{PMCA} : plasma membrane Ca^{2+} ATPase pump current; I_{ryr} : Ca^{2+} current due to CICR from an individual jSR; $I_{serca,sr}$: Ca^{2+} uptake current directed from the SERCA to the LSR; I_{tr} : Ca^{2+} current due to concentration gradient driven Ca^{2+} transport from LSR to jSR; jSR: junctional portion of the sarcoplasmic reticulum; k_{cl} : dissociation constant; k_{mp} : half saturation constant for the sarcolemmal Ca^{2+} pump; LCC: L-type DHP-sensitive Ca^{2+} channel; L-type: long lasting type; LSR: longitudinal portion of the sarcoplasmic reticulum; mM: milli molar; mV: milli volt; $[Na^+]_{dyad}$: Na^+ concentration in the dyadic space; $[Na^+]_{myo}$: Na^+ concentration in the cytosol; nM: nano molar; O_c : fractional occupancy of calmodulin by Ca^{2+} in the cytosol; O_{calse} : fractional occupancy of calsequestrin by Ca^{2+} in the jSR; O_{tc} : fractional occupancy of troponin-Ca sites by Ca^{2+} in the cytosol; O_{tmgc} : fractional ocupancy of troponin-Mg sites by Ca^{2+} in the cytosol; O_{tmgmg} : fractional occupancy of troponin-Mg sites by Mg^{2+} in the cytosol; pC: pico coulomb; P_o : Open probability; PKA: protein kinase A; PLB_{dp} : Unphosphorylated phospholamban; PLB_p : phosphorylated phospholamban; PSR: phospholamban to SERCA ratio; Ry: ryanodine; RyR: ryanodine receptor; SERCA: sarcoplasmic reticulum Ca^{2+} ATPase; SL: sarcolemma; SR: sarcoplasmic reticulum; Tc: Ca^{2+}-specific troponin binding site; T-tubule: transverse tubules; TT: transverse tubules; VC: voltage clamp; VDI: voltage dependent inactivation;

Acknowledgements

This work was supported by a research grant from Methodist Hospital Research Institute. The authors would like to thank Jing-Song Fan for his early contributions to this work.

Author details
[1]Department of Electrical and Computer Engineering, Rice University, 6100 Main Street, Houston, 77005, USA. [2]Proportional Technologies, Inc., 8022 El Rio Street, Houston, 77054, USA. [3]Methodist Hospital Research Institute, Methodist DeBakey Heart & Vascular Center, 6565 Fannin Street, Houston, 77030, USA. [4]Department of Pharmacology and Toxicology, University of Arkansas for Medical Sciences, 4301 West Markham Street, Little Rock, 72205, USA.

Authors' contributions
AK carried out the voltage clamp modeling studies and drafted the manuscript. LS substantially contributed to the development of the rat ventricular cell model. MV made substantial intellectual contributions to the study and in drafting of the manuscript. PTP provided the experimental voltage clamp data used to validate the model and contributed to the drafting of the manuscript. JWC made key contributions to the conception and design, analysis and interpretation of data, and drafting of the manuscript. All authors read and approved the final manuscript.

Competing interests
The authors declare that they have no competing interests.

Received: 17 June 2010 Accepted: 10 November 2010 Published: 10 November 2010

References

1. Fabiato A, Fabiato F: **Contractions induced by a calcium-triggered release of calcium from the sarcoplasmic reticulum of single skinned cardiac cells.** *J Physiol* 1975, **249**:469-495.
2. Beuckelmann DJ, Wier WG: **Mechanism of release of calcium from sarcoplasmic reticulum of guinea-pig cardiac cells.** *J Physiol(Lond)* 1988, **405**:233-235.
3. Stern MD: **Theory of excitation-contraction coupling in cardiac muscle.** *Biophys J* 1992, **63**:497-517.
4. Hilgemann DW, Noble D: **Excitation-contraction coupling and extracellular calcium transients in rabbit atrium: reconstruction of basic cellular mechanisms.** *Proc R Soc Lond B* 1987, **230**:163-205.
5. Isenberg G: **Cardiac excitation-contraction coupling: from global to microscopic models.** In *Physiology and Pathophysiology of the Heart.* Edited by: Sperelakis N. Kluwer Academic; 1995:289-307.
6. Stern MD, Song LS, Cheng H, Sham JSK, Yang HT, Boheler KR, Rios E: **Local control models of cardiac excitation-contraction coupling.** *J Gen Physiol* 1999, **113**:469-489.
7. Rice JJ, Jafri S, Winslow RL: **Modeling gain and gradedness of Ca^{2+} release in the functional unit of the cardiac diadic space.** *Biophys J* 1999, **77**:1871-1884.
8. Greenstein JL, Winslow RL: **An integrative model of the cardiac ventricular myocyte incorporating local control of Ca^{2+} release.** *Biophys J* 2002, **83**:2918-2945.
9. Winslow RL, Tanskanen A, Chen M, Greenstein JL: **Multiscale modeling of calcium signaling in the cardiac dyad.** *Ann NY Acad Sci* 2006, **1080**:362-375.
10. Hinch R, Greenstein JL, Tanskanen AJ, Xu L, Winslow RL: **A simplified local control model of calcium-induced calcium release in cardiac ventricular myocytes.** *Biophys J* 2004, **87(6)**:3723-3736.
11. Greenstein JL, Hinch R, Winslow RL: **Mechanisms of excitation-contraction coupling in an integrative model of the cardiac ventricular myocyte.** *Biophys J* 2006, **90**:77-91.
12. Hinch R, Greenstein JL, Winslow RL: **Multi-scale models of local control of calcium induced calcium release.** *Prog Biophys Mol Biol* 2006, **90**:136-150.
13. Wang SQ, Song LS, Lakatta EG, Cheng H: **Ca^{2+} signalling between single L-type Ca^{2+} channels and ryanodine receptors in heart cells.** *Nature* 2001, **410**:592-596.
14. Zima AV, Picht E, Bers DM, Blatter LA: **Termination of cardiac Ca^{2+} sparks: role of intra-SR [Ca^{2+}], release flux, and intra-SR Ca^{2+} diffusion.** *Circ Res* 2008, **103**:105-115.
15. Shiferaw Y, Watanabe MA, Garfinkel A, Weiss JN, Karma A: **Model of intracellular calcium cycling in ventricular myocytes.** *Biophys J* 2003, **85**:3666-3686.
16. Bers DM: *Excitation-Contraction Coupling and Cardiac Contractile Force.* 2 edition. Dordrecht: Kluwer Academic; 2001.
17. Fan JS, Palade P: **One calcium ion may suffice to open the tetrameric cardiac ryanodine receptor in rat ventricular myocytes.** *J Physiol (Lond)* 1999, **516**:769-780.
18. Marquardt DW: **An algorithm for least-squares estimation of nonlinear parameters.** *J Soc Ind Appl Math* 1963, **11**:431-441.
19. Lau HT: **Overdetermined nonlinear systems.** *A Numerical Library in C for Scientists and Engineers.* 1 edition. 2000 Corporate Blvd. N.W., Boca raton, Florida 33431: CRC Press; 1995, 354-358.
20. Merson RH: **An operational method for the study of integration processes.** *Proceedings Symposium on Data Processing* Weapons Research Establishment, Salisbury, South Australia; 1957.
21. Butcher JC: *Numerical Methods for Ordinary Differential Equations.* 2 edition. West Sussex: Wiley; 2003.
22. Smith GD, Keizer JE, Stern MD, Lederer WJ, Cheng H: **A simple numerical model of calcium spark formation and detection in cardiac myocytes.** *Biophys J* 1998, **75**:15-32.
23. Despa S, Brette F, Orchard CH, Bers DM: **Na/Ca exchange and Na/K-ATPase function are equally concentrated in transverse tubules of rat ventricular myocytes.** *Biophys J* 2003, **85**:3388-3396.
24. Kawai M, Hussain M, Orchard CH: **Excitation-contraction coupling in rat ventricular myocytes after formamide-induced detubulation.** *Am J Physiol* 1999, **277**:603-609.
25. Terentyev D, Viatchenko-Karpinski S, Vedamoorthyrao S, Oduru S, Gyorke I, Williams SC, Gyorke S: **protein protein interactions between triadin and calsequestrin are involved in modulation of sarcoplasmic reticulum calcium release in cardiac myocytes.** *J Physiol* 2007, **583**:71-80.
26. Crank J: *The mathematics of diffusion.* 2 edition. Oxford, London: Clarendon Press; 1975.
27. Cheng H, Lederer WJ, Cannell MB: **Calcium sparks: elementary events underlying excitation-contraction coupling in heart muscle.** *Science* 1993, **262**:740-744.

28. Blatter LA, Hüser J, Riós E: **Sarcoplasmic reticulum Ca^{2+} release flux underlying Ca^{2+} sparks in cardiac muscle.** *Proc Natl Acad Sci USA* 1997, **94**:4176-4181.
29. Diaz ME, O'Neill SC, Eisner DA: **Sarcoplasmic reticulum calcium content fluctuation is the key to cardiac alternans.** *Circulation Research* 2004, **94**:650-656.
30. Sun L, Fan JS, Clark JW, Palade PT: **A model of the L-type Ca^{2+} channel in rat ventricular myocytes: ion selectivity and inactivation mechanisms.** *J Physiol (Lond)* 2000, **529**:139-158.
31. Yuan W, Bers DM: **Ca-dependent facilitation of cardiac Ca current is due to Ca-calmodulin-dependent protein kinase.** *Am J Physiol* 1994, **267**:H982-H993.
32. Hashambhoy YL, Winslow RL, Greenstein JL: **CaMKII-induced shift in modal gating explains L-type Ca^{2+} current facilitation: a modeling study.** *Biophys J* 2009, **96(5)**:1770-1785.
33. Bers DM, Grandi E: **Calcium/Calmodulin-dependent Kinase II Regulation of Cardiac Ion Channels.** *J Cardiovasc Pharmacol* 2009, **54**:180-187.
34. Hilgemann DW, Collins A, Cash DP: **CaMKII tethers to L-type Ca^{2+} channels, establishing a local and dedicated integrator of Ca^{2+} signals for facilitation.** *J Cell Biol* 2005, **171(3)**:537-547.
35. Tandan S, Wang Y, Wang TT, Jiang N, Hall DD, Hell JW, Luo X, Rothermel BA, Hill JA: **Physical and Functional Interaction Between Calcineurin and the Cardiac L-Type Ca^{2+} Channel.** *Circ Res* 2009, **105**:51-60.
36. Schouten VJ, Morad M: **Regulation of Ca^{2+} current in frog ventricular myocytes by the holding potential, c-AMP and frequency.** *Pflügers Arch* 1989, **415**:1-11.
37. Soldatov NM: **Ca^{2+} channel moving tail: link between Ca^{2+}- induced inactivation and Ca^{2+} signal transduction.** *TRENDS in pharmacological Sciences* 2003, **24(4)**:167-171.
38. Saucerman JJ, Bers DM: **Calmodulin Mediates Differential Sensitivity of CaMKII and Calcineurin to Local Ca^{2+} in Cardiac Myocytes.** *Biophysical Journal* 2008, **95**:4597-4612.
39. Post JA, Langer GA, Op den Kamp JA, Verkleij AJ: **Phospholipid asymmetry in cardiac sarcolemma. Analysis of intact cells and 'gas-dissected' membranes.** *Biochem Biophys Acta* 1988, **943(2)**:256-266.
40. Post JA, Langer GA: **Sarcolemmal calcium binding sites in heart: I. Molecular origin in "gas-dissected" sarcolemma.** *J Membr Biol* 1992, **129**:49-57.
41. Cens T, Rousset M, Leyris JP, Fesquet P, Charnet P: **Voltage- and calcium-dependent inactivation in high voltage-gated Ca^{2+} channels.** *Prog Biophys Mol Biol* 2006, **90**:104-117.
42. Keizer J, Levine L: **Ryanodine receptor adaptation and Ca^{2+}-induced Ca^{2+} release-dependent Ca^{2+} oscillations.** *Biophys J* 1996, **71**:3477-3487.
43. Gyorke S, Fill M: **Ryanodine receptor adaptation: control mechanism of Ca^{2+}-induced Ca^{2+} release in heart.** *Science* 1993, **263**:986-988.
44. Zahradnikova A, Zahradnik I: **A minimal gating model for the cardiac calcium release channel.** *Biophys J* 1996, **71**:2996-3012.
45. Keizer J, Smith GD: **Spark-to-wave transitions: salutatory transmission of calcium wave in cardiac myocytes.** *Biophys Chem* 1998, **72**:87-100.
46. Stern MD, Pizarro G, Rios E: **Local control model of excitation-contraction coupling in skeletal muscle.** *J Gen Physiol* 1997, **110**:415-440.
47. Li L, Satoh H, Ginsburg KS, Bers DM: **The effect of Ca^{2+}-calmodulin-dependent protein kinase II on cardiac excitation-contraction coupling in ferret ventricular myocytes.** *J Physiol* 1997, **501(1)**:17-31.
48. Maier L, Zhang T, Chen L, DeSantiago J, Brown JH, Bers DM: **Transgenic CaMKIIδ_C overexpression uniquely alters cardiac myocyte Ca^{2+} handling: reduced SR Ca^{2+} load and activated SR Ca^{2+} release.** *Circ Res* 2003, **92(8)**:904-911.
49. Currie S, Loughrey CM, Craig MA, Smith GL: **Calcium/calmodulin-dependent protein kinase IIδ as-sociates with the ryanodine receptor complex and regulates channel function in rabbit heart.** *Biochem J* 2004, **377(2)**:357-366.
50. Guo T, Zhang T, Mestril R, Bers DM: **Ca^{2+}/Calmodulin-dependent protein kinase II phosphorylation of ryanodine receptor does affect calcium sparks in mouse ventricular myocytes.** *Circ Res* 2006, **99(4)**:398-406.
51. Lukyanenko V, Wiesner TF, Gyorke S: **Termination of Ca^{2+} release during Ca^{2+} sparks in rat ventricular myocytes.** *J Physiol (Lond)* 1998, **507**:667-677.
52. Wier WG, Egan TM, Lopez-Lopez R, Balke CW: **Local control of excitation-contraction coupling in rat heart cells.** *J Physiol (Lond)* 1994, **474**:463-471.
53. Zucchi R, Ronca-Testoni S: **The sarcoplasmic reticulum Ca^{2+} channel/ryanodine receptor: modulation by endogenous effectors, drugs and disease states.** *Pharmacol Rev* 1997, **49**:1-51.
54. Zhang L, Kelley J, Schmeisser G, Kobayashi YM, Jones LR: **Complex formation between junctin, tri-adin, calsequestrin, and the ryanodine receptor. Proteins of the cardiac junctional sarcoplasmic reticulum membrane.** *J Biol Chem* 1997, **33**:233-247.
55. Franzini-Armstrong C, Protasi F: **Ryanodine receptors of striated muscles: a complex channel capable of multiple interactions.** *Physiol Rev* 1997, **77**:699-729.
56. Bers DM: **Macromolecular complexes regulating cardiac ryanodine receptor function.** *J Mol Cell Cardiol* 2004, **37**:417-429.
57. Meissner G: **Ryanodine receptor/Ca^{2+} release channels and their regulation by endogenous effectors.** *Annu Rev Physiol* 1994, **56**:485-508.
58. Fill M, Copello JA: **Ryanodine receptor calcium release channels.** *Physiol Rev* 2002, **82**:893-922.
59. Mitchell RD, Simmerman HK, Jones LR: **Ca^{2+} binding effects on protein conformation and protein interactions of canine cardiac calsequestrin.** *J Biol Chem* 1988, **263**:1376-1381.
60. Beard NA, Laver DR, Dulhunty AF: **Calsequestrin and the calcium release channel of skeletal and cardiac muscle.** *Prog Biophys Mol Biol* 2004, **85**:33-69.
61. Jones LR, Zhang L, Sanborn K, Jorgensen AO, J K: **Purification, primary structure, and immunological characterization of the 26-kDa calsequestrin binding protein (junctin) from cardiac junctional sarcoplasmic reticulum.** *J Biol Chem* 1995, **270**:30787-30796.
62. Kobayashi YM, Jones LR: **Identification of triadin 1 as the predominant triadin isoform expressed in mammalian myocardium.** *J Biol Chem* 1999, **274**:28660-28668.

63. Kobayashi YM, Alseikhan BA, Jones LR: **Localization and characterization of the calsequestrin-binding domain of triadin 1. Evidence for a charged β-strand in mediating the protein-protein interaction.** *J Biol Chem* 2000, **275**:17639-17646.
64. Shannon TR, Wang F, Puglisi J, Weber C, Bers DM: **A mathematical treatment of integrated Ca dynamics within the ventricular myocyte.** *Biophys J* 2004, **87(5)**:3351-3371.
65. Ikemoto N, Ronjat M, Meszaros LG, Koshita M: **Postulated role of calsequestrin in the regulation of calcium release from sarcoplasmic reticulum.** *Biochemistry* 1989, **28**:6764-6771.
66. Gyorke I, Hester N, Jones LR, Gyorke S: **The role of calsequestrin, triadin, and junctin in conferring cardiac ryanodine receptor responsiveness to luminal calcium.** *Biophys J* 2004, **86**:2121-2128.
67. Knollmann BC, Chopra N, Hlaing T, Akin B, Yang T, Ettensohn K, Knollmann BE, Horton KD, Weissman NJ, Holinstat I, Zhang W, Roden DM, Jones LR, Franzini-Armstrong C, Pfeifer K: **Casq2 deletion causes sarcoplasmic reticulum volume increase, premature Ca^{2+} release, and catecholaminergic polymorphic ventricular tachycardia.** *J Clin Invest* 2006, **116**:2510-2520.
68. Lauger P: **Conformational transitions of ionic channels.** In *Single-Channel Recording.* Edited by: Sakmann B. New York: Plenum Press; 1983:177-189.
69. Finkelstein A, Peskin CS: **Some unexpected consequences of a simple physical mechanism of voltage-dependent gating in biological membranes.** *Biophys J* 1984, **46**:549-558.
70. Sham JSK, Cleemann L, Morad M: **Functional coupling of Ca^{2+} channels and ryanodine receptors in cardiac myocytes.** *Proc Natl Acad. Sci* 1995, **92**:121-125.
71. Adachi-Akahane SL, Cleemann MM: **Cross-signaling between L-type Ca^{2+} channels and ryanodine receptors in rat ventricular myocytes.** *J Gen Physiol* 1996, **108**:435-454.
72. Potter JD, Zott HG: **The role of actin in modulating Ca^{2+} binding to troponin.** *Biophys J* 1982, **37**:43A.
73. Cannell MB, Allen D: **Model of calcium movements during activation in the sarcomere of frog skeletal muscle.** *Biophys J* 1984, **45**:913-925.
74. Lindblad DS, Murphey CR, Clark JW, Giles WR: **A model of the action potential and underlying membrane currents in a rabbit atrial cell.** *Am J Physiol Heart Circ Physiol* 1996, **271**:H1666-H1696.
75. Shannon TR, Ginsburg KS, Bers DM: **Potentiation of fractional sarcoplasmic reticulum calcium release by total and free intra-sarcoplasmic reticulum calcium concentration.** *Biophys J* 2000, **78**:334-343.
76. Lytton J, Westlin M, Burk SE, Shull GE, MacLennan DH: **Functional comparisons between isoforms of the sarcoplasmic or endoplasmic reticulum family of calcium pumps.** *J Biol Chem* 1992, **267**:14483-14489.
77. Koivumäki JT, Takalo J, Korhonen T, Tavi P, Weckström M: **Modelling sarcoplasmic reticulum calcium ATPase and its regulation in cardiac myocytes.** *Phil Trans R Soc A* 2009, **367**:2181-2202.
78. Xu A, Hawkins C, Narayanan N: **Phosphorylation and activation of the Ca^{2+}-pumping ATPase of cardiac sarcoplasmic reticulum by Ca^{2+}/calmodulin-dependent protein kinase.** *J Biol Chem* 1993, **268(12)**:8394-8397.
79. Bassani RA, Mattiazzi A, Bers DM: **CaMKII is responsible for activity-dependent acceleration of relaxation in rat ventricular myocytes.** *American J Physiol* 1995, **268**:703-712.
80. Schaeffer PJ, Desantiago J, Yang J, Flagg TP, Kovacs A, Weinheimer CJ, Courtois M, Leone TC, Nichols CG, Bers DM, Kelly DP: **Impaired contractile function and calcium handling in hearts of cardiac-specific calcineurin b1-deficient mice.** *American J Physiol Heart Circ Physiol* 2009, **297**:1263-1273.
81. Wolska BM: **Calcineurin and cardiac function: is more or less better for the heart?** *Am J Physiol Heart Circ Physiol* 2009, **297(5)**:H1576-H1577.
82. Caroni P, Zurini M, Clark A, Carafoli E: **Further characterization and reconstitution of the purified Ca-pumping ATPase of heart sarcolemma.** *J Biol Chem* 1983, **258**:7305-7310.
83. Kimura J, Miyamae S, Noma A: **Identification of sodium-calcium exchange current in single ventricular cells of guinea-pig ventricular cells.** *J Physiol (Lond)* 1987, **384**:199-222.
84. Luo CH, Rudy Y: **A dynamic model of the cardiac ventricular action potential: I. Simulations of ionic currents and concentration changes.** *Circ Res* 1994, **74**:1071-1096.
85. Weber CR, Ginsburg KS, Philipson KD, Shannon TR, Bers DM: **Allosteric regulation of Na/Ca exchange current by cytosolic Ca in intact cardiac myocytes.** *J Gen Physiol* 2001, **117(2)**:119-131.
86. Bridge JHB, Smolley JR, Spitzer KW: **The relationship between charge movements associated I_{Ca} and $I_{Na\text{-}Ca}$ in cardiac myocytes.** *Science* 1990, **248**:376-378.
87. Overend CL, Eisner DA, O'Neill SC: **The effect of tetracaine on spontaneous Ca^{2+} release and sarcoplasmic reticulum calcium content in rat ventricular myocytes.** *J Physiol* 1997, **502(3)**:471-479.
88. Glitsch HG: **Electrophysiology of the sodium-potassium-ATPase in cardiac cells.** *Physiol Rev* 2001, **81(4)**:1791-1826.
89. Rang HP, Ritchie JM: **On the electrogenic sodium pump in mammalian non-myelinated nerve fibres and its activation by various external cations.** *J Physiol* 1968, **196**:183-221.
90. Akaike N: **Activation of electrogenic sodium pump in mammalian skeletal muscle by external cations.** *Pflügers Arch* 1975, **355(4)**:281-290.
91. Akera T, Gubitz RH, Brody TM, Tobin T: **Effects of monovalent cations on (Na^+ + K^+)-ATPase in rat brain slices.** *Eur J Pharmacol* 1979, **55(3)**:281-292.
92. Eisner DA, Lederer WJ: **The role of the sodium pump in the effects of potassium-depleted solutions on mammalian cardiac muscle.** *J Physiol* 1979, **294**:279-301.
93. Kasamaki Y, Guo AC, Shuba LM, Ogura T, McDonald TF: **Sodium-pump potentials and currents in guinea-pig ventricular muscles and myocytes.** *Can J Physiol Pharmacol* 1999, **77(5)**:339-349.
94. Hansen PS, Buhagiar KA, Kong BY, Clarke RJ, Gray DF, Rasmussen HH: **Dependence of Na^+-K^+ pump current-voltage relationship on intracellular Na^+, K^+, and Cs^+ in rabbit cardiac myocytes.** *Am J Physiol Cell Physiol* 2002, **283(5)**: C1511-C1521.
95. Marban E, Tsien RW: **Enhancement of calcium current during digitalis inotropy in mammalian heart: positive feed-back regulation by intracellular calcium?** *J Physiol* 1982, **329**:589-614.
96. Wang Y, Tandan S, Cheng J, Yang C, Nguyen L, Sugianto J, Johnstone JL, Sun Y, Hill JA: **Ca^{2+}/calmodulin-dependent protein kinase II-dependent remodeling of Ca^{2+} current in pressure overload heart failure.** *J Biol Chem* 2008, **283(37)**:25524-25532.

97. Lee KS, Marban E, Tsien RW: **Inactivation of calcium channels in mammalian heart cells: joint dependence on membrane potential and intracellular calcium.** *J Physiol* 1985, **364**:395-411.
98. Sher AA, Hinch R, Noble PJ, Gavaghan DJ, Noble D: **Functional significance of Na^+/Ca^{2+} exchangers co-localization with ryanodine receptors.** *Ann N Y Acad Sci* 2007, **1099**:215-220.
99. Mejia-Alvarez R, Kettlun C, Rios E, Stern M, Fill M: **Unitary Ca^{2+} current through cardiac ryanodine receptor channels under quasiphysiological ionic conditions.** *J Gen Physiol* 1999, **113**:177-186.
100. Cannel MB, Berlin JR, Lederer WJ: **Effect of membrane potential changes on the calcium transient in single rat cardiac muscle cells.** *Science* 1987, **238**:1419-1423.
101. Cleemann L, Morad M: **Role of Ca^{2+} channel in cardiac excitation-contraction coupling in the rat: evidence from Ca^{2+} transients and contraction.** *J Physiol* 1991, **432**:283-312.
102. Cannell MB, Cheng H, Lederer WJ: **The control of calcium release in heart muscle.** *Science* 1995, **268**:1045-1050.
103. Song LS, Wang SQ, Xiao RP, Spurgeon H, Lakatta EG, Cheng H: **β-Adrenergic stimulation synchronizes intracellular Ca^{2+} release during excitation-contraction coupling in cardiac myocytes.** *Circ Res* 2001, **88**:794-801.
104. Altamirano J, Bers DM: **Voltage dependence of cardiac excitation-contraction coupling: unitary Ca^{2+} current amplitude and open channel probability.** *Circ Res* 2007, **101(6)**:590-597.
105. Picht E, DeSantiago J, Blatter LA, Bers DM: **Cardiac alternans do not rely on diastolic sarcoplasmic reticulum calcium content fluctuations.** *Circ Res* 2006, **99**:740-748.
106. Sobie EA, Song LS, Lederer WJ: **Local recovery of Ca^{2+} release in rat ventricular myocytes.** *J Physiol* 2005, **565**:441-447.
107. Eisner DA, Venetucci LA, Trafford AW: **Life, Sudden Death and Intracellular Calcium.** *Circulation Research* 2006, **99**:223-224.
108. Diaz ME, Trafford AW, O'Neill SC, Eisner DA: **Measurement of sarcoplasmic reticulum Ca^{2+} content and sarcolemmal Ca^{2+} fluxes in isolated rat ventricular myocytes during spontaneous Ca^{2+} release.** *J Physiol (Lond)* 1997, **501**:3-16.
109. Trafford AW, Sibbring GC, Diaz ME, Eisner DA: **The effects of low concentrations of caffeine on spontaneous Ca release in isolated rat ventricular myocytes.** *Cell Calcium* 2000, **28(4)**:269-276.
110. Diaz ME, Graham HK, O'Neill SC, Trafford AW, Eisner DA: **The control of sarcoplasmic reticulum Ca content in cardiac muscle.** *Cell Calcium* 2005, **38**:391-396.
111. Negretti N, Varro A, Eisner DA: **Estimate of net calcium fluxes and sarcoplasmic reticulum calcium content during systole in rat ventricular myocytes.** *J Physiol (Lond)* 1995, **486**:581-591.
112. Barcenas-Ruiz L, Wier WG: **Voltage dependence of intracellular $[Ca^{2+}]_i$ transients in guinea pig ventricular myocytes.** *Circ Res* 1987, **61**:148-154.
113. Fleig A, Penner R: **Silent calcium channels generate excessive tail currents and facilitation of calcium currents in rat skeletal myoballs.** *J Physiol* 1996, **494(1)**:141-153.
114. Bers DM, Eisner DA, Valdivia HH: **Sarcoplasmic reticulum Ca^{2+} and heart failure: roles of diastolic leak and Ca^{2+} transport.** *Circ Res* 2003, **93**:487-490.
115. Sun XH, Protasi F, Takahashi M, Takeshima H, Ferguson DG, Franzini-Armstrong C: **Molecular architecture of membranes involved in excitation-contraction coupling of cardiac muscle.** *J Cell Biology* 1995, **129(4)**:659-667.
116. Franzini-Armstrong C, Protasi F, Ramesh V: **Shape, size, and distribution of Ca^{2+} release units and couplons in skeletal and cardiac muscles.** *Biophys J* 1999, **77**:1528-1539.
117. Tanaka H, Sekine T, Kawanishi T, Nakamura R, Shigenobu K: **Intrasarcomere Ca^{2+} gradients and their spatio-temporal relation to Ca^{2+} sparks in rat cardiomyocytes.** *J Physiol* 1998, **508**:145-152.
118. Cheng H, Lederer MR, Lederer WJ, Cannell MB: **Calcium sparks and $[Ca^{2+}]_i$ waves in cardiac myocytes.** *American Journal of Physiology* 1996, **270(1.1)**:148-159.
119. Langer GA, Peskoff A: **Calcium concentration and movement in the diadic cleft space of the cardiac ventricular cell.** *Biophys J* 1996, **70**:1169-1182.
120. Sobie EA, Dilly KW, Dos Santos Cruz J, Lederer WJ, Jafri MS: **Termination of cardiac Ca^{2+} sparks: an investigative mathematical model of calcium-induced calcium release.** *Biophys J* 2002, **83**:59-78.
121. Bers DM: **Dynamic imaging in living cells: windows into local signaling.** *Sci STKE* 2003, **2003(177)**:pe13.
122. Hilgemann DW, Collins A, Cash DP: **Cardiac Na^+-Ca^{2+} exchange system in giant membrane patches.** *Annu NY Acad Sci* 1991, **639**:127-139.
123. Pásek M, Simurda J, Christé G: **The functional role of cardiac T-tubules explored in a model of rat ventricular myocytes.** *Philos Transact A Math Phys Eng Sci* 2006, **364(1842)**:1187-1206.
124. Li HY, Quamme GA: **Effect of pH on intracellular free Mg^{2+} in isolated adult rat cardiomyocytes.** *Biochim Biophys Acta* 1994, **1222(2)**:164-170.
125. Harkins AB, Kurebayashi N, Baylor SM: **Resting myoplasmic free calcium in frog skeletal muscle fibers estimated with fluo-3.** *Biophys J* 1993, **65(2)**:865-881.

doi:10.1186/1742-4682-7-43
Cite this article as: Krishna *et al.*: Modeling CICR in rat ventricular myocytes: voltage clamp studies. *Theoretical Biology and Medical Modelling* 2010 **7**:43.